Entergy Operations, Inc.
P. O. Box 756
Port Gibson, MS 39150

Michael A. Krupa
Director, Extended Power Uprate
Grand Gulf Nuclear Station
Tel. (601) 437-6684

Attachment 1 contains proprietary information.

GNRO-2012/00011

February 20, 2012

U.S. Nuclear Regulatory Commission
Attn: Document Control Desk
Washington, DC 20555

SUBJECT: Response to Request for Additional Information Regarding
Extended Power Uprate
Grand Gulf Nuclear Station, Unit 1
Docket No. 50-416
License No. NPF-29

REFERENCES:

1. Entergy Operations, Inc. letter to the NRC (GNRO-2010/00056), *License Amendment Request - Extended Power Uprate*, September 8, 2010 (ADAMS Accession No. ML102660403)
2. NRC Letter, Request for Additional Information for the Steam Dryer Evaluation, dated February 14, 2012 (ADAMS Accession No. ML120400216)
3. Entergy Operations, Inc. letter to the NRC (GNRO-2012/00006), *Request for Additional Information Regarding Extended Power Uprate*, dated February 6, 2012 (ADAMS Accession No. ML12039A071)
4. Entergy Operations, Inc. letter to the NRC (GNRO-2012/00009), *Request for Additional Information Regarding Extended Power Uprate*, February 15, 2012

Dear Sir or Madam:

The Nuclear Regulatory Commission (NRC) has requested additional information (Reference 2) regarding the steam dryer discussed in the Grand Gulf Nuclear Station, Unit 1 (GGNS) Extended Power Uprate (EPU) License Amendment Request (LAR) (Reference 1). Attachment 1 provides responses to the requests for additional information items 8, 10 and 12 requested by the Mechanical and Civil Engineering Branch. Responses to items 2, 3, 5, and 6 were provided in Reference 3, RAI 7 was dropped during the review, and responses to items 1, 4, 9, 11, and 13 were provided in Reference 4. Note that the response to RAI 10 refers to a revision to the Steam Dryer Analysis Report (SDAR), which was originally included as Attachment 11 in Reference 1; the revised SDAR is included in an Enclosure to Attachment 1.

When Attachment 1 is removed, the entire letter is non-proprietary.

GE-Hitachi Nuclear Energy Americas, LLC (GEH) considers portions of the information provided in support of the responses to the request for additional information (RAI) in Attachment 1 to be proprietary and therefore exempt from public disclosure pursuant to 10 CFR 2.390. An affidavit for withholding information, executed by GEH, is provided in Attachment 3. The proprietary information was provided to Entergy in a GEH transmittal that is referenced in the affidavit. Therefore, on behalf of GEH, Entergy requests Attachment 1 be withheld from public disclosure in accordance with 10 CFR 2.390(b)(1). A non-proprietary version of the RAI responses, including the revised SDAR, is provided in Attachment 2.

No change is needed to the no significant hazards consideration included in the initial LAR (Reference 1) as a result of the additional information provided. There are no new commitments in this letter.

If you have any questions or require additional information, please contact Jerry Burford at 601-368-5755.

I declare under penalty of perjury that the foregoing is true and correct. Executed on February 20, 2012.

Sincerely,

MAK/FGB

Attachments:
1. Response to Request for Additional Information, Mechanical and Civil Engineering Branch, Steam Dryer (Proprietary)
2. Response to Request for Additional Information, Mechanical and Civil Engineering Branch, Steam Dryer (Non-Proprietary)
3. GEH Affidavit for Withholding Information from Public Disclosure

cc: Mr. Elmo E. Collins, Jr.
Regional Administrator, Region IV
U. S. Nuclear Regulatory Commission
612 East Lamar Blvd., Suite 400
Arlington, TX 76011-4125

NRC Senior Resident Inspector
Grand Gulf Nuclear Station
Port Gibson, MS 39150

U. S. Nuclear Regulatory Commission
ATTN: Mr. A. B. Wang, NRR/DORL (w/2)
ATTN: ADDRESSEE ONLY
ATTN: Courier Delivery Only
Mail Stop OWFN/8 B1
11555 Rockville Pike
Rockville, MD 20852-2378

State Health Officer
Mississippi Department of Health
P. O. Box 1700
Jackson, MS 39215-1700

Attachment 2

GNRO-2012/00011

Grand Gulf Nuclear Station Extended Power Uprate

Response to Request for Additional Information

Mechanical and Civil Engineering Branch, Steam Dryer (Non-Proprietary)

This is a non-proprietary version of Attachment 1 from which the proprietary information has been removed. The proprietary portions that have been removed are indicated by double square brackets as shown here: [[ ]].

Non-Proprietary

Response to Request for Additional Information
Mechanical and Civil Engineering Branch

By letter dated September 8, 2010, Entergy Operations, Inc. (Entergy) submitted a license amendment request (LAR) for an Extended Power Uprate (EPU) for Grand Gulf Nuclear Station, Unit 1 (GGNS). The NRC has requested additional information regarding the steam dryer in a letter dated February 14, 2012. The responses to items 1 through 6, and 9, 11, and 13 were provided in Entergy letters dated February 6 and 15; the responses to items 8, 10, and 12 are provided below. (Note – RAI 7 was dropped from the request.)

RAI 8

GGNS Steam Dryer Finite Element Model Verification

a. The licensee is requested to perform a thorough re-verification of the FE models (global model, sub-models, and shell-to-solid transition areas) used in the steam dryer analysis for GGNS and confirm that in the FE models used in the steam dryer analysis for GGNS: (a) all nodes are appropriately connected; (b) nodes that are supposed to be connected are not left free inadvertently, and the load path is not shifted away from the critical areas, and (c) in case that there are any unconnected nodes, the licensee is requested to provide a description of such locations and the impact on the GGNS steam dryer stresses at EPU conditions.

b. The licensee is also requested to verify and confirm that the quality of the finite element mesh (shape or aspect ratios) is acceptable to ensure that there are no regions with poor mesh quality in the global model, in the submodels, and in shell to solid transition areas of the GGNS steam dryer FE model. In case that there is a poor quality mesh, the licensee is requested to provide a description of the impact on the GGNS steam dryer stresses at EPU conditions.

c. The licensee is further requested to provide a summary of the results from the FE model mesh density convergence studies used in the steam dryer analysis for GGNS, to validate proper stress convergence.

Response

a. The structural Finite Element (FE) model of the Grand Gulf Nuclear Station (GGNS) replacement dryer is relatively large ([[ ]]) and represents a somewhat complex structure. In order to check the nodal connections (“connectivity”) in the steam dryer FE model, a detailed review was conducted for the global model and submodels (including shell-to-solid transition areas). The review was accomplished by performing a check, in which unit accelerations were applied to the steam dryer structure

Non-Proprietary

in the global X and Y directions, as well as a vertical acceleration replicating gravity (in positive global Z direction). Discontinuities in the resulting displacement plots could then be used to identify disconnected nodes.

1. Global Model Evaluation

Some nodal disconnects were identified in the global model. There are totally [[ ]] that were misaligned. Two sets of disconnected nodes ([[ ]] adjacent node pairs at each location) are in the [[ ]] interconnection, which are symmetric about the dryer neutral axis, as depicted in Figure 1. Figure 2 shows the corrected model with connected nodes at these locations. The corrected model was used to evaluate the impact of the disconnected nodes on the dryer response.

After the [[ ]] of disconnected nodes were corrected, the global model was reanalyzed using the Flow Induced Vibration (FIV) nominal loads. Note that the reanalysis applied the [[ ]], which was shown to be consistent with the [[ ]] technique as discussed in the response to Round 5, RAI-04 (see Reference 1). Table 1 provides a comparison of maximum percentage stress intensity results for all thirty-three dryer components before and after the corrections of nodal disconnects. The maximum increase in stress intensity is observed in the [[

]] Figures 3 and 4 show the maximum stress intensity contour plots with disconnected nodes and corrected nodes in the [[ ]] junction, respectively. [[

]]

It should be noted that in the cover plate and divider plate components, the maximum stress intensity decreased by [[ ]] respectively once nodal connectivity was restored. In total, fifteen (15) of the thirty-three (33) GGNS steam dryer components showed a decrease in maximum stress intensity.

From the above results, it can be concluded that (1) the original calculated global model stresses are not substantially different from the corrected case and (2) new results did not show an increase in the limiting component stress. Considering a single figure of merit to characterize the impact of the change, based on the percent difference values

Non-Proprietary

from Table 1, the mean bias of all components is [[ ]], which is comparable to the accuracy of the finite element model (i.e., [[ ]]).

The other [[ ]] misaligned node pairs that were identified are all at different locations in the global model. Several disconnected node pairs are illustrated in Figure 5. The disconnected nodes are not located at corners or adjacent to one another. In all cases the disconnected nodes are along an edge with connected nodes on either side. The disconnected nodes are not located in the vicinity of maximum stress locations of the thirty three evaluated components. It was shown in the above analysis that the connecting [[ ]] nodal pairs in 2 locations did not significantly impact the stress results in any component, which further supports that the impact of these individual disconnections is negligible to the global stress results. The Grand Gulf Nuclear Station (GGNS) replacement dryer global finite element model (FEM) is based on the prototype Susquehanna Replacement dryer model with modifications in several dryer components due to the design changes. The SSES and GGNS models have very similar mesh density in most of the dryer components.

2. Submodel Evaluation

Four submodels with much finer mesh and employing solid elements were built and analyzed for GGNS replacement dryer. The stress ratios from [[ ]] submodel and [[ ]] submodel were used to adjust the final stress margins for these two components. Although the peak stress calculated from [[ ]] submodel was lower than that from shell global model, the more conservative stresses from global model were used to calculate the fatigue margin on the [[ ]] The last submodel, the [[ ]] submodel was used to disposition a modeling discrepancy in the connection of top cap to divider plate. The results showed that the submodeling area is not the stress limiting location. So the results from this submodel were not applied to the final stress table as well.

All four GGNS dryer submodels were checked for possible nodal disconnects.

[[ ]] **Submodel**

All nodes are appropriately connected in this submodel region. The disconnected nodes in global model are relatively distant from the area of interest of the submodel and are not expected to impact the tie bar stress intensity results in the submodel.

Non-Proprietary

[[ ]] **Submodel**

All nodes are appropriately connected in this submodel region. The disconnected nodes in the global model are relatively distant from the area of interest of the submodel and are not expected to impact the cover plate stress intensity results in the submodel.

One discrepancy was identified in this submodel compared to design. [[

]] This reinforcement fillet weld was not modeled in the submodel although nodal connectivity was modeled correctly. However, it is considered conservative not to model the fillet weld material. By not modeling the fillet weld, the [[

]]

[[ ]] **Submodel**

Disconnected nodes were identified in two locations in top cap submodel. One set is located across the [[ ]] edge length (as shown in Figure 6), which was [[ ]] (Figure 7). The maximum stress intensity in the submodel could be influenced by these disconnected nodes. However, examining the model configuration, mesh size and applying engineering judgment, it would be expected that if nodal connectivity were restored and node-to-node contact established between these two local surfaces, the localized stress intensity results would not be changed significantly.

The other disconnected nodes are along the [[ ]] interface as shown in Figure 8. These disconnected nodes are away from the critical locations that through-wall linearized stresses are extracted; also the [[ ]] So they are not expected to impact the stress intensity results in the submodel as well.

To validate the above observations, [[ ]] to the two [[ ]] submodels, i.e., the current submodel with disconnected nodes and submodel with both locations fixed. Figures 9a and 9b show the stress intensity contour plots for disconnected nodes and merged nodes at the [[ ]] edge length respectively, when [[

]] to the structure, focusing on the maximum stress intensity region. The maximum stress intensity reduces by [[ ]] when nodal connectivity is corrected.

Non-Proprietary

Figures 10a and 10b show the stress intensity contour plots for disconnected nodes and merged nodes at the [[ ]] The maximum stress intensity reduces by [[ ]] when nodal connectivity is established.

All other model connections have been verified as correct.

[[ ]] **Submodel**

In the [[ ]] submodel, [[ ]] There are two elements that join coincident nodes adjacent to the [[ ]] See Figure 11 for the detailed locations. The maximum stress intensity from this submodel for the transient dynamic FIV loads stress analysis was [[ ]]. The same load step was analyzed using a static analysis, which produced a maximum stress intensity of [[ ]], shown in Figure 12(a). To confirm the influence on localized stress intensity results, the nodes were disconnected and the stresses were reevaluated using a static analysis for the same load step. Figure 12(b) shows the maximum stress intensity at the stress location of interest, i.e., the [[ ]]. The two stress intensity magnitudes are within [[ ]] of each other ([[ ]]). It can be concluded that the erroneously connected nodes have a negligible effect on the calculated maximum stress intensity at the location of interest.

All other nodes are appropriately connected in this submodel region.

In summary, the disconnected nodes found in global model and submodels have been justified to have negligible impact on the GGNS steam dryer stresses.

b. Mesh quality was checked by using automated ANSYS routines to test for shape and aspect ratios, and to verify that any elements flagged with “warnings” were remote relative to the areas of interest.

In the global model, there are [[ ]], as shown in Figure 13(a). The mesh at this location resulted in a stress singularity and caused the stress intensity to diverge when an [[ ]] The mesh was corrected to address this issue. Figure 13(b) shows the modified mesh at the same location. The maximum stress intensity values presented in Figures 14 and 15 show that the [[ ]] component stress was reduced after the mesh modification. From the RAI 04 study (Reference 1), it is found that [[

Non-Proprietary

]]. Thus the mesh modification at [[
]] does not impact the most limiting stress on the skirt.

There are also several [[
]], as shown in Figure 16 (a). Figure 16 (b) shows the modified mesh at the same location. Figures 17 and 18 are stress intensity contour plots for the [[ ]] before and after the mesh modification (global model with [[ ]]) at the shell-to-solid interface. As stated in the response to RAI 04 (Reference 1), a detailed solid element submodel analysis was also performed in the area of interest, i.e., [[

]], which indicates that the global model using the [[ ]] method provides a conservative stress prediction.

The submodels were also evaluated for mesh quality and determined to be adequate. All ANSYS warnings related to element aspect ratios are remote from the area of interest, i.e., the peak stress locations.

In summary, the locations discussed above (where the mesh was further evaluated to respond to questions regarding element shapes and aspect ratio) were determined to have adequately resolved dryer component stresses in the current analysis. Revising the mesh resulted in reductions in stresses in those locations. Thus, these mesh quality concerns were found to have no adverse impact on stresses in the dryer at EPU conditions.

c. The GGNS replacement dryer global FEM is based on the prototype Susquehanna replacement dryer model with modifications in several dryer components due to design changes. The SSES and GGNS models have very similar mesh density in most of the dryer components.

The mesh convergence study was performed in low frequency range for the SSES FEM to determine the adequacy of the mesh. The results are summarized in Table 2. For the top three (stress) limiting components, when the mesh is reduced by a factor of two, [[

]]

Non-Proprietary

Table 3 shows mesh size comparisons between the SSES and GGNS finite element models. The LF peak stress elements from GGNS flow induced vibration (FIV) analysis were selected for comparison.

[[
]] highlighted (bold text) in Table 3, the mesh sizes of other components in GGNS model are equivalent or finer than SSES model. Therefore, [[
]] is applicable to these components.

In continuous regions of a finite element model, the mesh is considered fine enough if the difference between an unaveraged stress (element stress) and averaged stress (nodal stress) is relatively small. The element and nodal stresses for the four components with coarse mesh sizes in GGNS model are compared in Table 4. [[

]] Good agreement between results indicates that the mesh is adequate to resolve the stresses in these components.

In summary, the GGNS replacement dryer model mesh is adequate to resolve the stresses throughout the model. [[

]]

Reference:

1. Entergy letter, *Response to NRC Request for Additional Information Regarding Extended Power Uprate*, GNRO-2012/00009, dated February 15, 2012.

Withheld from Public Disclosure in accordance with 10 CFR 2.390(b)(1)

Table 1: [[

]]

[[			
			]]

Non-Proprietary

Withheld from Public Disclosure in accordance with 10 CFR 2.390(b)(1)

Table 2: Summary of SSES Mesh Refinement Results

[[					
					]]

Withheld from Public Disclosure in accordance with 10 CFR 2.390(b)(1)

Table 3: Mesh Size Comparison at FIV Maximum Stress Location

[[				]]

Table 4: Element and Nodal Stress Comparison for GGNS model

[[						]]

Withheld from Public Disclosure in accordance with 10 CFR 2.390(b)(1)

[[

]]

Figure 1: [[ ]]

Withheld from Public Disclosure in accordance with 10 CFR 2.390(b)(1)

[[

]]

Figure 2: [[ ]]

Withheld from Public Disclosure in accordance with 10 CFR 2.390(b)(1)

[[

]]

Figure 3: [[

]]

[[

]]

Figure 4: [[

]]

Withheld from Public Disclosure in accordance with 10 CFR 2.390(b)(1)

[[

]]

Figure 5: [[ ]]

Withheld from Public Disclosure in accordance with 10 CFR 2.390(b)(1)

[[

]]

Figure 6: [[ ]]

Withheld from Public Disclosure in accordance with 10 CFR 2.390(b)(1)

[[

]]

Figure 7: [[ ]]

[[

]]

Figure 8: [[ ]]

Withheld from Public Disclosure in accordance with 10 CFR 2.390(b)(1)

[[

]]

Figure 9: [[

]]

Withheld from Public Disclosure in accordance with 10 CFR 2.390(b)(1)

[[

]]

(a)

[[

]]

(b)

Figure 10: [[

]]

Withheld from Public Disclosure in accordance with 10 CFR 2.390(b)(1)

[[

]]

Figure 11: [[ ]]

Withheld from Public Disclosure in accordance with 10 CFR 2.390(b)(1)

[[

]]

(a)

[[

]]

(b)

Figure 12: [[

]]

Withheld from Public Disclosure in accordance with 10 CFR 2.390(b)(1)

[[

]]

(a)

[[

]]

(b)

Figure 13: [[

]]

Withheld from Public Disclosure in accordance with 10 CFR 2.390(b)(1)

[[

]]

Figure 14: [[

]]

[[

]]

Figure 15: [[

]]

Withheld from Public Disclosure in accordance with 10 CFR 2.390(b)(1)

[[

]]

(a)

[[

]]

(b)

Figure 16: [[

]]

Withheld from Public Disclosure in accordance with 10 CFR 2.390(b)(1)

[[

]]

Figure 17: Stress Intensity Contour Plot of the Cover Plate before Mesh Modification

[[

]]

Figure 18: Stress Intensity Contour Plot of the Cover Plate after Mesh Modification

Withheld from Public Disclosure in accordance with 10 CFR 2.390(b)(1)

RAI 10

Reference to ESBWR LTRs

The Economic Simplified Boiling Water Reactor (ESBWR) Licensing Topical Reports (LTRs) will be revised due to recently identified errors. In addition, the GGNS EPU LAR predates the approval dates of the Economic Simplified Boiling Water Reactor (ESBWR) Licensing Topical Reports (LTRs). The review of PBLE methodology will be a plant specific review for the GGNS application. Therefore the licensee is requested to remove the following references to ESBWR LTRs, as noted in Attachment 11 of the GGNS LAR:

- Appendix-B, NEDC-33408P, Revision 1: "ESBWR Steam Dryer-Plant Based Load Evaluation Methodology", June 2009;
- Appendix C, NEDC-33408, Supplement 1, Revision 2: "ESBWR Steam Dryer - Plant Based Load Evaluation Methodology", July 2010; and
- Appendix D, NEDC-33436: "GEH BWR Steam Dryer - Plant Based Load Evaluation Methodology", November 2008.

Response

In September 2010, GGNS submitted its License Amendment Request (LAR) for an extended power uprate (EPU). The evaluation of the steam dryer under uprated power conditions was presented in NEDC-33601P, "Grand Gulf Replacement Steam Dryer Fatigue Stress Analysis Using PBLE Methodology", which was included as Attachment 11 of the EPU LAR. That report, also known as the Steam Dryer Analysis Report, or SDAR, has been revised to delete references to the ESBWR topical reports and to correspondence related to the ESBWR application. In this regard, the SDAR now more clearly reflects the GGNS-specific power uprate application. Appendix D has been deleted in its entirety. References to these documents and appendices elsewhere in the SDAR have been reviewed and adjusted to ensure that the appropriate information to support the plant-specific review of the EPU LAR has been provided. In addition, information regarding partial penetration welds, which had been provided in the response to Round 5 RAI 06 (see Entergy letter dated February 6, 2012, *Request for Additional Information Regarding Extended Power Uprate*), has been incorporated into Revision 1.

Revision 1 of the SDAR is included as Enclosure 3 to this attachment. In addition, there was significant information supporting the bias and uncertainty approach and values used in the GGNS analysis provided in one of the references that was removed. This information has been retained in Enclosures 1 and 2 to this attachment.

Withheld from Public Disclosure in accordance with 10 CFR 2.390(b)(1)

RAI 12

Dryer Stress: Analysis-vs-Operating Dryer Cracking Experience

Fatigue cracking was observed in the Susquehanna steam dryer (which is a prototype for Grand Gulf) near the dryer support. The licensee is requested to describe what was deficient in the finite element modeling at that location of the Susquehanna dryer in order that the dynamic finite element stress analysis did not predict high alternating stresses to cause a fatigue crack. The licensee is requested to provide the fatigue stress at the cracked location. The staff notes that the licensee made design improvements to the Grand Gulf dryer at the location corresponding to crack in the SSES steam dryer. However, the licensee is requested to describe whether a similar deficiency is present at one or more locations in the GGNS dryer. The staff requests that the applicant review the finite element model of the GGNS dryer by comparing it with the design drawings to confirm whether a deficiency similar to that of the Susquehanna steam dryer model is present at any location in the GGNS dryer. If present, the licensee is requested to explain how the deficiency in the GGNS steam dryer FE model will be corrected.

Response

Susquehanna Dryer Cracking

In general, considering the steam dryer physical design and its representation as a structural Finite Element (FE) model, the seismic block is not important with respect to Flow Induced Vibration (FIV) and can be represented as [[
]] The blocks are relatively small features on the dryer and a representation of explicit geometry is unnecessary. The seismic blocks, as well as other similar features (*e.g.*, [[ ]] do not need to be explicitly modeled in order to adequately resolve stresses due to FIV loads. This simplification also helps manage the model size and complexity, as well as the corresponding CPU/memory requirements. However, in the case of Susquehanna, the seismic block design included [[
]], which created some degree of localized stress intensification. Although the seismic block was not included in the original finite element model, the submodel FE analyses performed for the root cause evaluations showed that the stresses in this region did not exceed the fatigue limit. Therefore, the modeling simplification was not identified as a causal factor for the crack. The omission of the seismic block features in the model did not lead to a failure to predict high alternating stresses that caused a fatigue crack. A summary of the causal analysis is provided below.

Scheduled visual inspections of the Susquehanna Steam Electric Station (SSES) Unit 2 replacement steam dryer conducted in April 2011, revealed a crack indication in the vicinity of the 4^{o} seismic block location. This steam dryer replaced the original equipment installed at SSES Unit 2 and was being inspected as part of the spring 2011 outage. First cycle inspections

Withheld from Public Disclosure in accordance with 10 CFR 2.390(b)(1)

were performed on both the exterior and interior steam dryer surfaces and an indication that was approximately 4.5 inches long and through-wall was found in the steam dryer skirt. The indication ran through the dryer skirt panel to the mid-support ring weld at 0^{o}. The indication was found after one 2-year cycle of operation at 113% OLTP. In order to allow continued operation, a stop-drill repair was performed to arrest the crack propagation (with a commitment to re-inspect during the next refueling outage). The assessment and repair were performed in compliance with Boiling Water Reactor Owners' Group Vessel & Internals Project (BWRVIP) guidelines documented in BWRVIP-181-A [1].

The subsequent Root Cause Analysis (RCA) determined that there were two major causal factors. First, the design did not sufficiently account for the risks of [[
]] as shown in Figure 1. The design incurred potential risks related to [[
]] Second, the [[
]]. The investigation into the manufacture of the block [[

]] These findings have been addressed through the corrective action process; the GGNS dryer manufacturing process incorporated corrective actions (lessons learned) into the welding process. In-depth training of all fabrication personnel on the preparation of the weld's HAZ was performed. This training included the following interactive sessions:

- All welding, grinding, and inspection personnel were trained on why polishing of the weld's HAZ is necessary to reduce surface cold work.
- All welding, grinding, and inspection personnel were shown examples of properly prepared samples of HAZs with blended weld toes, and 63rms finish applied.
- All welding, grinding, and inspection personnel were instructed on the use of a visual surface comparator so that they could check their own work prior to final inspection.
- All inspection personnel were trained on the use of a profilometer to perform final inspection of the final surface finish of weld's HAZs, and other surface polished areas.

Training was provided to all welders pertaining to weld heat input, and autogenous welding. This training was focused on heat input control, travel speed, and following the parameters of the approved Welding Procedure Specifications (WPS). The training for autogenous welding

Withheld from Public Disclosure in accordance with 10 CFR 2.390(b)(1)

outlined the reason why fusion welding is not permitted. This training also identified the detrimental effects of autogenous welding.

The original global dryer model used in the EPU licensing analysis for SSES was (by definition) relatively coarse and included simplifications. The geometric details of the seismic blocks were not included. [[
]] as shown in Figure 1, [[
]] As part of the causal investigation of the spring 2011 observed indication in the skirt, sub-models for the seismic block to the dryer skirt region at the 4^{o} seismic block location were generated to model the detailed seismic blocks and the load path from the vessel support lug through the seismic block tab to the dryer skirt weld. The results of this evaluation indicated that the maximum predicted stress intensity in the as-built condition at the 4^{o} seismic block to dryer skirt weld location was [[
]] However, this stress level is still not of sufficient amplitude to initiate a fatigue crack and growth similar to the spring 2011 observed indication. Therefore, additional causal factors must have been present in order to create the conditions necessary to initiate a high cycle fatigue crack. The additional causal factors must have included [[

]]

In summary, the causal factors identified in the RCA for the SSES crack are associated with design and manufacture, but not with supporting finite element modeling and fatigue evaluation.

Withheld from Public Disclosure in accordance with 10 CFR 2.390(b)(1)

[[

]]

Figure 1: Susquehanna Replacement Steam Dryer Seismic Block

Withheld from Public Disclosure in accordance with 10 CFR 2.390(b)(1)

GGNS Seismic Block Design

The design of the GGNS seismic block is a result of combining critical to quality requirements and Lessons Learned from the Susquehanna seismic block installation. The result is a [[ ]] with the following differences from the Susquehanna dryer:

- The GGNS seismic block represents a [[ ]] over the SSES seismic block.
- The [[ ]] is attributed to a larger [[ ]] on the vessel lug at each seismic block location to accept ASME Code bounding loads through the vessel lug.
- The GGNS seismic block [[ ]] is rounded to minimize the risk of interference during dryer installation in the RPV.
- Two seismic block versions have a [[ ]] to alleviate a potential interference with the dryer skirt tee at those locations.
- Figure 2 shows the GGNS seismic block installation with [[ ]]

[[

]]

Withheld from Public Disclosure in accordance with 10 CFR 2.390(b)(1)

[[

]]

Figure 2: GGNS Replacement Steam Dryer Seismic Block

Review of the GGNS Dryer Design

As discussed in the first part of this RAI response, there were no deficiencies in the finite element model that contributed to high stresses leading to fatigue cracks in the Susquehanna replacement steam dryer. However, as requested by the staff, the finite element (FE) model for the GGNS replacement steam dryer was reviewed in detail by comparing the finite element model to the 3-D CAD model and design drawings to identify potential areas where the modeling and determination of peak stress did not explicitly include consideration of details in the design. There were two such areas identified and the results of evaluations of each are presented below.

Withheld from Public Disclosure in accordance with 10 CFR 2.390(b)(1)

1. Hood tee (outer) connects to the hood support with a plate thickness transition from [[ ]] as shown in Figure 3. This thickness transition was not modeled in the dryer FE model for GGNS. Thus, the resulting stress needed to be adjusted to include the effect of the thickness reduction. A thickness reduction factor, which is [[

]] has been applied to the final predicted maximum stress intensity for the hood tee-outer. The adjusted maximum stress intensity, including consideration of all biases and uncertainties and EPU scale factors, was calculated as [[

]]

[[

]]

Figure 3: Hood Tee – Outer

2. In the as-designed hood support component, there is a thickness reduction from the hood support plate thickness of [[ ]], as shown in Figure 4. This thickness reduction was not modeled in the dryer FE model for GGNS. The resulting stresses thus need to be adjusted to include the effect of the thickness reduction. The stresses in all weld lines along this thickness reduction section were scoped for all low frequency and high frequency load cases. The stress intensity values were calculated by determining [[

Withheld from Public Disclosure in accordance with 10 CFR 2.390(b)(1)

]]

By applying the corresponding weld factor and bias and uncertainty including the EPU factor to the adjusted stress intensity, the final maximum stress intensity is [[

]]

[[

]]

Figure 4: Hood Support

These changes to the margins of the outer hood tee and hood support are included in the updated GGNS replacement dryer final stress table.

References

1. BWRVIP-181-A, “BWR Vessel and Internals Project, Steam Dryer Repair Design Criteria,” EPRI Technical Report 1020997, July 2010.

Enclosure 1 to Attachment 2

GNRO-2012/00011

Grand Gulf Nuclear Station Extended Power Uprate

Response to Request for Additional Information

Mechanical and Civil Engineering Branch, Steam Dryer (Non-Proprietary)

Note

A non-proprietary version of this Enclosure is not being submitted in accordance with NRC Information Notice 2009-07, Requirements for Submittals, (2): "In instances in which a non-proprietary version would be of no value to the public because of the extent of the proprietary information, the agency does not expect a non-proprietary version to be submitted."

Withheld from Public Disclosure in accordance with 10 CFR 2.390(b)(1.

Enclosure 2 to Attachment 2
GNRO-2012/00011

Grand Gulf Nuclear Station Extended Power Uprate

Response to Request for Additional Information

Mechanical and Civil Engineering Branch, Steam Dryer (Non-Proprietary)

Note

A non-proprietary version of this Enclosure is not being submitted in accordance with NRC Information Notice 2009-07, Requirements for Submittals, (2): "In instances in which a non-proprietary version would be of no value to the public because of the extent of the proprietary information, the agency does not expect a non-proprietary version to be submitted."

Enclosure 3 to Attachment 2

GNRO-2012/00011

Grand Gulf Nuclear Station Extended Power Uprate

Response to Request for Additional Information

Mechanical and Civil Engineering Branch, Steam Dryer (Non-Proprietary)

This Enclosure provides Revision 1 of the GGNS SDAR, NEDC-33601

Withheld from Public Disclosure in accordance with 10 CFR 2.390(b)(1.

ENCLOSURE 6

173280-JB-060

NEDO-33601
GGNS Replacement Dryer Fatigue Stress Analysis Using PBLE Methodology
GEH Non-Proprietary Information-Class I (Public)

NON-PROPRIETARY NOTICE

This is a non-proprietary version of the Enclosure 5 of 173280-JB-060 which has the proprietary information removed. Portions of the document that have been removed are indicated by an open and closed bracket as shown here [[ ]].

HITACHI

GE Hitachi Nuclear Energy

NEDO-33601
Revision 1
Class I
DRF 0000-0094-9515
February 2012

Non-Proprietary Information

ENGINEERING REPORT

GRAND GULF REPLACEMENT STEAM DRYER FATIGUE STRESS ANALYSIS USING PBLE METHODOLOGY

INFORMATION NOTICE

This is a non-proprietary version of the document NEDC-33601P, Revision 0, which has the proprietary information removed. Portions of the document that have been removed are indicated by an open and closed bracket as shown here [[ ]].

IMPORTANT NOTICE REGARDING CONTENTS OF THIS REPORT

Please Read Carefully

The design, engineering, and other information contained in this document is furnished for the purpose of supporting the Grand Gulf Nuclear Station license amendment request for an extended power uprate in proceedings before the U.S. Nuclear Regulatory Commission. The only undertakings of GEH with respect to information in this document are contained in the contracts between GEH and its customers or participating utilities, and nothing contained in this document shall be construed as changing that contract. The use of this information by anyone for any purpose other than that for which it is intended is not authorized; and with respect to any unauthorized use, GEH makes no representation or warranty, and assumes no liability as to the completeness, accuracy, or usefulness of the information contained in this document.

REVISION HISTORY

Revision	Date	Changes	Comment
0	September 2010	Initial issue	None
1	February 2012	Table Changed Appendices B and C to be specific to Grand Gulf. Incorporated editorial changes to Appendix E. Corrected Appendix G, Plant Data Table on page 97. Remove references to ESBWR LTRs, NEDC-33436 and ESBWR MFNs. Revisions to Main Body and Appendix E per RAI-6.	

TABLE OF CONTENTS

LIST OF TABLES

LIST OF FIGURES

LIST OF ACRONYMS

Short Form	Description
1-D	One-dimensional
3-D	Three-dimensional
με	Micro Strain (10^{-6} length/length)
ASME	American Society of Mechanical Engineers
B&PV	Boiler and Pressure Vessel
BWR	Boiling Water Reactor
CLTP	Current Licensed Thermal Power
DAS	Date Acquisition System
DOF	Degree of Freedom
EPU	Extended Power Uprate
FEA	Finite Element Analysis
FEM	Finite Element Model
FFT	Fast Fourier Transform
FIV	Flow Induced Vibration
FRF	Frequency Response Function
GEH	GE Hitachi Nuclear Energy
GGNS	Grand Gulf Nuclear Station
HCF	High Cycle Fatigue
HF	High Frequency
Hz	Hertz
IGSCC	Intergranular Stress Corrosion Cracking
LF	Low Frequency
MASR	Minimum alternating stress ratio
Mlbm/hr	Millions pounds mass per hour
MSIV	Main Steam Isolation Valve
MSL	Main Steam Line
MSLB	Main Steam Line Break
MW_t	Megawatt Thermal

Short Form	Description
NRC	Nuclear Regulatory Commission
OBE	Operating Basis Earthquake
OLTP	Original Licensed Thermal Power
Pa	Pascal
PATP	Power Ascension Test Program
PBLE	Plant Based Load Evaluation
PSD	Power Spectral Density
psi	Pounds per square inch
PT	Penetrant Test
QC2	Quad Cities Unit 2
RCIC	Reactor Core Isolation Cooling
RFO	Refueling Outage
RIO	Refueling Inspection Outage
RMS	Root-Mean-Squared
RPV	Reactor Pressure Vessel
SCF	Stress Concentration Factor
SF	Singularity Factor
SRF	Stress Reduction Factor
SRV	Safety Relief Valve
SSE	Safe Shutdown Earthquake
TC	Test Condition
TSV	Turbine Stop Valve
[[	]]
VPF	Vane Passing Frequency
ZPA	Zero Period Acceleration

1.0 EXECUTIVE SUMMARY

This report documents the finite element stress analyses of the replacement steam dryer for the Grand Gulf Nuclear Station (GGNS). The focus of these analyses is to predict the replacement dryer's susceptibility to fatigue under flow-induced vibration and hydrodynamic loads during normal operation as well as for established design conditions, including normal, upset, emergency and faulted conditions at extended power uprate (EPU) power levels. A detailed finite element model (FEM) is used to perform the structural dynamic analyses. The results of these analyses are used to assess dryer component stresses versus fatigue design criteria under the operating conditions at EPU.

The GE Hitachi Nuclear Energy (GEH) Plant Based Load Evaluation (PBLE) methodology (Appendices B and C) was used to develop the fluctuating pressure loading that is applied to a finite element model of the replacement steam dryer to calculate the steam dryer transient dynamic responses. The pressure loads were developed from main steam line (MSL) strain gauge instrumentation data obtained during the power ascension of GGNS in November 2008. The MSL strain gauge data at 100% Current Licensed Thermal Power (CLTP) level and additional potential safety relief valve (SRV) acoustic resonance signals at high frequency range were used as the input to the PBLE for the determination of the fluctuating pressure loading.

To evaluate uncertainties in the steam dryer structural frequency response, [[
]] from the nominal value to create frequency shifts in the load definition. Trending of power ascension test measurements of MSL strain gauge data and associated dryer pressure loads were used to develop frequency dependent EPU scaling factors, to project FEM stress results to EPU conditions.

After incorporating end-to-end bias and uncertainty values, the results from fatigue evaluations confirm that at EPU conditions, the replacement dryer is structurally adequate to accommodate flow-induced vibration (FIV) loads. All dryer components meet the fatigue acceptance criteria with a minimum alternating stress ratio (MASR) greater than 2.0.

The GGNS replacement steam dryer was analyzed for the applicable American Society of Mechanical Engineers (ASME) load combinations under normal, upset, emergency and faulted conditions (primary stress). Results demonstrated that at EPU conditions, stresses for all structural components are below the ASME Code allowable limits.

The comparison of steam dryer geometry, plant geometry and operating conditions, as well as the comparison of FIV loads between GGNS and its valid prototype, justify and support the non-prototype designation, obviating the need for on-dryer instruments.

A Power Ascension Test Program (PATP) will be followed at GGNS for the initial cycle of EPU operation. MSL strain gauges will be monitored and the resulting steam dryer pressure loads compared to acceptance limit criteria to ensure that the dryer stresses remain below the fatigue limit.

2.0 PRODUCT DESCRIPTION

2.1 Original Grand Gulf Dryer

The original Grand Gulf steam dryer is a curved hood six-bank dryer. Inspections of the original Grand Gulf dryer have reported only a few indications. Three indications have been found on the dryer support ring. These indications were determined to be intergranular stress corrosion cracking, which is common for support rings in dryers of this vintage. Other indications were found on the lifting eye-to-lifting rod tack welds. These cracks were determined to be caused by low cycle fatigue during handling of the dryer, not high cycle fatigue (HCF) during power operation of the reactor. When compared to other curved hood dryers, the Grand Gulf indications have been minor.

Other original equipment curved hood dryers have required repairs to drain channels, end plates, hoods and tie bars to address fatigue cracking. Since 2004 the interiors of several curved hood dryers have been inspected. These inspections have shown cracking at the junction of the interior hood supports, the hood panel and base plate, as well as the junction of the interior hood support and the trough. The configuration at these locations is very stiff (the junction of three perpendicular planes). It is believed that the cracks formed early in life and once formed, the cracks introduced sufficient flexibility in the structure. Of those affected dryers that have been re-inspected, the results indicate that the existing cracks are relatively stable.

2.2 Replacement Dryer Design

The Grand Gulf replacement steam dryer design is based on the design of a curved hood six-bank replacement dryer used in a prototype Boiling Water Reactor (BWR)/4 reactor. To satisfy the current MASR and maximum allowable stress limits, the BWR/4 replacement dryer design uses [[

]] In addition, [[

]] This steam dryer also uses [[

]] to improve the stress distribution and move the welds away from the stress concentration at these panel junctions. The replacement steam dryer also uses an improved [[

]] As a result, the BWR/4 prototype replacement steam dryer design is significantly more robust than the steam dryer it replaces. Both the Grand Gulf reactor vessel and the BWR/4 reactor vessel where the BWR/4 prototype replacement dryer was installed have the same internal diameter so the Grand Gulf replacement

steam dryer design remains essentially unchanged from the BWR/4 prototype design. Differences between the BWR/4 dryer and the Grand Gulf replacement steam dryer will be discussed in Section 2.2.1 below. The Grand Gulf replacement dryer is very similar in profile to the original Grand Gulf dryer but has the improvements incorporated in the [[ ]]design.

2.2.1 Modifications Made for Grand Gulf

Several minor changes were made to the BWR/4 prototype dryer design to match the fit and form of the original Grand Gulf steam dryer. First, the Grand Gulf reactor design uses six vessel supports for the steam dryer as opposed to four supports for the BWR/4 design. The six support locations are included in the Grand Gulf replacement steam dryer design. The steam dryer skirt was lengthened by 9.5 inches to match the original Grand Gulf dryer. The Grand Gulf reactor is designed with six hold-down locations on the vessel head to hold the dryer in place during a postulated MSL break. Four of these are the lifting rods as in the BWR/4 design. The additional two hold-down channels in the BWR/6 design are located in the end closure plates between the two center banks. [[

]] Section 5 provides additional information comparing the BWR/4 prototype dryer and the GGNS replacement dryer.

2.2.2 Design Improvements to BWR/4 Replacement Design

A minor change to the BWR/4 prototype steam dryer was [[

]], reducing the stress in this location. [[ ]]

3.0 STEAM DRYER EVALUATION PROCESS DESCRIPTION

3.1 Evaluation Process Overview

The following process is used to evaluate the capability of the steam dryer to withstand the vibration and hydrodynamic loadings during normal operation, as well as transient and accident conditions (see Figure 3-1).

- The MSL geometry is evaluated for potential acoustic resonances that may occur in the expected range of EPU operating conditions. This evaluation is based primarily on an acoustic evaluation of the safety relief valve (SRV) standpipe and MSL geometry, as well as measurements taken in plants with similar geometries and operating conditions. (Reference Appendix A.)
- The potential acoustic resonance frequencies are used in conjunction with the vessel and MSL acoustic models to determine optimum locations for the MSL pressure measurements. Measurements of the acoustic pressures in the MSLs are taken during the plant power ascension to CLTP. (Reference Appendix A.)
- The power ascension trend data is used to develop scaling factors for projecting the dryer acoustic loads to EPU conditions. (Reference Appendix A)
- The dryer fluctuating pressure load definition for the FIV analysis is developed based on the plant MSL pressure measurements and the potential SRV resonances identified in the source screening using the PBLE methodology. (Reference Appendices A, B, and C.)
- The fatigue analysis of the dryer is performed using the fluctuating pressure load definition, the stress analysis is adjusted for all bias and uncertainties and the results are confirmed to meet the fatigue acceptance criteria. (Reference Appendix E.)
- The power ascension monitoring program and acceptance limits are defined for confirming the steam dryer meets the fatigue acceptance criteria at EPU conditions. (Reference Appendix F.)
- The dryer is evaluated under defined load combinations to demonstrate that the dryer will maintain structural integrity under normal, upset, emergency and faulted conditions. (Reference Appendices A and E.)

3.2 Steam Dryer Load Definition

3.2.1 Screening for Potential Acoustic Sources

The purpose of this section is to describe the process of screening GGNS for potential acoustic sources. Regulatory Guide 1.20, Revision 3, Section C 2.0 (Reference 1) indicates studies of past failures have determined that flow-excited acoustic resonances within the valves, stand-off pipes and branch lines in the MSLs of BWRs can play a significant role in producing mid- to high-frequency pressure fluctuations and vibration that can damage MSL valves, the steam dryer and other reactor pressure vessel (RPV) internals and steam system components. The screening for acoustic sources is plant specific because the BWR models are not all alike. The MSL configuration for BWR/6 plants is generically similar across the plant fleet, particularly within the containment drywell where the limited space dictates a standardized pipe routing configuration. The MSLs exit the vessel symmetrically offset about 18-20° from the 90-270° vessel line, then collect and exit the drywell along the 0-180° vessel line towards the turbine, as shown in Figure 3-2. Outside the drywell, after the outboard main steam isolation valves (MSIVs), the MSL configuration varies from plant to plant.

The different containment types introduce only a minor difference in the MSL configuration within the drywell. For the BWR/6 Mark III containments, the MSLs drop to roughly mid-height of the RPV and exit the drywell.

GGNS has the typical four MSL configuration where the steam line nozzles are offset ± 18^{o} from the 90-270° line. There are no dead-legs so no prominent low frequency (LF) acoustic loads are expected. GGNS uses a common standpipe configuration for all of the SRV branches. There are two SRV layouts in the MSL configuration, with MSLs B and D being mirror images of MSLs A and C. The short lines, A and D, have four SRVs, as shown in Figure 3-3. The long lines, B and C, have six SRVs, with the last two just downstream of a slight bend. There is a Reactor Core Isolation Cooling (RCIC) line and a Reactor Vent line on MSL A at 107 inches and 81 inches below the centerline of the nozzle, respectively, as shown in Figure 3-4. This line typically falls between the SRVs and the RPV in most BWR/3 through BWR/6 plants.

The acoustic FEM modal analysis has been used to predict the expected range of steam acoustic resonant response of the standpipe using a small single valve model and full multi valve models.

The FEM acoustic analysis of the single Grand Gulf SRV indicates [[
]], as shown in Figure 3-5.

However, the SRV and MSL acoustics will interact and the combined system may resonate at frequencies different from that of the single valve standpipe fundamental frequency. For that reason, acoustic modes in the full model, including all valves, must be evaluated. The acoustic FEM for the short MSL line with [[ ]] SRVs shows [[ ]], as shown in Figure 3-6.

The acoustic FEM for the long line with [[ ]] SRVs shows prominent modes at [[ ]], as shown in Figure 3-7.

A test program was performed following Refueling Outage (RFO)-16 at GGNS to obtain MSL strain gauge data. (See Section 3.2.2 for more details regarding the test.) The test report is contained in Appendix G of this report. From the MSL strain gauge testing done in November 2008, maxima appear in the 95% CLTP and 100% CLTP measurements in the frequency range of [[ ]]

In the GGNS MSL measurements at 95% power, there are [[ ]] (see Figure 3-8). These peaks are believed to be associated with a single standpipe resonance. At 100% power, the amplitude for the [[ ]] In addition, the coherence at [[ ]] between the measurement locations on MSL C is very high (~0.9) whereas the coherence is only about 0.2 for the [[ ]] The [[ ]] peak appears to be a true SRV resonance and is modeled in the load definition.

In the GGNS MSL measurements, a strong [[ ]] peak (see Figure 3-8) develops at 100% CLTP power (MSL flow velocity ~141 ft/sec). The associated 0V measurements [[ ]] This peak shows in all MSL measurement locations, though at varying amplitudes. This peak has the appearance of [[ ]]; however, it is most apparent in the 100% power measurements. [[

]]

An FEM acoustic model of an SRV at a similar [[ ]] predicted [[ ]] resonance for a standpipe with similar dimensions to the GGNS standpipe (see Table 3-1). The MSL measurements taken in 2009 at this [[ ]] show an SRV resonance at [[ ]] that begins between 95% and 100% Original Licensed Thermal Power (OLTP) (MSL flow velocity of [[ ]]). The GGNS [[ ]] peak is close to the [[ ]] peak seen in

the [[ ]] plant data. This could be the beginning of a resonance at 100% power. Therefore, this is assumed to be an SRV resonance and is modeled in the load definition.

The [[ ]] MSL measurements show an SRV resonance at [[ ]] (Figure 3-9) that begins between 100% and [[ ]] OLTP power (MSL flow velocity of [[ ]]). The SRV standpipe dimensions are about the same as GGNS (see Table 3-1). Therefore, this potential SRV resonance in this frequency range [[ ]] is considered in the load definition. A review of the acoustic mode shapes shows that modeling the SRV resonance frequency at [[ ]] will tend to maximize the pressure loading on the dryer.

Table 3-2 shows how the predicted resonant frequencies match up with the measurement data from GGNS and the similar [[ ]] plant.

From the combined FEM analysis and measurements, the first candidate frequency for the dryer analysis would be [[ ]] From the measurements, this frequency is [[ ]] and will probably [[ ]], and is close to the predicted [[ ]] Next would be [[ ]], which grows quickly with increased power. It is close to the predicted [[ ]] and the [[ ]] plant measured frequency of [[ ]] The next candidate would be the [[ ]] SRV resonance. [[ ]] The final frequency, the predicted [[ ]] mode, is close to the [[ ]] peak seen in the [[ ]] plant measurements.

Figure 3-10 shows the observed and predicted SRV resonances. [[ ]] The vertical lines are the average MSL flow velocities at CLTP and EPU. The sloped lines signify the possible interaction between the first acoustic mode of the SRV and the first and second shear wave modes associated with the flow instabilities. Figure 3-10 illustrates that the acoustic modes shown in the measurements and predictions are [[ ]] The flow velocities required to initiate [[ ]] resonances are well above the EPU range. However, resonances due to [[ ]] would be expected to occur during power ascension and CLTP and could continue at EPU.

The data points represent measured data during power ascension at GGNS and the [[ ]] plant, respectively. The horizontal lines represent the [[ ]] used in the GGNS dryer analysis.

3.2.2 Obtain Data for Dryer Load Evaluation

The methodology used to obtain data for the dryer load evaluation is outlined in more detail in Appendix A. This section provides a summary of the following topics: Optimization of Strain Gauge Locations, Data Acquisition Equipment, Data Acquisition Summary, and Data Filtering and Scaling.

3.2.2.1 Optimization of Strain Gauge Locations

The PBLE can be used with [[ ]] data to define the acoustic loads on a BWR steam dryer.

For MSL instrumentation, the methodology requires:

- A minimum of two measurement locations per steam line.
- [[ ]]
- That there are no significant acoustic sources between the measurement locations and the vessel nozzles.

The process for determining sensor locations that minimize singularities in the PBLE solution is described in Appendices B and C. The candidate sensor locations are chosen to [[ ]] The PBLE model is then run [[ ]] There were [[ ]] strain gauge mounting locations on the A and C lines and [[ ]] locations on the B and D lines. [[

]]

Figure 3-11 shows an example of the SF plot comparing the response of the [[ ]] Prior to installing the gauges, the as-built arrangement of the piping was evaluated and the pipe condition at the proposed locations was assessed to determine the final mounting location.

3.2.2.2 Data Acquisition Equipment

The data acquisition system (DAS) equipment used to gather MSL data at GGNS is an LMS ScaDAS-05. This system meets criteria outlined in Appendix A. This DAS is a computer-based

system capable of acquiring, storing and analyzing strain gauge data. This DAS was selected to have high immunity to electrical noise. This system is suitable for static and dynamic measurements for a frequency bandwidth of at least [[ ]] It is sensitive enough to detect and measure strain levels of [[ ]] Anti-aliasing filtering is sufficient to exclude aliasing of [[ ]] data with an anti-aliasing noise floor less than [[ ]] The anti-aliasing filtering requirement exceeds the noise floor requirement.

The DAS has an option to set bridge excitation to zero volts. [[ ]] Figure 3-12 shows a comparison of the strain gauge measurements with and without excitation. [[ ]]

3.2.2.3 Data Acquisition Summary

In 2008, during RFO-16 at GGNS, [[ ]] strain gauge sensors were installed at [[ ]] MSL locations. After RFO-16, a data acquisition test program was conducted to collect power ascension data. The tests performed during this event were as follows.

[[ ]]

This acquired test data serves as input to PBLE load generation as described in more detail in Appendix A.

In May 2010, a second data acquisition campaign was conducted to collect GGNS data. [[ ]] Tests performed during the May 2010 program are as follows:

- [[ ]]

- [[

]]

A more detailed summary of these test campaigns can be found in Appendix G. The DAS was left in place at GGNS and may be used again to support steam dryer limit curve monitoring in a future power ascension test program as described in Appendix F.

3.2.2.4 Data Filtering and Scaling

The first step in the filtering process for GGNS was to [[

]]

For all of these reasons the frequencies listed in Table 3-3 were judged [[

]]

The GGNS noise was filtered using a Fast Fourier Transform (FFT) to achieve reduced bandwidth and linear phase. These filters operate in the zero phase mode by passing the data in the forward direction and then passing the result back through in reverse time order. This method was used to avoid stability and roll-off issues with Butterworth filters with the narrow line rejection desired without substantial overlap to adjacent frequencies. The frequencies that were filtered had [[

]]

The result is [[

]]

[[ ]] it was treated as a potential SRV resonance frequency because it falls in the band of likely SRV sources.

Figure 3-13 shows an example of [[
]] The figure shows the unfiltered and filtered signal and also includes the 0V excitation signal for comparison. [[

]] Figure 3-14 shows the same filtered data but only includes the range from [[
]] so that the effects of [[
]] This figure demonstrates that the filtering [[
]] Figure 3-15 is an example of the filtering performed for the [[
]] It is noted that for the QC2 benchmark cases, [[ ]] These figures show that the filtering performed for the GGNS MSL data is consistent with the filtering performed for the benchmark data. The notch width used in the GGNS filtering was narrower than that used on the benchmark plant; therefore, the generic PBLE bias and uncertainty values are bounding for the GGNS application.

The time histories were [[
]] from GGNS-acquired plant data and then [[

]] The common conversion factor from pressure in psi to pressure in Pascals was applied to each station average stream. More information is provided in Appendix A on calibration testing of strain gauge pressure data using pre-operational leak test data.

The full frequency range filtered and back-filled and scaled to Pascals was also output in the PBLE format to be used in generating the dryer acoustic node pressure time histories from PBLE over the full time record.

3.2.3 Steam Dryer Fluctuating Load Definition

3.2.3.1 Load definition

The replacement steam dryer FIV response analysis uses the filtered MSL strain gauge data to develop the load. The methodology is described in Appendices B and C [[
]]

- [[

]]

A 3-D acoustic FEM of the GGNS replacement steam dryer and RPV was constructed [[

]] Additional key input [[

]] to the steam dryer. Table 3-4 shows these parameters for the GGNS acoustic FEM. The parameters are within the range of the PBLE sensitivity assessment shown in Appendix G of Appendix C.

MSL strain gauges were placed at [[ ]] locations, including [[ ]] locations on MSLs B and D and [[ ]] locations on MSLs A and C. Strain time histories from GGNS Test Condition J (100% CLTP) were converted [[

]] The MSL steam properties are derived by the PBLE as described in Section 2.4 of Appendix C.

The nozzle acoustic velocities and amplitudes are then used to excite the dome acoustic FEM. The relationship between MSLs spectral content and the RPV spectral content is modeled with a [[ ]] transfer matrix (Transmatrix – Section 2.3.3 of Appendix C). The Transmatrix also includes smaller internal RPV noise [[

]] (Section 3.1.2 of Appendix C). This noise contributes to dryer load when MSL signals are low or have been filtered to remove noise. Velocity of GGNS at EPU ([[ ]]) is well below QC2 at test condition 41a ([[ ]]). Therefore, in accordance with Appendix C, the QC2 source amplitude was used in the GGNS PBLE load development.

Pressure loads are calculated and recorded at specific nodes on the acoustic model that are adjacent or coincident with nodes on the surface of the structural FEM. A time segment of the pressure loads (i.e., pressure time histories) from the adjacent acoustic model nodes were mapped to the surface of the structural FEM. These mapped pressure loads were used to perform

the FIV structural analyses. This process is performed distinctly for both LF and HF PBLE pressure loadings.

3.2.3.2 Selection of Time Segments

The MSL strain gauge data acquisition for each GGNS power ascension test condition consisted of data sets [[

]], a subset of this data is used to attain a reasonable calculation time for the structural analyses.

Dividing the structural analysis into LF and HF ranges facilitates the management of the large data sets. A [[ ]] segment from the MSL pressure time histories was selected to capture the peak response for the LF [[ ]] acoustic loads, using a sampling rate of [[ ]] A [[ ]] time segment from the MSL pressure time histories was selected to capture the peak response for the HF [[ ]] acoustic loads, [[

]]

The length of the time segments was chosen to [[

]]

capture the peak response at each frequency. The time segments were selected by evaluating the spectral content of the [[ ]] MSL strain gauge data [[

]] The uncertainty in the various time intervals is addressed in Section 3.4 of this report and in Appendix A.

[[

]] This process was performed for [[

]] loads, respectively. Following preliminary structural analysis, stress time history results were used with the [[ ]] stress projection methods (Appendix E) to select the time segment used in the final stress analysis.

The steam dryer pressure and stress intensity PSDs were [[

]]

[[

]] The resulting stress intensity PSDs represent the projected stress [[ ]] These projected peak stress intensity values are compared on a component basis [[

]]

3.2.4 Basis for Projected FIV Loads to EPU

The GGNS dryer loads were projected to EPU amplitude [[ ]] It was determined that the majority of the dryer loads in the frequency span [[ ]] were [[ ]] as a function of MSL flow [[ ]] The scaling of GGNS dryer to EPU also included [[ ]] combinations of potential SRV resonance conditions [[ ]] scaled to EPU.

3.2.4.1 Trending and Projection of Non-SRV Resonance Dryer Loads

Section 3.2.2.3 and Appendix G discuss acquiring MSL strain gauge data. This data is used to project PBLE generated steam dryer loads for each condition. The load is projected to [[

]]

To derive the frequency dependent EPU scaling the load [[ ]] These loads were calculated at [[

]]

[[

]] Equation 3-2 provided a good fit to all the non-resonant data and supports previous observations that non-resonant loads [[

]]

Figure 3-16 through Figure 3-18 depict the CLTP PSD curve (green) and the EPU projection curve (light blue) [[

]] is included in Appendix A, Section 5.1.

3.2.4.2 Trend and Project SRV Resonance Data

The acoustic response will be tracked and projected during power ascension (See Appendix F). SRV acoustic resonance can be characterized [[

]] After an initial onset period the load projections can be reasonably made with modest power ascension power steps and linear projections to estimate the dryer load amplitude at the next test step. [[

]] Once the resonance is established, [[

]] When the resonance beings to peak, [[

]]

[[

]]

The SRV resonant loads at [[ ]] are in early onset. Scaling of those loads for dryer qualification at EPU is discussed in the next section. The 95% and 100% average power data was used with Equation 3-4 and the resulting projection for the [[ ]] loads are depicted by the light blue lines in Figure 3-16 through Figure 3-18. [[ ]], the projection is below the EPU design values (expected maximum response). Further discussion on SRV projection is included in Appendix A, Section 5.1.

3.2.4.3 Generation of SRV – Projected Loads.

A review of the GGNS power ascension data indicates that, [[ ]], there is evidence of [[ ]] SRV acoustic resonances. The initial onset was observed at [[ ]] as well as [[ ]] Based on the assessment in Appendix A, Section 3, there is potential for additional SRV resonances [[ ]]

To evaluate the acoustic response of the GGNS dome and the sensitivity of the replacement dryer to SRV acoustic resonances through this frequency range, [[ ]] The scaling [[ ]] is described in Appendix A, Sections 3 and 5.

[[ ]] different projected EPU conditions were evaluated for evaluation of the GGNS replacement dryer at EPU. These include:

[[

]]

[[

]]

The loads were scaled such that the projected GGNS design basis loads bounded the projected peak resonant response loads from plants with similar [[

]] design. The projected [[ ]] dryer load is scaled to the full GGNS projected Strouhal number at EPU for each of the Strouhal Adder Frequencies.

The resulting load amplitude is depicted as the purple lines in Figure 3-16 through Figure 3-18. These [[ ]] design conditions provide what is expected to be a conservatively high set of design loading conditions for the structural analysis. These loads, coupled with the modest resulting stress, provide high assurance that the GGNS replacement dryer will be acceptable at EPU conditions. The acceptance limit criteria presented in Appendix F will assure GGNS does not operate at conditions that will result in FIV stresses above the ASME Code endurance limit.

Additional information on the generation of projected SRV resonance loads is included in Appendix A, Section 5.

3.2.5 Comparison of Projected Loads with Industry Data

The previous sub-sections within this report have described the process to develop the GGNS dryer loads. This includes scaling acoustic data to EPU projected steam flows and adding [[

]] This was added at the following frequencies: [[ ]] The [[ ]] frequencies are directly observed in GGNS test data, and the signal amplitudes at these frequencies are expected to increase as the power is increased toward EPU conditions. The [[ ]] frequencies have also been observed in test data from other plants with similar steam line and SRV standpipe geometries.

This section presents a qualitative review of the GGNS loads with the available industry data. The key purpose of this section is to compare dryer loads from other plants and demonstrate the validity of [[ ]] the load definition.

Industry data [[ ]] is used in the comparison PSDs that follow. These comparisons demonstrate the consistent nature of steam dryer loads between similar plants and the [[ ]] SRV resonance load used in the replacement steam dryer design for GGNS.

The GGNS load used in these comparisons is the projected load at EPU conditions used in the stress evaluation of the replacement dryer. The simulated SRV resonances at [[ ]] were applied [[ ]] in each of the [[ ]] EPU load conditions used in design. The acceptance limits included in Appendix F assure that the GGNS loads during EPU will not exceed the peak response or [[ ]] response over the [[ ]] range in these [[ ]] SRV conditions. The [[ ]] peaks have been combined in the plots to facilitate comparisons with other plants. This demonstrates how the amplitude and frequency choice compares with plants with similar valve arrangements.

3.2.5.1 Comparison with [[ ]] *Plant Data*

A similar design [[ ]] plant [[ ]] and has obtained measured MSL strain gauge data at a steam velocity equivalent to GGNS at EPU (See Appendix A for more details).

The dryer load comparison is made for [[ ]] (see Figure 3-19 through Figure 3-21). The [[ ]] loads are representative of the loads [[ ]]

The PSD plots for GGNS and the [[ ]] plant are [[ ]] frequency range. The signal content at a given frequency is typically [[ ]] when compared to GGNS.

For the [[ ]] peaks of the GGNS dryer loads, the GGNS [[ ]] amplitudes are [[ ]] This is the result of scaling the [[ ]] load based on GGNS Strouhal values. As demonstrated, this approach ensures the simulated SRV resonant load bounds the [[ ]] loads.

The [[ ]] loads include a resonance peak at approximately [[ ]] Thus, the potential effect of the [[ ]] peak will be captured during the finite element analysis (FEA) [[ ]]

3.2.5.2 Comparison with [[ ]] *Plant Data*

The [[ ]] data, PSD plots shown in Figure 3-22 and Figure 3-23, includes peak hold data based on a [[ ]] test data sample. The resolution was [[ ]] The sensor selected for the comparison was [[ ]]

[[ ]] This sensor is located at the [[ ]]

The [[ ]] reactor developed [[ ]] that peaked at [[ ]] power and [[ ]]

Figure 3-22 and Figure 3-23 compare the amplitude of the [[ ]] SRV resonance with the GGNS [[ ]] dryer loads. The GGNS loads [[ ]] It is also noted that outside the [[ ]] SRV resonance band, the [[ ]] test data is [[ ]] than GGNS EPU projections between [[ ]] This difference is attributable in part to the [[ ]] and the conservative noise floor load produced by the PBLE with MSL strain gauge input.

3.2.5.3 Comparison with [[ ]] *Plant Data*

The [[ ]] data comparison with GGNS data is shown in Figure 3-24 through Figure 3-26. The [[ ]] loads are PBLE generated using [[ ]] Figure 5-2 through Figure 5-13 provide a comparison with [[ ]] loads generated using MSL strain gauge instrumentation.

The dryer load comparison is made for [[ ]] dryer regions [[ ]] The [[ ]] loads are representative of the loads [[ ]]

In general, the [[ ]] loads have a [[ ]] content [[ ]] and a [[ ]] content. The [[ ]] and GGNS have a comparable response in the [[ ]] band. The PBLE load based on dryer data drops off after [[ ]], but the conservative noise floor load produced by the PBLE with MSL strain gauge input produces a more comparable amplitude to GGNS above [[ ]]

The [[ ]] plant developed [[ ]] Strouhal resonance at [[ ]] during EPU [[ ]]

For the [[ ]] peaks of the GGNS dryer loads, the GGNS [[ ]] loads are [[ ]] the loads shown in the [[ ]] plant data. These

plots demonstrate the conservatism of the simulated SRV resonant load in comparison with that observed on the [[ ]]

3.3 Steam Dryer Stress Analysis

3.3.1 Dryer FEA Model

A typical steam dryer has been described in Section 2.0. The components of this dryer are included in the full steam dryer FEM and are specified later in this section. The commercial finite element software ANSYS 11 is used for the analyses. This section provides a detailed description of the FEM.

The FEM for the GGNS replacement dryer is based on [[ ]] dryer (Figure 3-27). Nominal dimensions are used at all locations. The global FEM includes all the structurally significant components of the dryer. The GGNS replacement dryer FEM is shown in Figure 3-28 through Figure 3-31 and incorporates the improvements and modifications from Sections 2.2.1 and 2.2.2.

3.3.1.1 General Description

3.3.1.1.1 Elements and Major Components

The element selection follows the element description in Section 5.1.1 of Appendix E. The FEM of the steam dryer contains [[ ]] elements. Additional element types include [[ ]] The tie bars on bank top caps, which provide the structural links among vane banks, are modeled [[ ]] ANSYS [[ ]] elements are used for the support ring [[ ]]

The major dryer components are shown in Figure 3-29 through Figure 3-31. [[ ]] are discussed separately in the next paragraphs.

An overview of the element types by component, real ID and material ID is provided in Table 3-5. Table 3-6 lists the ANSYS material ID separately, along with a description of their use in the model.

For material ID 1, temperature dependent properties were obtained from the ASME Code (Reference 2). Table 3-7 correlates the elastic modulus with temperature. The chemical composition of ASTM 304L Stainless Steel is 18Cr-8Ni, which points to Material Group G of Table TM-1 of the above mentioned code (Reference 2). Poisson's Ratio is 0.3, and the density is 8.0763E-04lb_f-s^2/in^4 [[ ]] Material ID 13 is used to [[ ]]

[[ ]] The Poisson Ratio and the temperature dependency of the elasticity modulus are identical to material ID 1.

The material properties for water (material ID 17) are discussed separately in Section 3.3.1.1.5.

3.3.1.1.2 [[ ]]

The vane bundles are enclosed [[

]]

The mass of the [[

]]

The stiffness reduction of the [[

]]

3.3.1.1.3 Element Mesh Density

Mesh element sizes for various components in the FEM are provided in Table 3-8. The dryer components listed in Table 3-8 are shown in Figure 3-29 through Figure 3-31. These typical mesh sizes follow the guidelines outlined in paragraph 5.1.2 of Appendix E. A mesh convergence study demonstrated that the FEM satisfied the [[ ]] convergence criterion of Appendix E.

3.3.1.1.4 Vane Bank Modules

An overall description of the dryer vane bank is provided in Section 2 of Appendix E. The mass, stiffness and damping distributions of the numerous vanes and their appendages are modeled to

account for their inertia and stiffness effect on the dryer in the FIV analysis. [[

]] A vane bundle is a vane module without end plates. There are a total of [[ ]] vane bundles in the GGNS replacement dryer. Figure 3-35 shows the vane bundle positioning.

The modeling of each of the vane bundles is described in Section 5.1.3 of Appendix E. A detailed mesh of each Vane Bundle [[ ]] is created. The mesh consists of [[ ]]

An overview of the element types by component, real ID and material ID is provided in Table 3-9. The temperature dependent properties were obtained from Reference 2. Table 3-7 correlates the elastic modulus with temperature. The chemical composition of AISI 304L Stainless Steel is 18Cr-8Ni, which points to Material Group G of Table TM-1 of the above mentioned code. Poisson's Ratio is 0.3. [[

]] Table 3-10 provides an overview of the density used for each of the vane bundles.

The detailed vane bundle modeling is used [[

]] input to the global model.

The master DOFs are defined at those locations where, per hardware design, certain vane bundle nodes in a super-element are interfacing with corresponding nodes of other dryer components in the global model.

In addition, [[ ]] are defined in the vane bundle models to properly capture the internal bundle dynamics consistent with the prototype dryer benchmark. Figure 3-36 shows the [[ ]] FEM of a vane bundle illustrating at the same time the interface points and master DOFs.

3.3.1.1.5 Water Coupling and Water Properties

The skirt of the dryer is partially submerged in water, which is modeled [[

]] to account for the fluid (i.e., water) structure interaction. Water volume is

modeled to represent the thermodynamic properties of the steam water mixture that exists in the annular region between the dryer skirt and the RPV wall as well as the skirt and steam separators.

ANSYS [[ ]] fluid elements are used to model the water as described in Section 5.1.4 of Appendix E. The water levels inside and outside were determined by a dryer performance calculation. [[

]] The displacement boundary conditions are applied to represent the solid boundary of either the reactor vessel wall or steam separator.

The water surrounding the skirt and drain channels contains a large number of steam bubbles rising from the reactor core and steam separators. The properties of the two-phase mixture, "bubbly water," are calculated using equations 5.1-1 and 5.1-2 in Section 5.1.4 of Appendix E. The bulk modulus and density are [[ ]]

3.3.1.1.6 Damping

For the flow-induced vibration of steam dryers, GE Hitachi (GEH) applies the ANSYS [[

]] (See Section 6.1.1 of Appendix E.)

Based on Equation 6.1-2 of Appendix E, the damping ratio, i.e., the ratio of the damping constant over critical damping constant, varies [[

]]

[[

]] In the time domain transient dynamic analysis with ANSYS, [[

]]

Figure 3-37 represents the [[ ]] damping curves for [[ ]] for the global model.

3.3.1.2 Comparison of GGNS Modeling with Benchmarked Model

As discussed above, the FEM structural modeling approach for the GGNS replacement dryer follows the methodology outlined in Appendix E, [[
]]

The [[ ]] model reflects the GGNS replacement dryer [[
]] The dynamic response corresponds well with published data for "Elastic Constants for Bending of Thin Perforated Plates with Triangular and Square Penetration Pattern" by O'Donnell. (See Reference 3.)

3.3.2 FIV Analysis

This section describes the process used to perform the FIV structural analysis. The commercial finite element software ANSYS is used in the solution. For the flow-induced vibration of steam dryers, GEH incorporates [[
]]

3.3.2.1 Vibration Analysis Approach

The structural responses of the GGNS replacement steam dryer components to the FIV loads are calculated [[ ]] (Section 6.1.2 of Appendix E). The acoustic load definition is [[

]]

Displacement boundary conditions are applied to the lug support locations in the dryer model. Displacement boundary conditions are also used to contain the fluid. The support ring rests on [[ ]] steam dryer support brackets that are welded attachments to the RPV wall. [[
]] The motion of the steam dryer in the circumferential direction is constrained [[

]] Motion in the vertical direction is constrained by the dryer dead weight.

3.3.2.2 Structural Uncertainty, Maximum Stresses and Weld Factors

3.3.2.2.1 Uncertainty in Structural Modes

There is an uncertainty in the predicted structural mode frequencies and dynamic response of steam dryers because of the approximations in the structural model and variations in the as-built dryer as compared to the nominal design dimensions (Section 6.1.2 of Appendix E).

The structural model's modal uncertainty is addressed [[
]] This is accomplished by [[

]] In addition to the nominal load case, [[ ]] cases are [[ ]]

3.3.2.2.2 Maximum Stresses

The results of the dynamic stress analysis consist of time histories of the structural response of all the elements in the FEM [[ ]] In the post-processing of the analysis results, the stresses [[ ]] are searched to determine the maximum stress intensities for the dryer components (Table 3-11 and Table 3-12 [[
]] [[ ]] In the global dryer FEM, the components of the dryer model are defined and grouped based on their common design features and relative loading. The resulting FIV stress table contains the maximum stress intensities [[ ]] for each dryer component.

3.3.2.2.3 Weld Factors

Weld Factors

A key component of the fatigue alternating stress calculation at a specific location is the appropriate value of the stress concentration factor (SCF). The weld types of relevance for the steam dryer stress analysis are the [[
]] (Section 4.2 of Appendix E). Because the use of a weld quality factor is for static rather than for fatigue applications, the peak stress is based on the calculated

[[ ]] Figure 4.2-1 of Appendix E shows the flow diagram for the calculation of fatigue stress with appropriate SCFs.

For the case of NG-3352 Type I and III full penetration welded joints, the recommended SCF value is 1.4. In this case, the finite element stress is directly multiplied by the appropriate SCF to determine the fatigue stress. Although the recommended 'f' factor for Type I and III welds in the NG table is 1.0, a SCF of 1.4 is recommended [[
]]

The weld factor value [[ ]] can be derived [[

]]

multiplier to obtain the fatigue stress.

In addition to full penetration welds and fillet welds, partial penetration groove welds also exist in the Grand Gulf replacement steam dryer as allowed by the ASME Section III Subsection NG-352. A partial penetration groove weld is expected to have root discontinuities similar to those in fillet welds.

]]

Weld Quality Factor

[[

]]

3.3.2.3 Weld Scoping and Initial Fatigue Assessment

3.3.2.3.1 Weld Scoping

[[

]] Stress concentrations due to welds are handled [[

]]

[[ ]] such that the actual weld geometries are fully captured. In addition to the primary scoping that was described in Section 3.3.2.2.2; the weld lines are scoped to determine the maximum stress intensities at each weld line. [[

]] To obtain the weld peak stress intensities, the [[

]] The maximum weld stress intensity is then determined for each component that is associated with welds (Table 3-13 and Table 3-14 [[

]]

3.3.2.3.2 Initial Fatigue Assessment

In performing the fatigue evaluation for steam dryers under FIV loading, the maximum stress intensity in each dryer component from both the primary scoping and the weld scoping is determined from the FIV stress analyses. As described in Section 3.3.2.3.1 the maximum stress intensities are adjusted as necessary by the appropriate weld SCF defined in the design criteria. [[

]] Table 3-15 and Table 3-16 are for [[ ]] nominal cases, and are provided here as a sample scoping output. These results are tabulated for the nominal and all other load cases.

3.3.2.4 Dryer Components Requiring Further Post Processing

Several dryer components included more refined stress processing to more accurately reflect the stress in these locations. The affected components include the [[

]]

3.3.2.4.1 [[ ]]

[[

]]

[[

]]

3.3.2.4.2 [[ ]]

[[

]]

[[

]]

3.3.2.4.3 [[ ]]

[[

]]

3.3.2.4.4 [[ ]]

[[

]]

[[

]]

3.3.2.4.5 [[ ]]

[[

]]

**3.3.2.4.6 [[
]]**

[[

]]

3.3.3 ASME Loads

The GGNS replacement steam dryer was analyzed for the primary structural stress assessment under ASME load combinations for normal, upset, emergency and faulted operation conditions at EPU power level. The ASME load combinations are shown in Table 3-23, and each individual load is calculated and specified in this section.

3.3.3.1 Steady State, Upset Transient, Emergency and Faulted Condition Pressure Loads

The pressure differentials across the steam dryer are calculated for four categories of events: normal, upset, emergency and faulted conditions. Normal conditions are the steady-state operating conditions. Upset conditions are the anticipated transient events. Emergency conditions are within the reactor internals design basis and are defined by the rapid vessel depressurization via operation of the automatic depressurization system relief valves. Faulted conditions are the design basis accident events (e.g., main steam line break). The loads have been developed for the original GGNS steam dryer at EPU conditions. These loads were confirmed to remain bounding for the replacement steam dryer [[

]]

3.3.3.1.1 Normal and Upset ΔP_N & ΔP_U

The normal and upset differential pressure loads are determined based on the methods defined in Appendix A, Section 9.3.1.3. The differential pressure loads are based on EPU conditions for GGNS and account for the higher steam flows at EPU conditions.

Table 3-24 shows the differential 'static' pressure load (ΔP_N) for the dryer outer hood. The static pressure is divided into two general regions: an outer hood region that includes the higher pressure drop of the nozzle region and the balance of the dryer. Figure 3-49 presents the pressure load applied on the dryer components.

As discussed in Section 9.3.1.3 of Appendix A, ΔP_U, the pressure differential load for the steam dryer for upset operation is determined [[

]]

3.3.3.1.2 Differential Pressure Load During Emergency and Faulted Conditions

For emergency and faulted conditions, the pressure differentials across the steam dryer components are calculated [[ ]] as discussed in Section 9.3.2.5 of Appendix A.

The limiting event for the emergency condition is [[ ]] For EPU conditions, the differential pressure load during emergency operation (ΔP_E) is [[ ]]

For the faulted condition, the limiting event is [[ ]] analyzed [[ ]] as described in Section 9.3.2.5 of Appendix A. For EPU conditions, the differential pressure load for these two conditions is [[ ]]

3.3.3.2 Main Steam Line Break Event Acoustic Loads [[ ]]

The methodology for determining the acoustic loads on the steam dryer hoods during a main steam line break (MSLB) event is described in Section 9.3.2.6 of Appendix A. [[ ]] The acoustic load is calculated at [[ ]] reactor operating conditions defined by the load combination table.

The peak normalized acoustic load distribution ($\Delta P/\Delta P_{Vessel}$) for the [[ ]] operating conditions is provided in Table 3-25. The multiplier P_0 is determined [[ ]] based on EPU conditions. The maximum acoustic loads [[ ]] on the steam dryer hood due to the MSLB are obtained [[ ]] The components in the dryer FEM for these acoustic pressure loads [[ ]] are shown in Figure 3-50.

3.3.3.3 Turbine Stop Valve (TSV) Closure Event Loads [[ ]]

The TSV closure event produces [[ ]] loads on the steam dryer. [[ ]] The methodology for determining these loads is similar to the methodology for determining the acoustic loads due to the MSLB and is described in Section 9.3.2.2 of Appendix A.

The peak normalized load distribution is shown in Table 3-26. For EPU conditions, [[ ]] The maximum load on the steam dryer hood is

obtained [[

]] pressure loads are shown in Figure 3-51 and Figure 3-52.

3.3.3.4 Seismic Loads

Seismic events transmit loads to the dryer through the vessel support brackets. Horizontal loads due to a seismic event are applied [[ ]] as shown in Figure 3-53. Vertical seismic loads are applied [[ ]] as shown in Figure 3-54. Safe shutdown earthquake (SSE) and operating basis earthquake (OBE) loads for spectral analysis are shown in Figure 3-55 through Figure 3-58. Structural damping [[ ]] is applied to the response spectra.

3.3.3.5 SRV Load

The SRV containment discharge loads are transmitted to the dryer through the vessel support brackets. The horizontal SRV discharge loads are applied [[
]] The vertical SRV discharge loads are applied [[
]] SRV discharge loads for the spectral analysis are selected [[

]] as shown in Figure 3-59 through Figure 3-61.
The applied structural damping is [[ ]]

3.3.3.6 Zero Period Acceleration (ZPA)

The static structure analyses were performed using ZPA accelerations for seismic loads and SRV discharge loads when frequency exceeds the ZPA frequency. The zero period accelerations applied in the ASME structural analysis are listed in Table 3-27.

3.3.3.7 Metal and Water Weight Load (DW)

The stresses caused by metal and water weight are obtained by applying G loading to the GGNS replacement dryer FEM.

3.3.3.8 FIV Stresses

The FIV analysis for GGNS replacement dryer during normal operation was performed and documented in Section 3.3.2. Because the ASME Code load combinations stress analysis is the primary structural assessment, [[ ]] The maximum

primary bending stresses and maximum primary membrane stresses will be adjusted using the methodology defined in Section 8 of Appendix A to account for biases and uncertainties. These will be applied [[ ]] for the ASME load combinations.

FIV loads for the steam dryer for upset operation (FIVU) are determined [[ ]]

3.3.4 Acceptance Criteria

The steam dryer, including the dryer units, is a non-safety related item and is classified as an Internal Structure as defined in Reference 2, Subsection NG, Paragraph NG-1122. The steam dryer is not an ASME Code component, but the structural evaluation methodology uses the Code as a design guide with the exception [[ ]] as discussed in Subsections 3.3.4.3 and 3.3.4.4.

3.3.4.1 Material Properties

The ASME Code material properties for 304L are listed in Table 3-28.

3.3.4.2 ASME Code Stress Limits for Load Combinations

The ASME Code, Subsection NG stress limits for the steam dryer analysis are listed in Table 3-29. Stress limits for Service Levels A, B and C are according to NG-3220 and for Service Level D are per ASME Code Section III Appendix F Paragraph F-1331 for Level D. Upset condition stress limits are increased by [[ ]] above the limits shown in this table per NG-3223 (a).

3.3.4.3 Static Evaluation

The limits outlined in Section 3.3.4.2 above are used for static analysis except when evaluating welds [[ ]] in lieu of ASME Code Table NG-3352-1, as explained in Section 3.3.4.3.1 below.

3.3.4.3.1 Weld Quality Factor

ASME Boiler and Pressure Vessel Code Subsection NG weld quality factors are used to evaluate the steam dryer, which is not a core support structure.

Samples of the original production welds have been taken as part of the root cause evaluations for the steam dryer failures that occurred at EPU conditions. Metallurgical evaluations of those samples showed [[

]]

To assure high quality welds, new or replacement steam dryer fabrication employs weld processes that have been fully qualified. [[

]], robust weld process qualifications are conducted to prevent weld defects from occurring during fabrication. Representative weld samples using the same joint design and material types as specified for the new or replacement steam dryer are destructively tested. Metallurgical evaluations demonstrating an acceptable weld root are required prior to weld procedure approval. These tests demonstrate that no defects are present at the root of production welds.

Therefore, [[ ]], as well as qualified weld processes [[ ]], are used [[ ]] for new dryer analyses.

3.3.4.4 Fatigue Evaluation

Steam dryers are subjected to cyclic acoustic pressures that cause flow-induced vibration during normal operation. They may experience on the order of [[ ]] stress cycles during a steam dryer's typical [[ ]] year life. Therefore, HCF constitutes a major structural acceptance criterion for the steam dryer. The steam dryer FIV fatigue evaluation described in this section is consistent with the ASME Boiler and Pressure Vessel (B&PV) Code Section III requirements. Other cyclic loads [[ ]], have not been significant contributors to fatigue damage and [[ ]] are considered to add minimal fatigue usage.

The steam dryer structural analyses are performed assuming that the dryer will be operated for [[ ]] years. The stresses are expected to be well within the elastic range when the dryer is subjected to FIV loading during normal operation. Therefore, the HCF life is the major design consideration. The fatigue stress limit is lower than the material yield stress. Steam dryer components are subjected to cyclic acoustic pressure in normal operation where HCF constitutes

the controlling structural acceptance criterion for steam dryers. Determination of the fatigue stress limit used in the FIV structural analysis is consistent with ASME B&PV Code Section III.

In performing the fatigue evaluation for steam dryers under FIV loading, the maximum stress intensity in each dryer component is found from the FIV stress analyses described in Section 3.3.2. The maximum stress intensities are then adjusted as necessary by the appropriate weld SCFs defined in Section 3.3.2.2.3. In support of a plant power uprate, the adjusted stress intensities are [[ ]] described in Section 3.2.4. Finally, the analysis biases and uncertainties described in Section 3.4 are incorporated into the results.

The design fatigue curves and curve selection criteria for Austenitic Ni-Cr stainless steel are given in the ASME code Section III, Division 1, Appendix I, Figure I-9.2.2 and Figure I-9.2.3. The ASME stress-cycle, or S-N curves plot the alternating stress intensity versus number of cycles. Alternating stress limit is dependent on mean stress. The selection criteria provided for the ASME S-N curves are based on the sum of local membrane, bending and secondary stresses on the dryer components evaluated. The summed stress includes mean stress. Curve C is the most conservative of the three curves in Figure I-9.2.2 [[ ]] Curve C also includes margin to address the residual stress from fabrication. The fatigue stress limit for the steam dryer is chosen to be the alternating stress intensity limit at [[ ]] cycles. The fatigue stress limit of Curve C at [[ ]] cycles is [[ ]]

The requirement for acceptance of a steam dryer component is that its maximum stress intensity has to be less than the fatigue limit. The MASRs are calculated and reported for each of the steam dryer components. The MASR is defined as follows.

$$MASR = \frac{Fatigue.Stress.Limit}{Maximum.Service.Stress} \quad (3\text{-}5)$$

A minimum alternating stress ratio less than 1.0 indicates the stress in the steam dryer component has exceeded its fatigue limit. For this evaluation, a MASR of 2.0 is specified as the acceptance criteria (Reference 4).

3.4 End to End Bias and Uncertainty

This section identifies the various biases and uncertainties that are applied for the evaluation of the GGNS replacement steam dryer. Section 8 of Appendix A provides a detailed description of

the methodology for applying the bias and uncertainty values that were applied for GGNS. This section summarizes the GGNS plant-specific inputs. These include:

1. Strain to Pressure Uncertainty (Bias addressed in Strain to Pressure conversion)
2. EPU Bias (for stress adjustment to EPU conditions)
3. CLTP Bias and Uncertainty (for adjustment of "Strouhal Adders" to observed CLTP amplitude)
4. PBLE Load Projection, [[ ]], Bias and Uncertainty
5. PBLE Load Projection, [[ ]], Bias and Uncertainty
6. GGNS Acoustic Mesh and Model Bias and Uncertainty
7. FEM Bias and Uncertainty
8. CLTP Time Interval Selection Bias

Table 3-1. GGNS-[[ ]] Plant SRV Dimension Comparison

	Standpipe Diameter (in.)	Standpipe Height (in.)
GGNS	[[	
[[ ]] Plant		]]

Table 3-2. Predicted and Measured Resonant Frequencies

	[[						
						]]	

Table 3-3. Filtered Frequencies

Center Frequency, (Hz)	**Full Width at [[ ]] Attenuation, (Hz)**	**Probable Source**	[[ ]]
[[			
			]]

Table 3-4. GGNS PBLE RPV Acoustic FEM Parameter Inputs

Parameter	Value
[[	
	]]

Table 3-5. Overview of Element Type by Component

[[

]]

Table 3-6. Material Definitions

Material ID	Description
[[	
	]]

Table 3-7. Temperature Dependent Modulus of Elasticity Used for 304L SS

Temperature, °F	Modulus, MSI
-100	29.1
70	28.3
200	27.6
300	27.0
400	26.5
500	25.8
600	25.3
700	24.8
800	24.1

Table 3-8. Component Element Mesh Sizes

Component	Approximate Element Size (inch)
Base Plate	[[
Top Cap	
Closure Plates	
End Plates	
Divider Plates	
Inner Hoods	
Outer Hoods	
Hood Supports	
Skirt	
Drain Channels	
Lower Ring	]]

Table 3-9. Overview of Vane Bank Element Type by Component and Real

[[

]]

Table 3-10. [[ ]] Material Densities After Adjustment

[[

]]

Table 3-11. Primary Stress Scoping for Nominal [[ ]] Case

[[

]]

Table 3-12. Primary Stress Scoping for Nominal [[ ]] Case

[[

]]

Table 3-13. Weld Scoping for Nominal [[ ]] Case

[[

]]

Table 3-14. Weld Scoping for Nominal [[ ]] Case

[[

]]

Table 3-15. Maximum Stress from Primary and Weld Scoping for Nominal [[ ]] Case

[[

]]

Table 3-16. Maximum Stress from Primary and Weld Scoping for Nominal [[ ]] Case

[[

]]

Table 3-17. [[ ]]

[[			
			]]

Table 3-18. [[ ]]

	[[		
			]]

Table 3-19. [[ ]]

	[[		
			]]

Table 3-20. [[ ]]

	[[		
			]]

Table 3-21. [[ ]]

	[[		
			]]

Table 3-22. [[ ]]

[[

		]]

Table 3-23. GGNS Replacement Dryer Load Combinations

Comb. No	Level	Combination
A-1	Normal	[[
B-1	Upset	
B-2	Upset	
B-3	Upset	
B-4	Upset	
B-5	Upset	
C-1	Emergency	
D-1	Faulted	
D-2	Faulted	
D-3	Faulted	
D-4	Faulted	
D-5	Faulted	]]

Note: For the D-2 case the load combination used in the analysis is [[
]] *which is conservative compared to the definition in the load combination as shown in Table 3-23.*

Definition of Load Acronyms:

[[

]]

[[

]]

Table 3-24. Differential "Static" Pressure Load for Dryer Outer Hood

Outer Hood Location	ΔP_N (psid)
[[	
	]]

Table 3-25. Peak Normalized Acoustic Loads for [[ ]]

y, Edge of Vertical Cover Plate (ft)	Normalized Pressure Differential								
[[									
									]]

Note: x = 0 at edge of dryer face nearest steam line with break, y = 0 at lower horizontal cover plate.

Table 3-26. Peak Normalized Acoustic Loads for [[ ]] Event [[ ]]

y, Edge of Vertical Cover Plate (ft)	Normalized Pressure Differential				
[[					
					]]

Note: x = 0 at edge of dryer face nearest steam line with break, y = 0 at lower horizontal cover plate.

Table 3-27. Zero Period Acceleration

	ZPA (inch/s^2)
SSE HOR	170.8
OBE HOR	93.7
SSE VT	52.5
OBE VT	27.7

	ZPA (inch/s^2)
SRV HOR NS	44.3
SRV HOR EW	34.7
SRV VT	62.8

Table 3-28. Material Properties

Steam Dryer Material SA240 Type 304L	Installation Temp	Operating Temp		
	[[			
Sm, Stress intensity limit, ksi				
Sy, Yield strength, ksi				
Su, Tensile strength, ksi				]]

Table 3-29. ASME Code Stress Limits

			Stress Value (ksi) at Temperature	
Service Level	**Stress Category**	**Stress Limit**	[[	
Design	P_m	S_m		
	P_m+P_b	$1.5S_m$		
Service Levels A & B	P_m	S_m		
	$Pm+P_b$	$1.5S_m$		
Service Level C	P_m	$1.5\ S_m$		
	P_m+P_b	$2.25\ S_m$		
Service Level D	P_m	Min ($0.7S_u$ or $2.4S_m$)		
	P_m or $P_L + P_b$	Min 1.5 ($0.7S_u$ or $2.4S_m$)		]]

Note: Upset condition service level limits are increased by 10% above the limits shown in this table per NG-3223(a).

Legend:

P_m: General primary membrane stress intensity

P_L: Local primary membrane stress intensity

P_b: Primary bending stress intensity

S_m: Design Stress Intensity

S_u: Ultimate tensile strength

[[

]]

Figure 3-1. Evaluation Process Overview

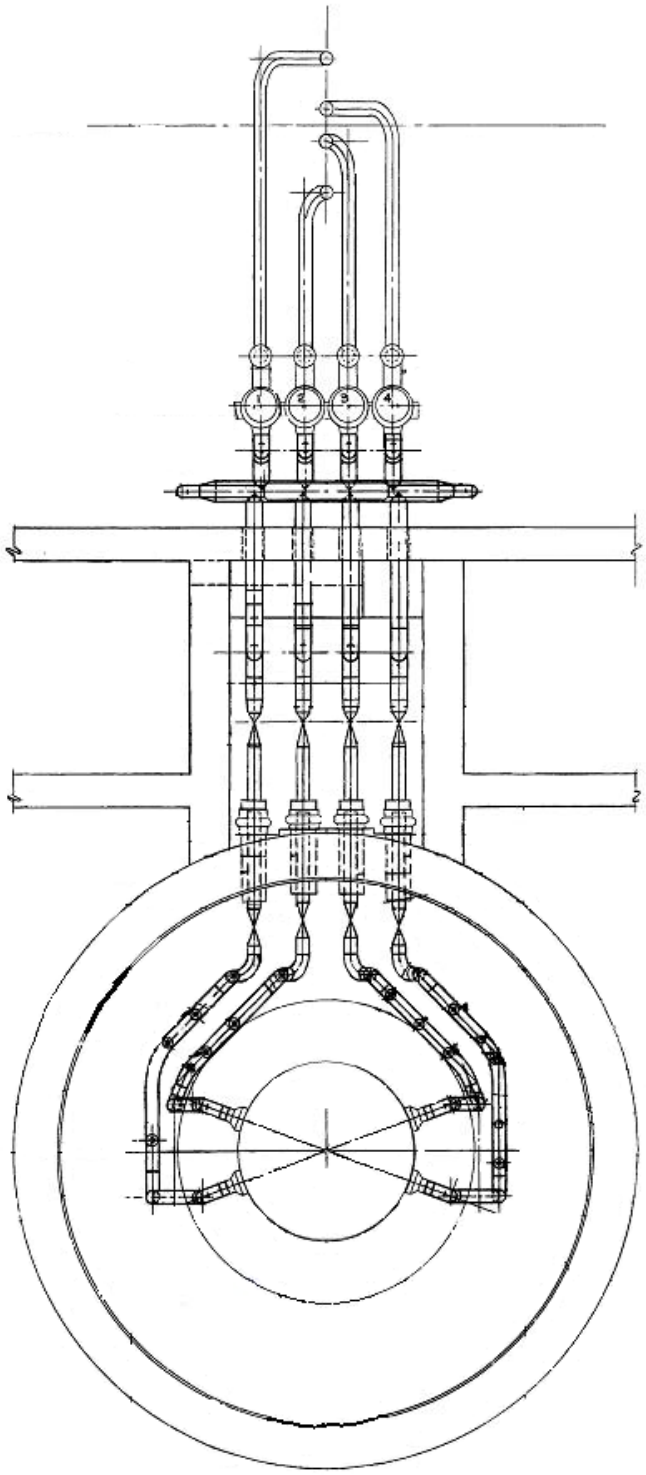

Figure 3-2. Typical MSL Layout Between RPV and Turbine (Plan View)

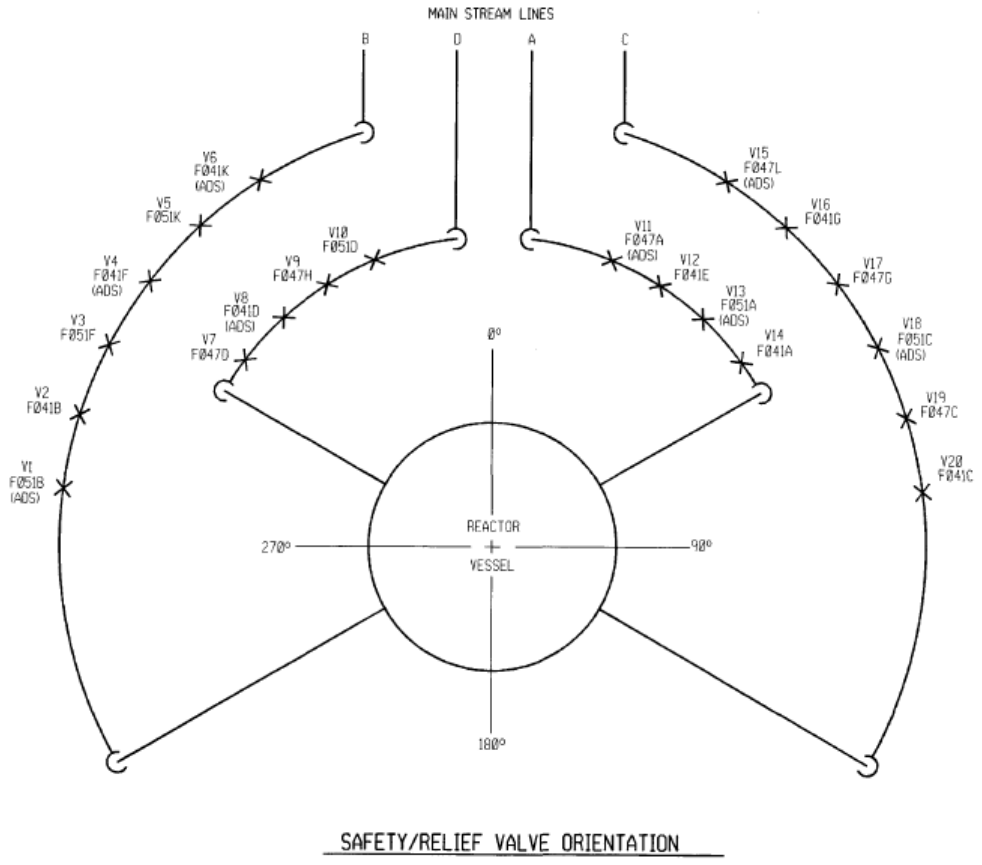

Figure 3-3. SRV Layout

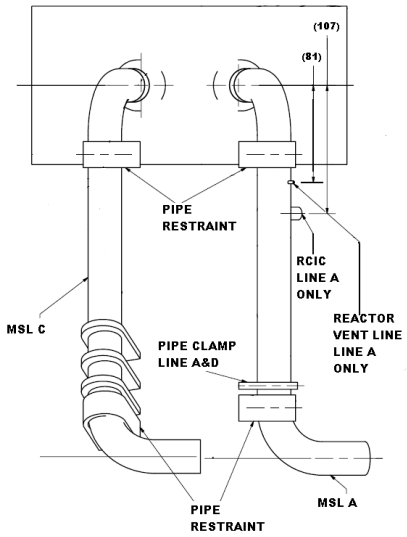

Figure 3-4. Branch Line Layout

[[

]]

Figure 3-5. Single Valve FEM Model

[[

]]

Figure 3-6. Results of [[ ]] Valve Model

[[

]]

Figure 3-7. Results of [[ ]] Valve Model

[[

]]

Figure 3-8. Waterfall from GGNS MSL Strain Gauge Measurements

[[

]]

Figure 3-9. Waterfall from [[ ]] Plant MSL Strain Gauge Measurements

[[

]]

Figure 3-10. Shear Wave Analysis-Observed and Predicted Resonances

[[

]]

Figure 3-11. Example Singularity Factor Plot Showing Installed Sensor Comparison Results
[[ ]]

[[

]]

Figure 3-12. [[ ]]

[[

]]

Figure 3-13. [[ ]] Strain Gauge Signal Filtering

[[

]]

Figure 3-14. [[ ]] Strain Gauge Signal Filtering [[ ]]

[[

]]

Figure 3-15. [[ ]] Strain Gauge Signal Filtering

[[

]]

Figure 3-16. CLTP Loads, Projected EPU Loads and EPU SRV Design Loads, [[
]]

[[

]]

Figure 3-17. CLTP Loads, Projected EPU Loads and EPU SRV Design Loads, [[ ]]

[[

]]

Figure 3-18. CLTP Loads, Projected EPU Loads and EPU SRV Design Loads, [[ ]]

[[

]]

Figure 3-19. Comparison of Grand Gulf PSDs to [[ ]] Plant Data – [[ ]]

[[

]]

Figure 3-20. Comparison of Grand Gulf PSDs to [[ ]] Plant Data – [[ ]]

[[

]]

Figure 3-21. Comparison of Grand Gulf PSDs to [[ ]] Plant Data – [[ ]]

[[

]]

Figure 3-22. Comparison of Grand Gulf PSD with [[ ]] Test Data – [[ ]]

[[

]]

Figure 3-23. Comparison of Grand Gulf PSD with [[ ]] Test Data – [[ ]]

[[

]]

Figure 3-24. Comparison of Grand Gulf PSD to [[ ]] Plant Data – [[ ]]

[[

]]

Figure 3-25. Comparison of Grand Gulf PSD to [[ ]] Plant Data – [[ ]]

[[

]]

Figure 3-26. Comparison of Grand Gulf PSD to [[ ]] Plant Data – [[ ]]

[[

]]

Figure 3-27. [[ ]] FEM

[[

]]

Figure 3-28. GGNS Replacement Dryer FEM

[[

]]

Figure 3-29. Nomenclature for Major Components

[[

]]

Figure 3-30. Nomenclature for Major Components

[[

]]

Figure 3-31. Nomenclature for Major Components

[[

]]

Figure 3-32. [[ ]]

[[

]]

Figure 3-33. [[ ]]

[[

]]

Figure 3-34. [[ ]] Model Used In The Dynamic Analysis Study: [[ ]] (Reference Case)

[[

]]

Figure 3-35. Top View of Dryer Showing the Vane Bundles

[[

]]

Figure 3-36. Vane Bundle FEM and Master DOFs

[[

]]

Figure 3-37. [[ ]]

[[

]]

Figure 3-38. Area of the Replacement Steam Dryer Submodeled

[[

]]

Figure 3-39. Components In and Near the Submodel Region

[[

]]

Figure 3-40. Cut Boundary Conditions Applied to the Submodel

[[

]]

Figure 3-41. Nominal Maximum Stress Time Point Unmodified Geometry

[[

]]

Figure 3-42. [[ ]] for the Bank End Plate

[[

]]

Figure 3-43. Stress Distribution After Geometry Modification

[[

]]

Figure 3-44. Inner Hood Tee Weld Line Stress [[ ]]

[[

]]

Figure 3-45. [[ ]]

[[

]]

Figure 3-46. Illustration Of The [[ ]]

[[

]]

Figure 3-47. Tie Rod to Bank End Plate Connection Geometry

[[

]]

Figure 3-48. Tie Bar Actual Geometry

[[

]]

Figure 3-49. Differential “Static” Pressure Loads for Dryer Components

[[

]]

Figure 3-50. Components for MSLB Acoustic Pressure Loads

[[

]]

Figure 3-51. Components in Dryer FE Model for [[ ]] Pressure Load

[[

]]

Figure 3-52. Components in Dryer FE Model for [[ ]] Pressure Load

[[

]]

Figure 3-53. Horizontal Seismic Model

[[

]]

Figure 3-54. Vertical Seismic Model

[[

]]

Figure 3-55. Horizontal SSE Seismic Spectra

[[

]]

Figure 3-56. Vertical SSE Seismic Spectra

[[

]]

Figure 3-57. Horizontal OBE Seismic Spectra

[[

]]

Figure 3-58. Vertical OBE Seismic Spectra

[[

]]

Figure 3-59. Horizontal SRV North-South Spectra

[[

]]

Figure 3-60. Horizontal SRV East-West Spectra

[[

]]

Figure 3-61. Vertical SRV Spectra (Vertical)

4.0 RESULTS

4.1 FIV Final Stress Table with Bias and Uncertainty

The FIV analysis of Section 3.3.2 generated peak stress intensities based on scoping analyses. [[

]] Following the methodology outlined in Section 8 of Appendix A, final peak stresses were determined accounting for bias and uncertainty. These peak stresses are selected from the [[ ]] load cases representing the [[ ]] cases as well as the nominal load case. Also, [[ ]] methods were used to evaluate the bias and uncertainty, and the peak stress [[ ]] was selected for each component [[ ]] The final peak stresses were then compared to the design limit, and the minimum alternating stress ratio was determined. These results are shown in Table 4-1. As specified in Reference 4, a minimum alternating stress ratio of 2.0 is required to demonstrate adequate margins. From Table 4-1, it is demonstrated that for all dryer components, using a load definition scaled to EPU conditions including the potential effects of SRV resonances, the minimum alternative stress ratio for all components is greater than 2.0. Therefore, these analyses demonstrate the acceptability of the GGNS replacement steam dryer design at EPU operating conditions.

Two additional tables of peak stresses are provided for the bending plus membrane stress intensity (Table 4-2) and membrane stress intensity (Table 4-3), as input to the ASME load combination analysis. These stresses also include the applicable bias and uncertainties defined in Section 8 of Appendix A.

4.2 ASME Code Load Case Stress Results

The GGNS replacement steam dryer was analyzed for the ASME Code load combinations (primary stresses) using the FEM as described in Section 3.3.1. The results of these analyses are used to assess dryer component primary stresses versus ASME design criteria as described in Section 3.3.4.2 for a [[ ]] load combinations described in Section 3.3.3 under normal, upset, emergency and faulted operation conditions at EPU power level. The summary of the results is presented in Table 4-4. The acceptance criteria used for these evaluations are the same as those used for safety-related components. The results indicate that the stresses for all structural components are below the ASME Code allowable limits at EPU operating conditions. The ASME load combination results demonstrate the acceptability of the GGNS replacement steam dryer design at EPU operating condition.

Table 4-1. Final Stress Intensity Table with Bias and Uncertainty

Dryer Component	CLTP Maximum Stress Intensity (psi)	EPU Maximum Stress Intensity (psi)					Max Stress Intensity (psi)	MASR
		[[				]]		
[[								
								]]

Table 4-2. FIV Bending Plus Membrane Stress Intensity with Bias and Uncertainty

[[										]]

* The maximum stress location is not on the welds, so primary stress intensity is the same as the peak stress intensity in Table 4-1.
** The component requires further post processing to refine the primary stress intensity prediction. The peak stress intensity in Table 4-1 is conservatively applied.

Table 4-3. FIV Membrane Stress Intensity with Bias and Uncertainty

[[										
										]]

Table 4-4. EPU ASME Results for Normal, Upset, Emergency and Faulted Conditions

[[

]]

5.0 NON-PROTOTYPE JUSTIFICATION

The GGNS replacement steam dryer design is based on the valid BWR/4 prototype replacement steam dryer and meets the non-prototype classification in accordance with Reference 1 as outlined by Regulatory Position 1. Replacement steam dryers have been installed at the two unit Susquehanna Steam Electric Station with on-dryer instrumentation included at Unit 1. The Unit 1 replacement steam dryer is designated as the BWR/4 prototype. The following sections contain information related to current operating experience with the BWR/4 prototype steam dryer, the similarities between the BWR/4 prototype design and proposed GGNS replacement steam dryer, and side-by-side comparison of the following areas: [[

]]

5.1 BWR/4 Prototype Test and Operating Experience

The replacement Susquehanna Steam Electric Station Unit 1 (SSES-1 or SSES) steam dryer was installed in March 2008 during Refueling Inspection Outage #15 (RIO-15). The Unit 1 replacement steam dryer assembly was operated until March 2010. During the March 2010 SSES-1 RIO-16 outage, the steam dryer was removed from the reactor vessel to the equipment pool where the following work was performed.

1. Vibration instrumentation was removed.
2. Planned comprehensive visual inspections were performed.
3. The lifting rod lugs, which had rotated during operation, were repaired.

The qualified Level 3 inspector, responsible for the March 2010 Unit 1 dryer inspections, documented the [[ ]] interior weld inspections and [[ ]] exterior inspections completed. There were a total of five deviation reports prepared. Four of these reports involved lifting lug set screw tack weld cracks and associated loose lifting lugs. One deviation report involved [[

]]

The corrective actions from these findings have resulted in the following changes that have been implemented for the GGNS replacement steam dryer:

- Revised fabrication procedures [[
]] and
- [[
]]
- Eliminated the use of tack welds.

5.2 GGNS Dryer Geometry Comparison With BWR/4 Prototype

Table 5-1 is a comparison of important plant parameters and dryer geometry. This comparison directly supports the non-prototype discussion by showing how similar the prototype dryer is compared to the design basis of the GGNS replacement dryer.

5.3 Plant Geometry and Operating Condition Comparison

The evolutionary design of the BWR plant has resulted in similar reactor vessel, steam dryer and MSL geometrical configurations, as well as similar plant operating conditions. As a result, the range of plant-to-plant variations that affect the steam dryer pressure loading is small. A consequence of this relatively small envelope of dryer conditions is that the prototype dryer experience can be applied to the GGNS replacement dryer. Section 5.2 provided a comparison of the GGNS replacement dryer design with the prototype dryer. Table 5-2 provides a comparison of the GGNS reactor-operating conditions compared to those for the prototype plant. This comparison is a side-by-side comparison of the operating conditions that are significant with respect to the fluctuating pressure loads that act on the steam dryer. Table 5-3 provides a comparison of the reactor vessel and MSL configuration for GGNS and the prototype plant.

With respect to fluctuating pressure loads on the dryer, reactor power is significant only in that it determines the steam flow rate through the system. The higher GGNS power level results in higher steam mass flow through the dryer compared to the prototype. The flow velocities are relatively low and the difference in turbulent loading is not significant. The steam flow velocity in the MSLs governs the pressure loads on the dryer. The GGNS MSLs are a larger diameter than the prototype plant to accommodate the higher steam output from the plant. The resulting flow velocities in GGNS and the prototype plant are essentially the same. Therefore, the fluctuating pressure loads acting on the dryer are also similar. Differences in the pressure loading arise due to the effects of plant-specific features, [[ ]] [[ ]] The effect that these differences may have on the dryer pressure loading is discussed in Section 5.5.

The geometric parameters may have an effect on the acoustic mode shapes within the vessel. The vessel and steam dome volumes are similar between the two plants. Therefore, differences in acoustic mode response are minimal as exhibited by the comparison of the acoustic model impedance of the MSL steam nozzle shown in Figure 5-1. The expected minor differences in acoustic properties are discussed in Section 5.4. The differences in the MSL geometry [[ ]] may affect the frequency content of the plant-specific pressure loads. The effect of these differences on the dryer pressure loading is described in Section 5.5.

The GGNS-specific load definition based on MSL measurements (Section 3.2) and the plant-specific FIV fatigue analysis (Section 3.3) address differences in plant geometry and operating conditions between GGNS and the prototype plant.

5.4 RPV Acoustic Property Comparison

Appendices B and C describe the important acoustic properties in the vessel and steam dome. The purpose of this section is to compare these acoustic properties between the BWR/4 prototype and GGNS.

RPV acoustic properties are listed in Table 5-4, which illustrates the similarities in these parameters between GGNS and the BWR/4 prototype. A sensitivity assessment is performed [[ ]] (Appendix C). The objective of the assessment is to confirm that the acoustic parameters are within the established range of application, so that bias and uncertainty values determined from the benchmarked plant can be applied. These PBLE input parameters are within the range of input parameters treated in the sensitivity assessment in Appendix C. The acoustic model is consistent with the benchmark assumptions.

Examining Table 5-4, the dome pressure determines vessel saturated steam properties and is provided, [[

]]

As described in Section 5.3, the GGNS and BWR/4 prototype steam dome and dryer geometries are very similar. Also, the operating conditions described in Section 5.3 are comparable. Because the acoustic properties, geometries and operating conditions are comparable, the vessel acoustic FRFs will be similar between the two plants as exhibited by Figure 5-1. Differences

between the BWR/4 prototype and GGNS are addressed by the GGNS-specific vessel acoustic model and the PBLE load definition.

5.5 Plant FIV Load Comparison

This section compares the FIV loads between the BWR/4 prototype plant and GGNS. MSL measurements from strain gauges mounted on the MSLs have been compared along with steam dryer loads from PBLE load definition predictions.

5.5.1 Steam Dryer Loads

MSL measurements taken at GGNS and the BWR/4 prototype plant are used as input to the PBLE to predict the steam dryer loads taken at [[ ]] locations on the acoustic finite element model. These predicted loads are averaged and the same regions of the dryer are compared. Figure 5-2 shows the loads comparison for the dryer outer hood quadrant 1. Below [[ ]] the BWR/4 prototype plant loads are [[ ]] particularly the [[ ]] peaks, likely associated with [[ ]] Between [[ ]] the loads are generally [[ ]] the GGNS loads, although [[ ]] the GGNS loads are [[ ]] in the GGNS data and at [[ ]] in the BWR/4 prototype plant data.

Figure 5-3 through Figure 5-13 and Table 5-5 show the load comparison for the other dryer outer hood [[ ]] along with the skirt and end plates and inner hood [[ ]] Similar trends are observed for those locations.

The comparison of the steam dryer loads between GGNS and the BWR/4 prototype plant demonstrate that the loads are very similar, with some differences attributed to plant-specific features and dimensions. These differences between the BWR/4 prototype plant and GGNS loads are addressed in the GGNS-specific pressure vessel acoustic model and the PBLE load definition.

5.6 Applicability of PBLE and FEM Bias and Uncertainty Values to GGNS

5.6.1 Overview – FIV Bias and Uncertainty

Bias and uncertainty values are applied to model predictions to account for variations in the expected plant operating state, as well as tendencies of the methodology to over or under-predict actual data. Correcting predictions for biases and uncertainties is an important consideration [[ ]] The corrections that are applied to the GGNS steam

dryer evaluation fall into several categories. These are discussed in detail in Section 8 of Appendix A.

Appendix C also contains a detailed discussion of the PBLE model qualification through plant benchmarks, as well as the application methodology (including the application of biases and uncertainties).

5.6.1.1 PBLE Bias and Uncertainty

Bias and uncertainty values derived from comparisons against plant data [[

]] Different types of data are available from instrumented dryers, including [[

]]

In general, corrections derived from instrumented dryer benchmark cases can account for the tendencies of the methodology to over or under-predict stress. Benchmark comparisons have demonstrated that the PBLE methodology [[ ]] The PBLE model has been benchmarked with dryer instruments [[

]] The peak stress is determined based on [[

]]

[[

]] Additional discussion regarding the applicability of these values to GGNS is provided in Section 5.6.2.

5.6.1.2 Structural FEM Bias and Uncertainty

The structural FEM has uncertainty that affects the dryer frequency response. For example, the dryer global model does not perfectly represent [[

]]

This is addressed by the methodology, [[

]] The dryer analysis methodology utilizes [[ ]]

[[ ]] as a means to [[ ]] assure that the uncertainty in the response frequency is adequately bounded.

[[

]] The [[ ]] values were used in the results shown in Section 4. The [[ ]] stress results [[ ]] are used in assessing the design margin.

The FEM for GGNS was developed following the same guidelines used for the benchmark FEM (for the purposes of the FEM benchmark, this is the [[ ]], Reference 6). In this process, the FEM mesh is refined by reducing the element sizes to demonstrate that the solution is converged [[ ]] The [[ ]] criterion is used to ensure that the plant-specific application is consistent with the benchmarked model.

Sections 5.2, 5.3, 5.4 and 5.5 demonstrate that the GGNS replacement dryer is adequately represented by the BWR/4 prototype design and operating conditions, including the similarity in pressure loads, as shown in Section 5.5. This confirms the applicability of the FEM bias and uncertainty for the GGNS replacement steam dryer.

5.6.1.3 Time Interval Bias

A time interval bias is considered in the final calculated peak stress values. [[

]] The time segment is not nominal. Regardless, a bias value is included, recognizing that [[ ]], the segment still represents a time sample.

5.6.1.4 Instrumentation Uncertainty

Instrumentation uncertainties can potentially affect the PBLE-based prediction. [[

]] For the GGNS application, the DAS and strain gauge system were calibrated during pre-operational hydro-test to minimize the uncertainty added by piping geometry and gauge field installation. These [[ ]] provide a means to

narrow instrument (inherent) uncertainty. The DAS and strain gauges used in the GGNS installation are consistent with those presented in Appendix C.

5.6.1.5 Plant Specific Uncertainties

Uncertainties are applied to account for variation in the anticipated plant operating state, [[

]] The acoustic model is sensitive to [[

]] These values are confirmed [[ ]] to assure that representative values are applied in the evaluation (see Appendix C, Section 4.4, [[ ]] The acoustic properties are summarized in Section 5.4.

5.6.2 Summary and Conclusions

The bias and uncertainty values applied to the GGNS steam dryer analysis are consistent with the benchmarked approach presented in Appendix C and discussed in Sections 5.6.1.1 through 5.6.1.5. In general, the biases and uncertainties associated with the PBLE methodology are attributable to the [[ ]] main components of the calculation, although measurement errors also have an impact on accuracy.

The "TransMatrix" is central to the PBLE methodology (Appendix C). It provides a means to [[ ]] Due to similarities in BWR operating conditions, as well as similar plenum and steam line configurations, the TransMatrix values can be applied to a wide range of plants. The bias and uncertainty values applied to GGNS (see Section 8.0 of Appendix A) reflect application of the TransMatrix developed from [[ ]] data. These bias and uncertainty values represent the result of benchmark comparisons against the instrumented [[ ]] steam dryer. It is worth noting that the [[ ]] dryer has the same diameter as the GGNS dryer and has a similar arrangement of [[ ]] hoods, which is also true for the prototype. Benchmark information for the prototype plant is included in Appendix C.

Given the similarities in the overall dryer geometry and acoustic parameters, the PBLE prediction for GGNS is expected to be consistent with prior benchmarks. It follows that the biases and uncertainties based on the benchmarks are valid for GGNS. However, recognizing that the qualification basis supporting broad application of PBLE is somewhat limited, the GGNS replacement dryer structural integrity evaluation demonstrates a MASR greater than 2.0,

consistent with Nuclear Regulatory Commission (NRC) requirements for application to other plants (Reference 4).

Table 5-1. GGNS Dryer Geometric Comparison

No.	Compared Item	[[	]]
[[			
			]]

Table 5-2. Comparison of Plant Operating Conditions - GGNS vs. Prototype Plant

Item	[[		Units
Rated Power			MWt
Dome Temperature			°F
Dome Pressure			psia
Total MSL Mass flow			lbm/hr
Flow velocity in steam line		]]	ft/Sec

Table 5-3. Comparison of Plant Geometry - GGNS vs. Prototype Plant

Plant Geometric Item	GGNS	Prototype	Units
[[			
			]]

Table 5-4. RPV Acoustic Property Comparison

Property	GGNS	BWR/4 prototype
[[		
		]]

Table 5-5. Comparison of Test Conditions for GGNS and BWR/4 Prototype Plant

	[[		]]
[[			
			]]

[[

]]

Figure 5-1. GGNS-BWR/4 Dome Acoustic Properties

[[

]]

Figure 5-2. GGNS-BWR/4 Prototype Plant Dryer Comparison [[ ]]

[[

]]

Figure 5-3. GGNS-BWR/4 Prototype Plant Dryer Loads Comparison [[
]]

[[

]]

Figure 5-4. GGNS-BWR/4 Prototype Plant Dryer Loads Comparison [[
]]

[[

]]

Figure 5-5. GGNS-BWR/4 Prototype Plant Dryer Loads Comparison [[
]]

[[

]]

Figure 5-6. GGNS-BWR/4 Prototype Plant Dryer Loads Comparison [[
]]

[[

]]

Figure 5-7. GGNS-BWR/4 Prototype Plant S Dryer Loads Comparison [[
]]

[[

]]

Figure 5-8. GGNS-BWR/4 Prototype Plant Dryer Loads Comparison [[
]]

[[

]]

Figure 5-9. GGNS-BWR/4 Prototype Plant Dryer Loads Comparison [[
]]

[[

]]

Figure 5-10. GGNS-BWR/4 Prototype Plant Dryer Loads Comparison [[
]]

[[

]]

Figure 5-11. GGNS-BWR/4 Prototype Plant Dryer Loads Comparison [[
]]

[[

]]

Figure 5-12. GGNS-BWR/4 Prototype Plant Dryer Loads Comparison [[
]]

[[

]]

Figure 5-13. GGNS-BWR/4 Prototype Plant Dryer Loads Comparison [[
]]

6.0 MONITORING DURING POWER ASCENSION AND FINAL ASSESSMENT AT EPU

6.1 Power Ascension Test Plan

During startup and power ascension above CLTP, monitoring of MSL data will be performed and the data will be compared to the acceptance limits to confirm acceptable steam dryer structural performance. These acceptance limits are based upon the FEA results for full EPU conditions (Appendix F).

Entergy plans to use strain gauges on the MSLs for GGNS to obtain acoustic vibration data during power ascension. [[

]]

Demonstrating that the dryer pressure loads remain within the allowable pressure loads confirms that the steam dryer alternating stresses remain within the structural analysis basis (reference Appendix E). The [[ ]] uncertainty analyses are accounted for in the development of the acceptance limits.

The primary function of the monitoring program is to confirm that the [[

]] steam dryer during power operation is consistent with the pressure loading assumed in the structural fatigue evaluation and to confirm that the steam dryer can adequately withstand the acoustic and hydrodynamic pressure loads. The primary objectives are as follows:

- [[

  ]]
- Confirm the steam dryer analyses performed for the EPU conditions.

[[

]]

- Evaluation of data against the acceptance criteria [[

]]

- Forwarding to the NRC the evaluation results taken [[

]] monitored against established acceptance limits to assure steam dryer structural integrity is maintained. [[

]] The acceptability of the steam dryer for the measured loading would then be evaluated [[

]] as required (reference Appendix F). [[

]]

6.2 Final Assessment at EPU

[[

]]

Station operating procedures will be used to monitor plant parameters potentially indicative of steam dryer failure as recommended in General Electric Service Information Letter 644, "BWR Steam Dryer Integrity." Results will be reviewed and evaluated on a defined basis to monitor moisture carryover conditions.

[[ ]] visual inspection of all accessible, susceptible locations of the steam dryer in accordance with General Electric Service Information Letter 644, “BWR Steam Dryer Integrity” will be performed.

7.0 REFERENCES

1. US Nuclear Regulatory Commission Regulatory Guide 1.20, Revision 3, March 2007.

2. 2001 ASME Boiler and Pressure Vessel Code, Section II - Materials (Includes 2002 and 2003 Addenda).

3. "Effective Elastic Constants for Bending of Thin Perforated Plates with Triangular and Square Penetration Patterns" by W.J. O'Donnell, February 1973, ASME Journal of Engineering Industry 95: 121-128.

4. MFN 10-219, Letter from S. Philpott (NRC) to J. Head (GEH), "Boiling Water Reactor Operating Fleet -- Extended Power Uprate Technical Basis for the Requirement of a Minimum Alternating Stress Ratio of 2.0," July 27, 2010.

5. Not used.

6. GNRO-2012-00011, Entergy letter to the NRC, Request for Additional Information Regarding Extended Power Uprate, dated February 20, 2012.

Appendix A

Steam Dryer Integrity Analysis Methodology

TABLE OF CONTENTS

Page

LIST OF TABLES

LIST OF FIGURES

1.0 OVERVIEW

The steam dryer in a boiling water reactor (BWR) nuclear power plant performs no safety function, but must retain its structural integrity to avoid the generation of loose parts that might adversely affect the capability of other plant equipment to perform safety functions. As a result of steam dryer issues at one BWR plant implementing an extended power uprate, the US Nuclear Regulatory Commission (NRC) has issued revised guidance that included a comprehensive structural evaluation and vibration assessment program for steam dryers in References 1 and 2, with supplementary guidance provided in Reference 3:

> "Applicants proposing to construct and operate a new nuclear power plant, or licensees planning to request a power uprate for an existing power plant, (that have prototype dryer design) should perform a detailed analysis of potential adverse flow effects (both flow-excited acoustic resonances and flow-induced vibrations) that can severely affect the steam dryer in BWRs and other main steam system components" (Reference 3).
>
> "Because adverse flow effects in reactors caused by flow-excited acoustic and structural resonances are sensitive to minor changes in arrangement, design, size, and operating conditions, even applications submitted for non-prototypes should include rigorous assessments of the potential for such adverse effects to appear. For any two nearly identical nuclear power plants, one may experience significant adverse flow effects, such as valve and steam dryer failures, while the other does not. Also, small changes in operating condition can cause a small adverse flow effect to magnify substantially, leading to structural failures. For example, severe acoustic excitation occurred in the steam system of one BWR nuclear power plant when flow was increased by 16 percent for extended power uprate (EPU) operation" (Reference 3).

This appendix describes the overall analysis and power ascension measurement programs used to verify structural integrity of the steam dryer. Techniques for conducting inspections of the steam dryer have been provided in References 4 and 5 and are not within the scope of this report.

Although the steam dryer is not a safety-related component, it is evaluated to ASME Code NG design rules and fabrication guidance as delineated in this appendix and other supporting appendices. This approach will assure that the dryer has no adverse effect on the operation of safety related components during normal operation, transient and accident conditions.

Because the steam dryer issues arising from extended power uprate operation were fatigue cracking, the most challenging area of the dryer evaluations is to demonstrate that the steam dryer (whether existing, modified, or a replacement dryer) will meet the fatigue acceptance criteria when subjected to the vibrations resulting from the acoustic and fluctuating pressure loading during normal operation. As described in this report, this requires:

- Review of the dryer construction details and industry data to identify relevant inspection findings.
- Evaluation of the main steam line (MSL) geometry for potential acoustic resonances that may occur over the expected range of conditions.
- Installation of instrumentation and measurement and trending of dryer or MSL data up to the current licensed thermal power (CLTP) conditions.
- Development of the dryer fluctuating pressure load definition, performance of a structural analysis, and demonstration that the dryer satisfies limits for the projected loads over the expected range of operation, including normal, upset, emergency and faulted conditions.
- Definition of dryer acceptance limits for power ascension testing.
- Implementation of a power ascension test program for confirming that the steam dryer alternating stresses remain within the fatigue acceptance criteria as reactor power is increased from CLTP to power uprate conditions.

In the event the current dryer is to be used or modified for power uprate, a baseline dryer inspection per Reference 4 guidance is required prior to operation at uprated power conditions. After operation at power uprate conditions, the dryer is re-inspected per the requirements of Reference 4. In the case of a replacement dryer, GEH will issue inspection guidance that is specific to the replacement dryer.

2.0 OVERVIEW OF STEAM DRYER EVALUATION APPROACH

The following process is used to evaluate the capability of the steam dryer to withstand the vibration and pressure loadings during normal operation as well as transient and accident conditions. This process is applicable to evaluating an existing steam dryer in consideration of a power uprate, evaluating modifications or repairs to an existing dryer, or evaluating the design for a new or replacement dryer. This process satisfies the structural analysis requirements of References 1 and 2 and incorporates the guidance provided in Reference 3.

The overall dryer evaluation process is shown in Figure 2-1. The major steps of the evaluation process are:

- The MSL geometry is evaluated for potential acoustic resonances that may occur in the expected range of EPU operating conditions. This evaluation is based primarily on an acoustic evaluation of the safety relief valve (SRV) standpipe and MSL geometry, as well as measurements taken in plants with similar geometries and operating conditions.
- The potential acoustic SRV resonance frequencies are used in conjunction with the vessel and MSL acoustic models to determine optimum locations for the MSL pressure measurements. Measurements of the acoustic pressures in the MSLs are taken during the plant power ascension to CLTP.
- The power ascension trend data is used to develop scaling factors for projecting the dryer acoustic loads to EPU conditions. The power ascension measurements are also used to identify SRV acoustic resonances that may be present at CLTP.
- The dryer fluctuating pressure load definition for the flow-induced vibration (FIV) analysis is developed based on the plant MSL pressure measurements and the potential SRV resonances identified in the source screening using the Plant Based Load Evaluation (PBLE) methodology.
- The fatigue analysis of the dryer is performed using the fluctuating pressure load definition. After incorporating the analysis bias and uncertainties, the results are confirmed to meet the fatigue acceptance criteria.
- The primary stress analysis of the dryer is performed to demonstrate that the dryer will maintain structural integrity under normal, upset, emergency and faulted conditions.
- The power ascension monitoring program and acceptance limits are defined for confirming the steam dryer meets the fatigue acceptance criteria at power uprate conditions.

The evaluation process is supported by the following appendices:

Appendix B – GGNS - Plant Based Load Evaluation Methodology: This appendix describes the GEH analytical model for determining the fluctuating pressure loads acting on the steam dryer.

Appendix C – GGNS Plant Based Load Evaluation Methodology, Supplement 1: This appendix describes the application of the PBLE model for determining the fluctuating pressure loads acting on the steam dryer based on MSL measurements.

Appendix D - Not Used.

Appendix E – Steam Dryer Structural Analysis Methodology: This appendix describes the modeling and analysis process for performing the structural fatigue and primary stress analysis of the steam dryer.

Appendix F – Power Ascension Test Plan: This appendix describes the development of the acceptance limits for the power ascension monitoring program, application of the acceptance limits during power ascension, and the methodology for updating the limits if necessary during power ascension.

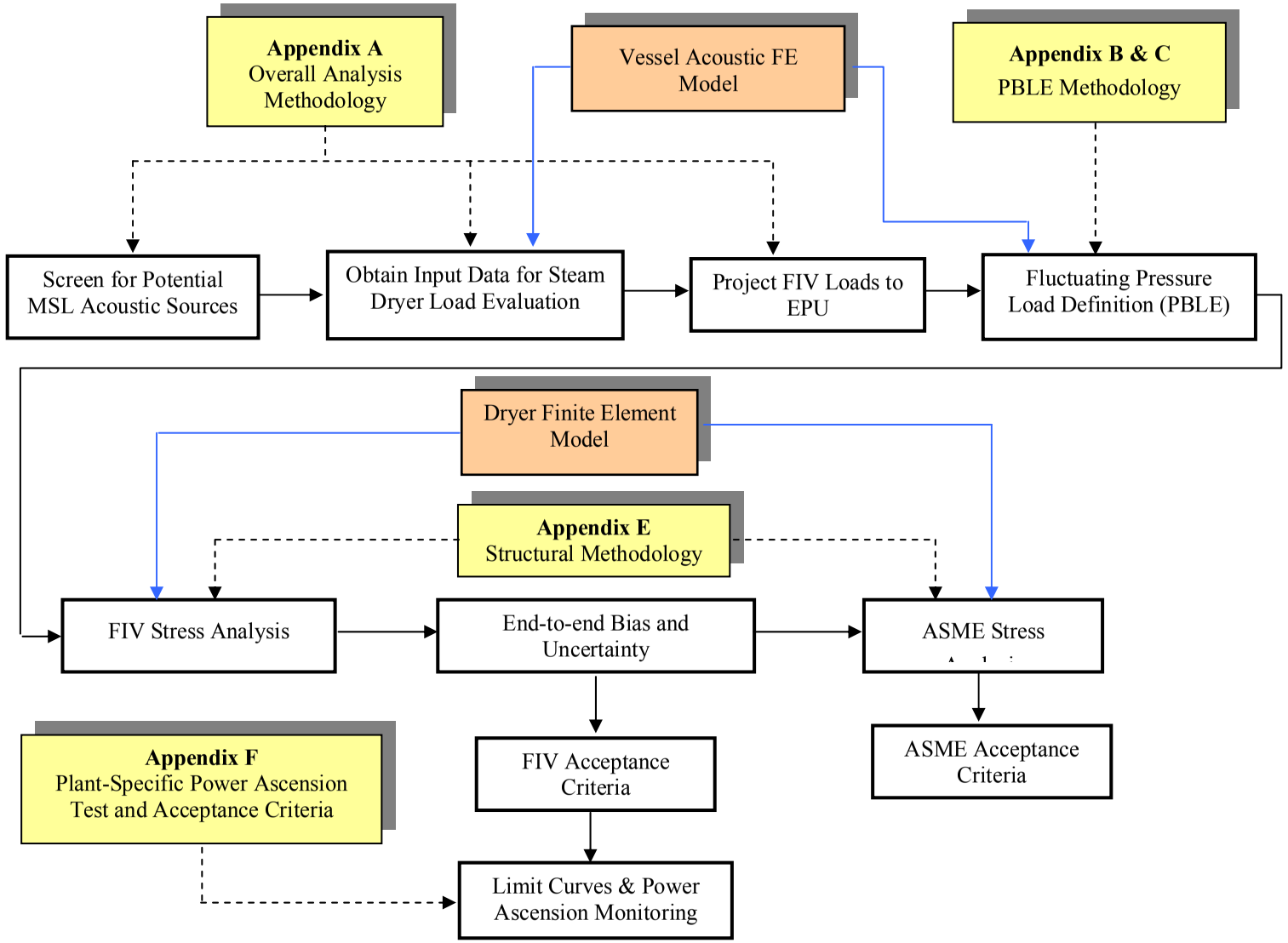

Figure 2-1 Steam Dryer Structural Evaluation Overview

3.0 SCREENING FOR POTENTIAL MSL ACOUSTIC SOURCES

The evolutionary design of the GE BWR plant has resulted in similar reactor vessel, steam dryer, and MSL geometrical configurations, as well as similar plant operating conditions. [[

]] The MSL geometrical configuration governs the frequency content in the pressure loads acting on the steam dryer. [[

]] The plant-specific frequency and amplitude and content must be determined for the dryer FIV fatigue load definition.

[[

]] A few plants have a stagnant branch line, or deadleg, on some of the MSLs. These deadlegs serve as a mounting location for safety relief valves (SRVs). Acoustically, the deadleg provides a resonating chamber that may amplify the low frequency pressure content of the fluctuating pressure loads acting on the dryer. The high quality factor SRV resonance peaks occur above 100 Hz. The frequency is dependent primarily on the SRV branch line cavity depth; the MSL flow velocity at which the SRV branch line begins to resonate is governed by the diameter of the standpipe. Whether or not the SRV acoustic resonance actually produces a pressure load that acts on the dryer depends on whether or not the SRV acoustically couples through the steamline to an acoustic mode in the vessel steam dome.

[[

]]

3.1 POTENTIAL SRV ACOUSTIC RESONANCE FREQUENCIES

The only significant potential acoustic sources in the MSLs that are not captured by the plant measurements are the SRV standpipe acoustic resonances that may occur at power levels above those at which the measurements are taken. The frequencies at which SRV resonances occur are determined primarily by the depth and shape of the SRV standpipe cavity between the MSL and the valve disc, and secondarily by acoustic interactions between other SRVs and interactions with the MSL acoustic modes. Because of these interactions, the MSL and the SRVs must be [[ ]].

First, a standalone acoustic finite element model of the SRV standpipe is analyzed to determine the basic resonance frequency. The SRV standpipe forms a closed end cavity. High velocity steam flow passing the entrance to the SRV may produce an acoustic resonance in this cavity. The prominent SRV acoustic resonance mode observed in BWR measurements is the fundamental quarter wave mode for the cavity. The frequency for this mode, f, is given by

$$f = \frac{c}{4L} \tag{3-1}$$

Where c is the speed of sound in steam and L is the depth of the standpipe cavity. This equation assumes that the cavity has a uniform diameter. However, the standpipe cavity for most SRVs is not uniform in diameter and tends to taper to smaller diameters towards the top (Figure 3-1). The taper increases the fundamental frequency of the cavity. Because the geometry of the cavity is complex, an acoustic finite element analysis of the standpipe cavity must be performed to determine the fundamental frequency.

[[

]] The resolution of the acoustic finite element model (FEM) must also be fine enough to replicate the details of the geometry. [[

]] The model is driven [[

]] The speed of sound is [[ ]] determined based on the PBLE modeling described in Section 2.4 of Appendix C.

Figure 3-1 shows the results of the acoustic FEM analysis for a typical SRV standpipe. [[ ]] This is almost 30 Hz higher than the frequency estimated by the idealized equation. Figure 3-2 shows the acoustic frequency response for the standpipe. The individual curves show the relative pressures along the centerline of the standpipe (highest pressure at the top of the standpipe). [[

]]

[[

]]

Figure 3-1 Acoustic Mode Shape for SRV Standpipe [[ ]]
(Relative Pressure)

[[

]]

Figure 3-2 Frequency Response for SRV Standpipe
(Relative Pressure at SRV Centerline Locations)

The frequencies at which SRV resonances occur are also determined by acoustic interactions between SRVs and with interactions with the MSL acoustic modes. Because of these interactions, [[

]] Each individual MSL [[

]]

The speed of sound is [[ ]] determined based on the PBLE modeling described in Section 2.4 of Appendix C.

Figure 3-3 shows the full steamline acoustic FEM for a GGNS MSL with six SRVs. [[

]]

Figure 3-12 is a waterfall plot showing the frequency content and amplitude of the MSL pressures [[

]]

Table 3-1 Comparison of [[

]]

[[	
	]]

Notes:
(1) [[

]]

The above analysis was repeated for a GGNS MSL with four SRVs in the MSL. [[

]] Assessing potential resonances at flow rates higher than measured will be addressed in the next section.

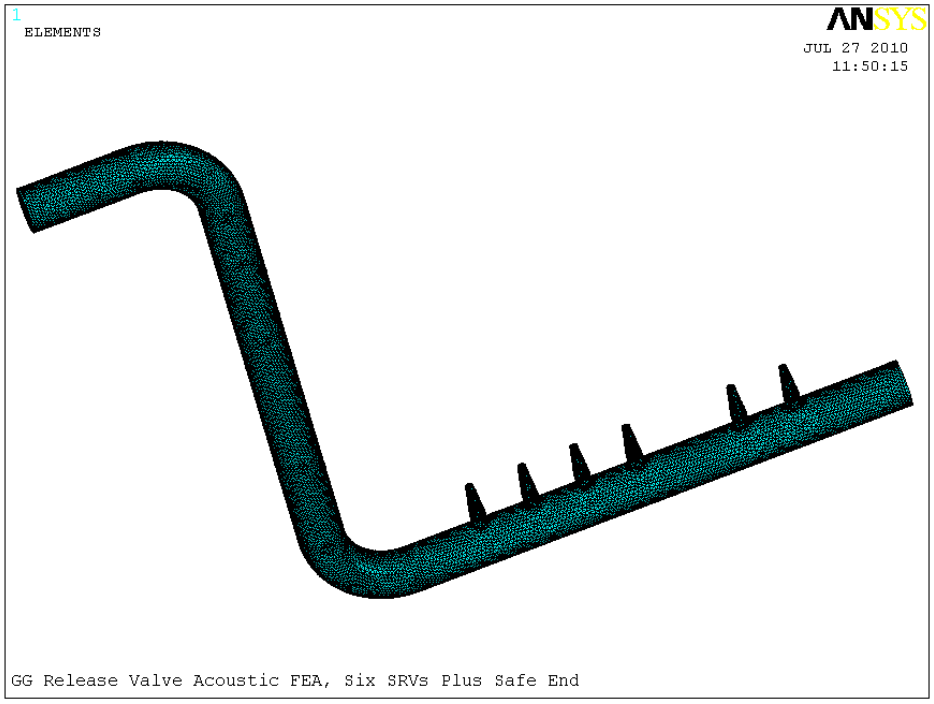

Figure 3-3 Full Steamline Acoustic FEM, Six SRVs

[[

]]

Figure 3-4 [[ ]]
(SRV nodes) (Relative Pressure at Top of SRVs)

[[

]]

Figure 3-5 [[ ]]

(Relative Pressure at MSL SG Locations)

[[

]]

Figure 3-6 [[ ]]

(Relative Pressure at Various MSL and SRV Locations)

[[

]]

Figure 3-7 [[ ]]

[[

]]

Figure 3-8 [[ ]]

[[

]]

Figure 3-9 **[[**]]

[[

]]

Figure 3-10 [[ ]]

[[

]]

Figure 3-11 [[ ]]

[[

]]

Figure 3-12 Power Ascension MSL PSD, [[ ]]

[[

]]

Figure 3-13 Frequency Response for Four SRV Steamline Acoustic FEM

[[

]]

Figure 3-14 [[ ]]

3.2 ONSET OF SRV ACOUSTIC RESONANCE

Once the potential SRV acoustic resonant frequencies have been identified, the MSL flow velocities at which the resonances are expected to appear must be determined. [[

]]

to determine which resonances need to be addressed in the load definition for the dryer FIV fatigue analysis.

Figure 3-15 shows the prominent SRV acoustic resonances [[

]]. A wide spread of frequencies are observed [[ ]] because of the differences in SRV standpipe height, as well as the interaction between the acoustics in the SRV standpipes and the MSL described in the previous section. [[

]]

The wide variation in the flow velocity at the onset of the resonances can be explained by the phenomena that produce the resonance. The SRV resonance is caused by an acoustic feedback loop between the disturbances in the shear layer across the SRV entrance and the acoustic standing wave in the SRV standpipe. In the resonance condition, large coherent vortices are generated in the shear layer. The SRV acoustic resonances observed in GE BWRs are the fundamental quarter wave mode of the standpipe as driven by the first or second mode (one or two vortices) of the shear layer instability.

Because the resonance is driven by a vortex shedding phenomenon, the Strouhal number can be used to characterize the conditions at which the resonances occur. The Strouhal number is defined as

$$S = \frac{fd}{V} \tag{3-2}$$

Where f is the resonance frequency (1/sec), d is the diameter of the standpipe (inches), and V is the average flow velocity in the steamline (inches/sec). First shear layer mode resonances typically occur with Strouhal numbers in the 0.3-0.6 range; second shear layer mode resonances typically occur with Strouhal numbers in the 0.8-1.0 range.

The plant observations in Figure 3-15 were replotted [[

]]. The replotted observations are shown in Figure 3-16. The plant observations line up [[

]]

Based on the plant observations, the resonance onset occurred at a Strouhal number of [[

]]. A simple prediction for the plant-specific SRV resonance onset can be made by using the onset Strouhal numbers based on [[

]] Potential SRV resonances predicted by the acoustic FEM analysis in Section 3.1 can then be screened [[ ]] with consideration of the range of steamline flow velocities for the plant-specific analyses.

Continuing with the example in Section 3.1, the [[

]].

3.3 SRV RESONANCE FREQUENCY SELECTION FOR ANALYSIS

[[ ]] are used to identify candidate frequencies to be considered in the plant measurements and analyses. The candidate frequencies are considered in Section 4 for determining the MSL measurement locations to [[

]].

Several factors must be taken into consideration when [[

]]. These are the SRV resonances observed in the MSL measurements taken at CLTP for the fluctuating pressure load definition (Section 4) and the potential resonances that may come up as the plant ascends in power (Section 3.2). [[

]]

SRV resonances may be observed in the MSL measurements taken at CLTP for the fluctuating pressure load definition (Section 4). These resonances must be addressed in the SRV resonance modeling when projecting the pressure loads to EPU conditions. [[

]]

[[

]]

It is desirable to analyze the dryer response through the full SRV resonance frequency range to address the uncertainty in predicting which resonance frequency may come up and to ensure that the structural response will be acceptable throughout the range. This can be accomplished while [[ ]] by taking advantage of the

nine frequency shift sensitivity cases in the structural analysis. [[ ]] Table 3-2 and Figure 3-18 show the analysis range covered by the nine frequency shift cases [[ ]]. Because of the frequency shifts, the dryer structure will be analyzed [[ ]]. In addition, the overlap between the various frequencies means that [[ ]].

Table 3-2 SRV Resonance Analysis Range

[[									
									]]

[[ ]] Figure 5-4 shows the pressure loading on various regions of the dryer as a function of frequency for the SRV resonance range. [[ ]]

Table 3-3 provides a summary of the SRV source screening evaluation. Based on the SRV screening evaluation results from Sections 3.1 and 3.2 as well as the plant measurements shown in Figure 3-17, the SRV resonance [[ ]]

Table 3-3 Summary of Modeled SRV Resonances

[[		
		]]

[[ ]]

3.4 SRV RESONANCE PROJECTION TO EPU CONDITIONS

It is difficult to analytically predict the amplitude of an SRV acoustic resonance. [[

]]

As can be seen in Figure 3-19, the change in [[ ]] velocity between the onset of the resonance and the peak [[

]]

[[

]]

Figure 3-15 [[ ]]

[[

]]

Figure 3-16 [[ ]]

[[

]]

Figure 3-17 [[ ]]

[[

]]

Figure 3-18 [[ ]]

[[

]]

Figure 3-19 [[ ]]

[[

]]

Figure 3-20 [[ ]]

4.0 OBTAINING INPUT DATA FOR STEAM DRYER LOAD EVALUATION

This section describes the plant instrumentation required for obtaining the input data necessary to develop the fluctuating pressure load definition for the fatigue analysis. This section describes the MSL and on-dryer instrumentation requirements and the methodology for determining the sensor locations. Data acquisition system and shielding requirements are defined. The process for data collection, signal evaluation and noise filtering are described.

- **Instrumentation Strategy**: [[

]]

- **Data Acquisition and Processing**: a measurement test program is conducted to obtain synchronized time measurements of the dynamic MSL piping strains or pressures; the electrical noise is filtered out of the measured strain or pressure signals; and pipe strains are converted to pressures.

4.1 PLANT MEASUREMENTS

The PBLE can be used with vessel pressure data or MSL pressure data to define the acoustic loads on a BWR steam dryer.

For MSL instrumentation (used for the GGNS analysis) the methodology requires:

- A minimum of two sensor locations per steam line
- [[

]]

The sensors can either be pressure transducers or arrangements of strain gauge bridges around the pipe circumference. If strain gauge bridges are used, the MSL pressures are calculated from the pipe hoop stress measurements. [[

]] More information on the methodology used for determining the MSL sensor locations is described in Appendix C.

[[

]]

Figure 4-1 Singularity Factor: Large versus Small Sensor Spacing

Red: 30 feet – Blue: 7.5 feet
Typical plant environment

As described in Appendix C, each location was instrumented with a minimum of four strain gauges distributed in pairs 180 degrees apart. When the signals from two diametrically opposed gauges are averaged together, the pipe bending effects in that plane are canceled out. The remaining strain signal represents the hoop stress in the pipe, which is proportional to the pressure inside the pipe. It is best if the pairs of gauges are equally spaced around the pipe. Where possible, the gauges should be located away from pipe supports, 6" from welds, one pipe diameter from elbows or tees, and 6" from welded attachments. All of these can affect the local pipe deformation and the subsequent strain to pressure conversion process. [[

]]

Figure 4-2 and Table 4-1 show a sample comparison of two different strain gauge spacings for the GGNS MSL illustrating how the spacing affects [[

]]

[[

]]

Figure 4-2 [[ ]]

Table 4-1 Comparison of [[ ]] for Different Strain Gauge Spacings

SG Location Plans	[[		SG Locations, Distance from Nozzle (inches)							
			A1	A2	B1	B2	C1	C2	D1	D2
Preliminary										
Uneven spacing										]]

[[

]]

[[

]]

Figure 4-3 [[ ]]

Prior to installing the gauges, the as-built arrangement of the piping is evaluated and the pipe condition at the proposed locations is assessed to determine the final mounting locations. The final sensor locations represent a compromise between the physical constraints [[ ]] Table 4-2 shows the upper and lower MSL sensor locations for the two PBLE benchmark plants described in Appendix C. Both of these plants had long straight section pipe runs immediately downstream of the vessel nozzle that allowed for the large spacing between sensor locations that is desirable for resolution at low frequencies. [[ ]]

Table 4-2 Strain Gauge Distance from Vessel, PBLE Benchmark Plants

Plant	MSL	Upper Location (ft)	MSL Diameters from Nozzle, Upper Location	Lower Location (ft)	Spacing Between Locations (ft)
QC2	A	[[			
QC2	B				
QC2	C				
QC2	D				
SSES	A				
SSES	B				
SSES	C				
SSES	D				]]

Table 4-3 provides the sensor locations and spacing for GGNS. [[ ]]

Table 4-3 GGNS Linear Distance from Vessel Nozzle to Strain Gauge Locations

MSL	Upper Location (ft)	MSL Diameters from Nozzle, Upper Location	Lower Location (ft)	Spacing Between Locations (ft)
A	[[			
B				
C				
D				
	]]			

To ensure an accurate strain-to-pressure conversion for each strain gauge, ultrasonic test (UT) pipe thickness measurements are made at each mounting location [[

]]

The data acquisition system (DAS) is a computer-based system capable of acquiring, storing, and analyzing the strain gauge data. The measurement system is designed to provide a well-shielded system with low noise so that only minimal electrical noise filtering is required. [[

]] The preferred method for grounding the DAS is to ground the system with the existing plant instrument ground. [[

]] The higher frequency bandwidth will enable higher frequencies to be recorded, making that content available if needed. [[

]] Anti-aliasing filtering must be sufficient to exclude aliasing of high frequency data [[

]] The strain gauge bridge excitation must have an option to set

the bridge excitation to zero volts. Measurements will be taken with and without the bridge excitation and comparisons between the two measurements will be to differentiate between electrical noise and acoustical sources.

4.2 DATA ACQUISITION AND TEST PLAN

The data acquisition test plan for taking MSL pressure measurements using strain gauges includes a system checkout, sensor pre-calibration, [[
]] low power testing, power ascension and steady state test hold points, and sensor post-calibration (final test acceptance).

Measurements are taken during [[

]]

Low power testing is performed for the purpose of comparing the noise floor from the plant being analyzed with the noise floor of the PBLE benchmark plants. The low power testing is performed at conditions where the reactor is at normal operating temperature and pressure with the recirculation pumps and drywell equipment operating, but the steam flow is low (approximately 10 - 30% of CLTP flow). These conditions minimize the contribution of the acoustic and hydrodynamic pressure loads to the measured signal. The noise floor from the plant being analyzed is then compared with the noise floor of the benchmark plant measurements. [[

]]

Figure 4-4 (GGNS) and Figure 4-5 (BWR/4 prototype) compare low power data from GGNS with low power data from the DAS used in MSL monitoring at the BWR/4 prototype plant during initial power ascension testing in 2008. While the NRC has asked that GEH maintain a 100% margin to the 13,600 psi allowable, to account in part for potential bias due to a lower noise floor, [[

]]

Steady-state measurements are taken at several hold points during the plant power ascension to CLTP in order to define the change in FIV loads as the power increases and to provide a basis for projecting the loads to higher power levels. These measurements form the basis for the inputs to the load generation process.

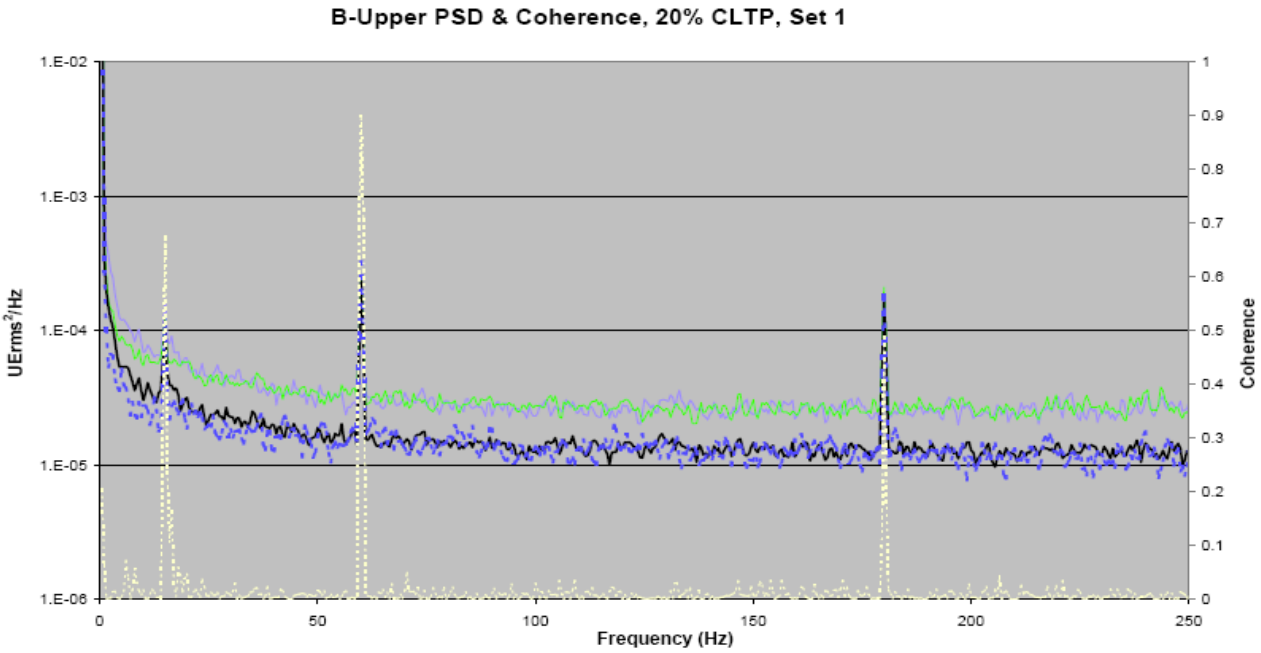

Figure 4-4 GGNS Low Power Data from Strain Gauge DAS

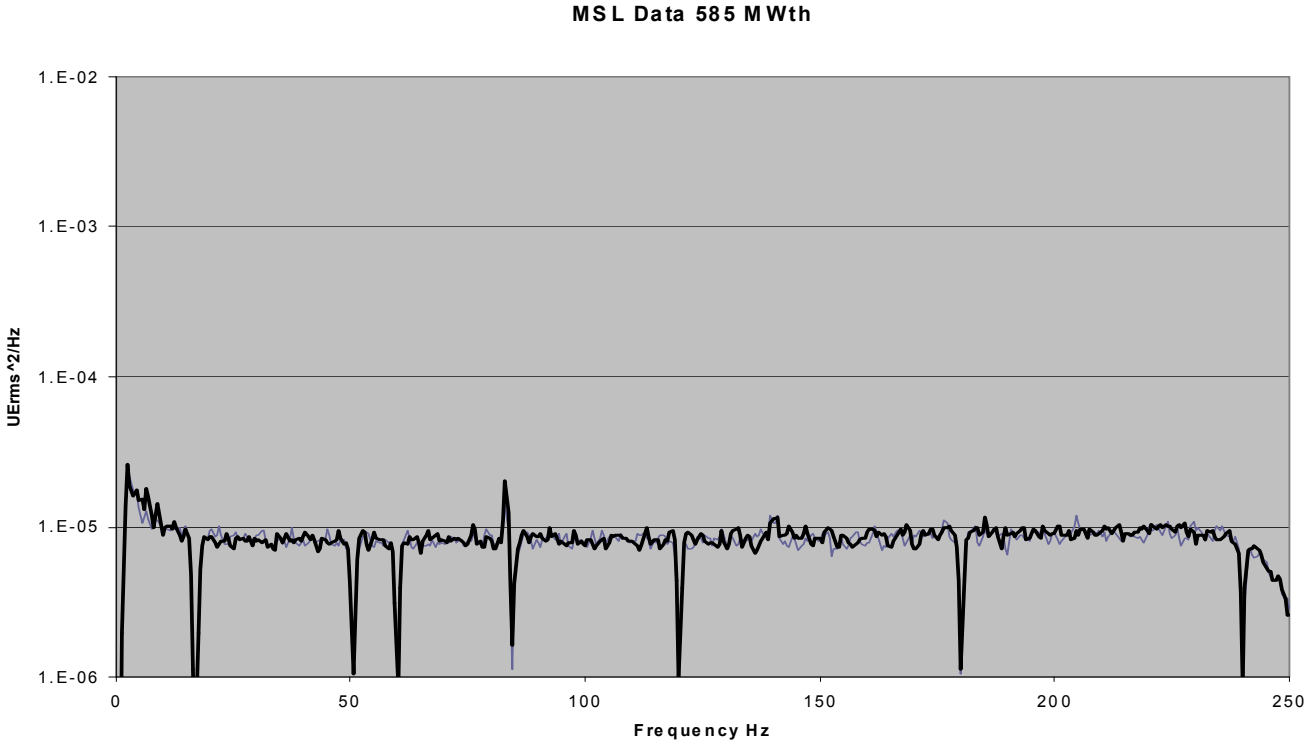

Figure 4-5 Prototype Plant Low Power Data from SG DAS (585MWth)

4.3 DATA ACQUISITION OF PLANT MSL PRESSURES

During plant operation, MSL data is recorded at various plant conditions to form the basis for the inputs to the load generation process. These measurements are taken with strain gauges located on the MSLs and are used to infer the variation in the pressure waves moving along the MSLs and into the RPV. Data taken at CLTP is used as the basis for the load generation using the PBLE methodology (described further in Appendix C).

Steady-state measurements are taken at several hold points during the plant power ascension to define the change in FIV loads as the power increases and to provide a basis for projecting the loads to higher power levels. Each steady-state measurement taken is [[

]] The measurements are taken at approximately 5% increments in power levels from 75% to 100% CLTP. When the plant is in steady-state operation at approximately 100% CLTP, multiple sets of test data are collected over a long period of time to determine whether the data is stationary. [[

]] During the load definition process described in Section 6, one set is then selected for further processing as the CLTP input data set for the analysis load definition.

The data acquisition and evaluation during power ascension is performed by first null and balancing the strain gauge bridge. Only anti-aliasing filtering is used during collection. The bridge excitation voltage must be chosen to balance between measurement sensitivity and measurement stability. Higher excitation voltages provide a better signal to noise ratio; however, the voltage must be limited to limit gauge heating and the associated signal drift. For each test condition measurements will also be taken at each test hold point with zero bridge excitation to facilitate identifying electrical interference in each data set.

4.4 SIGNAL PROCESSING OF EXPERIMENTALLY MEASURED DATA

4.4.1 Signal Processing During Power Ascension

Following data collection at each test point, the measured signal data are processed and plotted in the frequency domain for review before the ascending to the next power step. The initial evaluation of the data is performed by reviewing power spectral density (PSD) data averaged over long periods of time. This process is now described in detail.

The individual strain gauge signals, the averaged strain gauge signals (both excited and non-excited), and coherence between averaged strain gauge signals at the upper and lower sensor locations on the same MSL are plotted and reviewed. The individual strain gauge signals are reviewed to identify non-functional gauges. The averaged signal excited and non-excited curves are compared to identify frequency bands that can be identified as electric noise. Electrical noise signals are typically narrow band and have similar excited and non-excited signal amplitudes. This typically includes AC electrical noise at 60 Hz (US plants) and one or more harmonics of the AC noise as well as the recirculation pump drive frequency noise and/or drive frequency noise harmonics. Electrical or mechanical interference associated with the recirculation pump vane passing frequency may also be present.

Figure 4-6 provides a frequency domain PSD plot [[
]] for GGNS. The PSDs are [[
]]. The sensor locations consisted of eight strain gauges mounted in the circumferential direction at a spacing of 45 degrees. In this setup, pairs of gauges 180 degrees apart were wired together in series to average the signals, thus canceling out the pipe bending effects in that plane. The signals from the individual pairs are plotted in purple, green, yellow, and blue. As can be seen in the figure, the individual gauge signals in many frequency bands diverge as a result of the pipe vibration. The black line shows the PSD for the time domain average of the signals for the four pairs of strain gauges. The signals are averaged to define the average hoop strain that is proportional to the average dynamic pressure at the monitoring location. To evaluate data integrity, the individual signals are plotted and reviewed to identify potential problems with individual channels that could skew the averaged data.

For the data set shown in Figure 4-6, the bridge excitation was set at 10 VDC. Higher excitation voltages provide a better signal to noise ratio; however, the voltage must be limited to limit gauge heating and the associated signal drift. The blue dotted line is non-excited data set that was taken immediately following the 10 VDC data collection. This data set helps identify signals caused by electrical noise ([[ ]]). The plot also shows the coherence between the averaged signals at this location (A-Upper) and at the other sensor location on the line (A-Lower). [[

]] Acoustic resonances in the SRV standpipes will also show a high degree of coherence. [[

]]

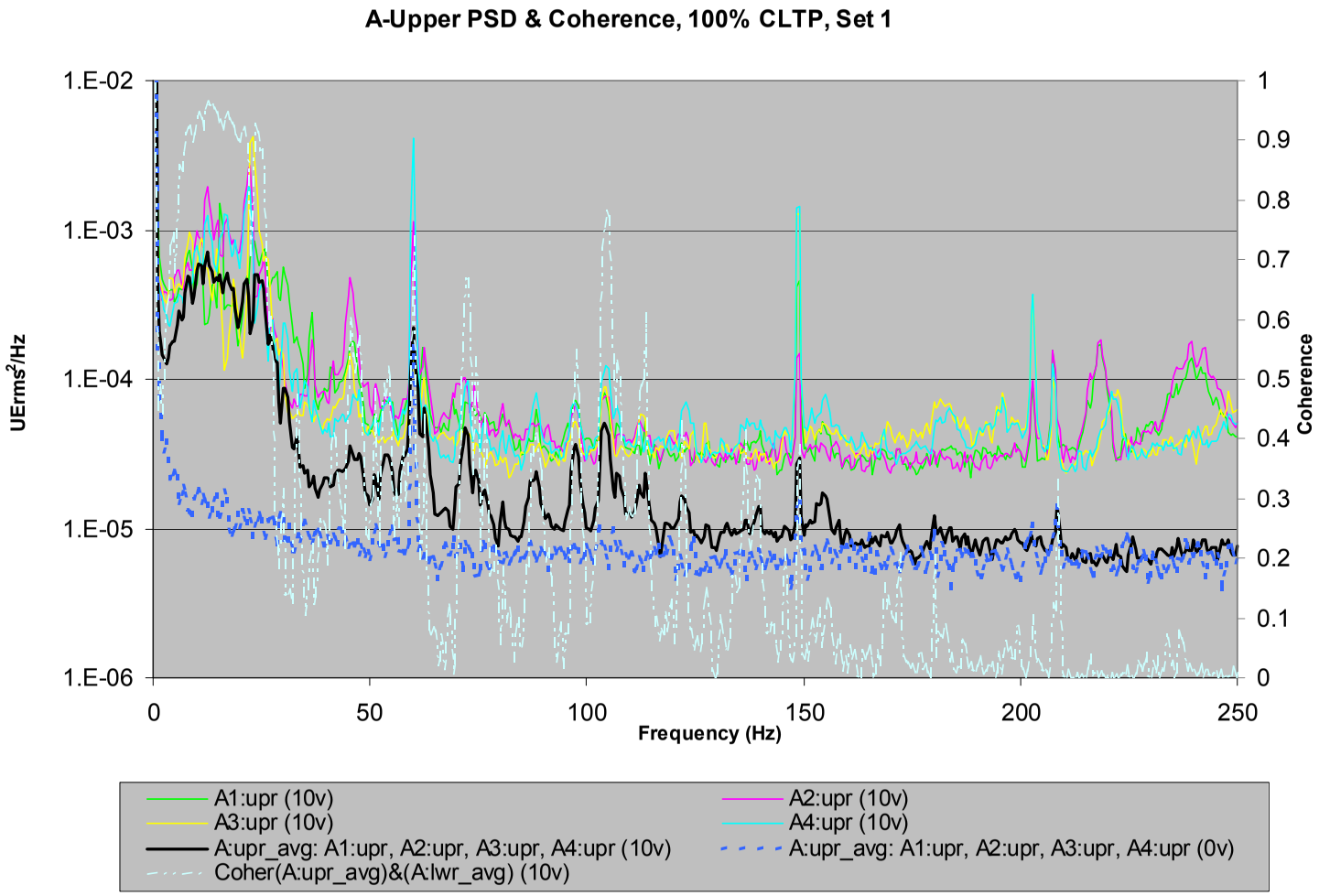

Figure 4-6 A-Upper PSD & Coherence, 100% CLTP, Set 1

4.4.2 Signal Filtering

Electrical noise is filtered from the measurements before using the strain gauge data to develop the dryer load definition. The electrical noise bands are identified and the basis for defining electrical noise bands documented. Comparisons of measurements taken with and without the bridge excitation help to differentiate between electrical noise and acoustical sources. Figure 4-7 illustrates this excitation/no excitation comparison. Without excitation, the acoustic signal content is removed and only the 60 Hz fundamental and 180 Hz third harmonic electrical line interference remain.

[[

]]

Figure 4-7 Identification of Electrical Interference

The potential for masked acoustic response in the electrical noise frequency bands were evaluated with other available dynamic plant instrumentation. Waterfall plots of the measurements taken during power ascension (e.g., Figure 3-17) are also useful for differentiating between electrical interference (relatively constant amplitude) and FIV content (amplitude grows with increasing steam flow). For example, in Figure 4-7, the narrow band maxima in the averaged signal coincide with the blue dotted non-excitation signal [[

]]

The width of the electrical peak on the zero excitation measurement is used to determine the width of the notch filter used to remove the electrical interference. The electrical frequencies that were notch filtered can be filled at the amplitudes of the neighboring non-filtered measurements to minimize the potential non-conservative bias introduced by the notch filtering. The filtered bands are compared with the filtering performed for the benchmark plants to assess whether the plant-specific filtering may contribute additional bias to the dryer load predictions.

The data is high- and low-pass filtered to remove the signal content below 2 Hz and above 250 Hz. Filtering out the data below 2 Hz removes any residual DC signal that was not removed by the strain gauge null and calibrating process.

4.4.3 Strain Conversion to Pressure and Measurement Bias

This section describes the method used to determine and quantify the bias and uncertainty involved with a given MSL instrumentation system. [[

]]

The strain gauge measurement bias (or correction factor) is determined by:

[[ ]] (4-1)

Where:

[[

]]

The individual strain gauge time domain signals at each location are averaged and converted to pressure by applying the strain-to-pressure conversion factor determined [[

]]. The resulting pressure time histories are then input to the PBLE calculation of the loads for each load case and frequency range. Because the correction factor or bias is already included in the loads that are used to determine the peak stresses, it is not included as a separate bias term in the final calculation of the peak stress.

5.0 BASIS FOR PROJECTED FIV LOAD TO EPU

5.1 TRENDING TEST DATA

5.1.1 Trend and Project Non-Resonance Data

Trending is performed to characterize the increase in FIV load as a function of frequency and MSL flow velocity and project the load to EPU conditions. The EPU scaling factor is [[

]].

Plant MSL data for GGNS was obtained at 75% through 100% CLTP in 2008. Waterfall plots of PSD data are provided in Appendix G. The MSL data provides a benchmark of the local and aggregate change in acoustic loading. However, for this methodology, the EPU Scaling Factor is developed [[

]]

This provides a direct assessment of the change in [[ ]] a function of MSL steam velocity. [[

]]

[[

]]

Figure 5-1 Acoustic Mesh Points

The trending evaluation was performed for [[

]]. For each test condition the [[ ]] at each test condition. [[

]] For each test condition, measured plant operating data recorded by the plant process computer was used for temporal mass flow and steam property data that was used to calculate the MSL velocity. A typical set [[ ]] is included Figure 5-2.

The MSL velocities used in Section 3 of this appendix were based on reactor steam density and mass flow. [[

]] and therefore provide a more accurate assessment. The adjusted values are provided in Table 5-1. The projected velocity for GGNS at EPU conditions is [[ ]].

Table 5-1 Steam Velocity Adjusted for Flow Losses (GGNS)

Test Condition	Mass Flow (Mlbs/hr)	MSL Velocity (ft/sec)
[[		
		]]

[[

]]

Figure 5-2 [[ ]]

The pressure load data is trended using the following formulation:

[[ ]] (5-1)

Where,

[[ ]] (5-2)

[[

]]

An example of a trending evaluation [[ ]] is included in Figure 5-2. The trend lines for GGNS were calculated [[ ]] conditions. The data points for the highest steam velocity [[

]]

Data trends were performed with different trending equations prior to settling on equation 5-1. This relation provided a good fit [[ ]] and supports previous observations that non-resonant loads grow in relation to velocity squared. [[

]] Figures 5-3 through 5-7 show trend plots [[ ]]. These trend plots demonstrate that Equation (5-1) adequately represents the trend [[ ]].

[[

]]

Figure 5-3 Typical Trending Plot [[ ]]

[[

]]

Figure 5-4 Typical Trending Plot [[ ]]

[[

]]

Figure 5-5 Typical Trending Plot [[ ]]

[[

]]

Figure 5-6 Typical Trending Plot [[ ]]

[[

]]

Figure 5-7 Typical Trending Plot [[ ]]

The EPU Scaling Factor is then defined as [[

]]. As described in Section 8, the EPU Scaling Factor is applied to the calculated peak stresses in the form of a bias term.

The EPU Scaling Factor can then be determined [[

]]:

[[ ]] (5-3)

[[ ]]

[[ ]] (5-4)

For consistency with definitions of model biases, the bias associated with the EPU Scaling Factor is defined as:

$$B_{EPU} = 1 - SF_{EPU} \quad (5\text{-}5)$$

The EPU Scaling Factor is determined by [[

]].

5.1.2 Trend and Project SRV Resonance Data

During power ascension it is necessary to track and project the SRV acoustic response. The SRV resonance is characterized by response that is similar to a half-sine wave shape as shown below in Figure 5-8 (Ziada, Reference 6) and in Figure 3-19. After an initial onset period the load projections can be reasonably made with modest power ascension power steps and linear projections to estimate the dryer load amplitude at the next test period. The load at step *n*, can be predicted as

[[ ]] (5-6)

Where,

[[

]]

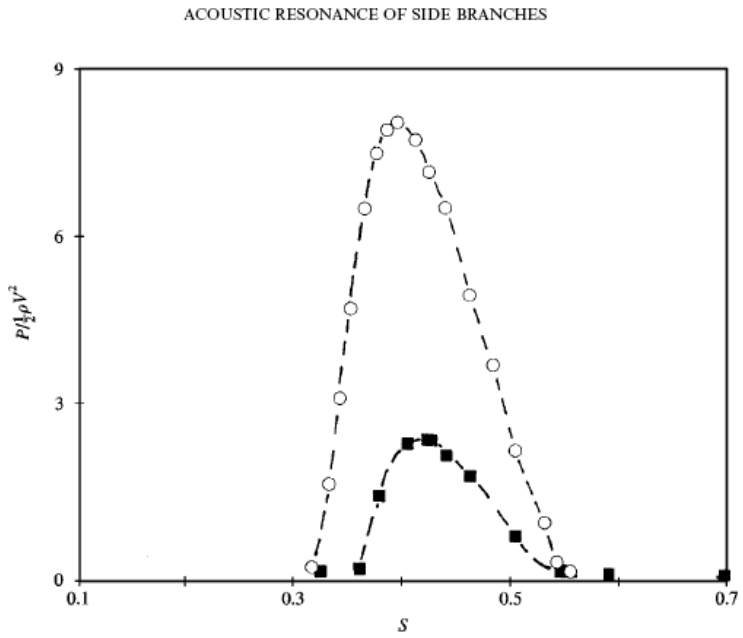

Figure 5-8 Strouhal Numbers of Flow-Excited Acoustic Resonances of Closed Side Branches (Reference 6)

5.2 CLTP LOAD SET SELECTION FOR PBLE LOAD DEVELOPMENT

The [[ ]] CLTP data were evaluated and demonstrated to be [[ ]]. Table 5-2 provides [[

]]

Table 5-2 Evaluation of CLTP Data

[[

]]

Test Condition 100%-J was selected for the development of the PBLE loads. This test condition is compared in Table 5-3 [[

]].

Table 5-3 Comparison of Test Condition 100%-J [[ ]]

[[

]]

5.3 SRV SCALING FACTOR

When an SRV branch line resonance is in early onset or not yet observed in the MSL data, [[

]], and to assess the effect on the GGNS replacement dryer.

5.3.1 Development of Simulated SRV Loading for FE Analysis

This section discusses the development of SRV resonance load adders that are used in the base load for performing the structural analysis. For a plant with multiple SRV valves in each MSL with similar geometry, a band of potential frequency responses can be predicted for each line. The exact frequency response, location of prevailing acoustic source, and phase relationship between the acoustic source and the MSL mode at increased steam flow is difficult to predict. The load source location and relative phase can have a significant effect on the magnitude and distribution of dryer load.

The approach used for GGNS was to [[

]]

- The method used to create simulated SRV resonance loads at potential SRV frequencies [[ ]],
- The evaluation of the acoustic load sensitivity [[ ]],
- The determination of the best parameter [[ ]], and
- The combination of the SRV resonance load adders with CLTP data for the structural FE analysis.

5.3.1.1 SRV Resonance Load Generation

To create a simulated SRV resonance load, [[

]]

[[ ]]

The equations are then rearranged to provide the solution for

[[ ]]

[[
]]

5.3.1.2 SRV Load Source [[ ]]

The above solution was executed [[
]]. The results demonstrated that [[

]]. Therefore a relatively simple method was developed to define [[ ]] simulated SRV loads [[
]].

To evaluate the acoustic load sensitivity, [[

]]. As expected, the GGNS dome acoustic response shows

variability in loading as the driving frequencies are changed. The key observation is that with a good selection [[ ]] can be provided with high loading for the analysis.

[[

]]

Figure 5-9 Sensitivity Study for SRV Acoustic Loads [[ ]]**.**

5.3.1.3 SRV Resonance Modeling in Structural Analyses

[[ ]] SRV resonance frequencies [[ ]] were selected to be included in the GGNS structural analysis (See Section 3 of this Appendix). These loads were scaled and combined with PBLE acoustic loads developed from CLTP data and this combined load is used in the FE structural analysis of the dryer.

The [[ ]] SRV resonance load adders [[

]]. This methodology provides a load definition for finite element structural analysis [[
]] in combination with turbulence driven CLTP FIV loads [[
]] to be used for evaluation. With the nine load definition time step sensitivity cases, the four SRV resonance load adders provide ample data to conservatively characterize the relation between potential SRV resonance dryer loads and dryer stress. Figure 5-10 provides an example [[ ]] load input with the [[ ]] SRV resonance load adders and compares that load with the average and peak hold CLTP data [[ ]].

The scaling of the SRV resonance load adders [[
]] is performed [[ ]] and [[
]] the bias and uncertainty evaluations performed after completion of the structural analysis. This methodology is described in Section 8 of this Appendix.

[[

]]

Figure 5-10 Comparison of FE Structural Model FIV Input with SRV Resonance Load Adders with Projected Loads at CLTP.

5.3.1.4 Power Ascension Monitoring

During power ascension testing by Entergy at Vermont Yankee in 2006 and at the prototype BWR/4 in 2009 and 2010 with GEH criteria, monitoring and acceptance limits were based on MSL strain gauge limits. With the exception of SRV resonances the change in steam line signals are very gradual and MSL strain gauge limits are practical for monitoring the power ascension for these loads. [[

]]

[[

]]

Figure 5-11 Variation of MSL Indicated Pressure [[ ]]

5.3.2 Projecting Simulated SRV Loading to EPU

Section 5.3.1 of this Appendix discussed the development of SRV resonance load adders that were used to develop the base load for performing the structural analysis. This section discusses the development of scaling factors that are designed to project potential SRV loading up to EPU conditions. These scaling factors are used with other scaling factors and biases and uncertainties in determining the final peak stresses as discussed in Section 8 of this Appendix. [[ ]] different projected EPU conditions were evaluated. These include:

1. [[

]]

The SRV resonance loads were scaled such that the projected GGNS design basis loads bounded the projected peak resonant response loads from plants with similar [[

]]

design. The projected [[ ]] SRV resonance dryer load is scaled to the full GGNS projected Strouhal number at EPU for each of the SRV resonance load adder frequencies. This evaluation is performed in Section 3 of this Appendix.

5.3.2.1 Comparison of Projected Loads to Plant Data

The FE element input loads for GGNS SRV resonance load adders were compared with the projected dryer load data at test conditions for the [[ ]] plants. The loads at the [[ ]] plants were projected [[

]] with a PBLE model for each plant. [[

]]

There was insufficient test data for [[ ]] a PBLE load definition. Therefore the [[ ]] was compared with loads projected on the GGNS dryer at the same location. (See Figure 5-12.)

[[

]]

Figure 5-12 Pressure Sensor Location [[ ]]

For the [[ ]] plants (including GGNS), there were long periods of test data available. The [[ ]] value used in the comparison were the [[ ]]. For the [[ ]], only [[ ]] was available. Therefore the [[ ]] were conservatively compared with a [[ ]] value based on [[ ]]. Figures 5-13 through 5-17 show the GGNS load definitions (including the SRV resonance load adders) compared with the [[ ]] plants based on measured plant data.

As shown in Figure 3-20, both the [[ ]] plant data, the branch line response had peaked prior to maximum plant steam flow. For the [[ ]], it was [[ ]] and for the [[ ]] plant it was prior to [[ ]]. The test conditions at both plants bracketed the projected peak response. Based on the data trend curve, it is expected

that the amplitude may have increased [[ ]] above the test condition amplitude.

The [[ ]] plant has a very similar branch line arrangement when compared to GGNS. The [[ ]] plant was at [[ ]] of OLTP for the test condition shown in Figures 5-13 through 5-15. This is the maximum test condition available. The branch line resonance is [[ ]]. At this plant there are [[ ]] main response frequencies, [[ ]]. The projected [[ ]] is scaled to the full GGNS projected Strouhal number at EPU for each of the SRV resonance frequencies. This evaluation is performed in Section 3 of this Appendix.

Table 5-4 summarizes the [[ ]] factors applied to the test conditions from each of these plants for comparison with the GGNS EPU design conditions. These factors are then converted to a Bias for consistency with the conversion used for load scaling.

Table 5-4 SRV Load Factors Applied to [[ ]] for Comparison with GGNS EPU SRV Load Conditions

Factor=PlantProj/PlantTest	[[					
Target Bias=1-PlantTest/PlantProj						]]
Minimum Scaling Requirements	**Min Factor**	**Target Bias**	**Min Factor**	**Min Bias**	**Min Factor**	**Min Bias**
[[						
						]]

[[

]]

Figure 5-13 Comparison of FE Structural Model FIV Input [[
]]

[[

]]

Figure 5-14 Comparison of FE Structural Model FIV Input [[
]]

[[

]]

Figure 5-15 Comparison of FE Structural Model FIV Input [[
]]

[[

]]

Figure 5-16 Comparison of FE Structural Model FIV Input [[
]]

[[

]]

Figure 5-17 Comparison of FE Structural Model FIV Input [[
]]

The following adjustment factors shown in Table 5-5, when applied to the SRV resonance load adders, will provide dryer loads that match or exceed the projected loads for the [[ ]] comparison plants. [[

]]

Table 5-5 SRV Resonance Load Factors Applied to Define SRV Resonance Conditions at EPU

[[						

[[						
						]]

Table 5-6 compares the minimum Target Bias values from Table 5-3 with those realized with the EPU design conditions. The applied EPU design load will meet or exceed the projected EPU load from the [[ ]] comparison plants.

Table 5-6 Comparison of Dryer SRV Loads from [[ ]] GGNS EPU Conditions with Dryer SRV Loads from [[ ]] Test Conditions.

[[				
				]]

5.3.3 Projecting Simulated SRV Loading to CLTP

Load scaling for CLTP and EPU are treated as bias and uncertainties in the GEH adjusted stress methodology. This facilitates proper accounting for all model bias and uncertainties when the model is used for projection.

The SRV resonance load adders are compared with CLTP loads at GGNS [[

]].

The CLTP bias and uncertainty is then expressed as:

[[ ]] (5-7)

[[ ]] (5-8)

The input for the adjusted stress routine requires that the bias and uncertainty be expressed [[

]].

Table 5-7 CLTP SRV Resonance Load Adder Bias and Uncertainties

[[

]]

6.0 STEAM DRYER FLUCTUATING PRESSURE LOAD DEFINITION

The dryer structural analysis must demonstrate that the dryer will maintain its structural integrity without failing due to fatigue during normal plant operation when subjected to the vibrations resulting from acoustic and fluctuating pressure loads. During normal operation, fluctuating pressure loads are created by the flow adjacent to the dryer (FIV loads) and from acoustic pressures generated by sources in the reactor dome and MSLs (e.g., acoustic resonances in the safety/relief valve standpipes). Appendix B provides the methodology for developing the fluctuating pressure load definition using measurements from on-dryer instrumentation. Appendix C provides the methodology for developing the load definition using measurements taken from the MSLs.

The following steps provide a brief summary of the dryer FIV load definition calculation with the PBLE from the MSL measurements described in Section 4 of this appendix. The same process is followed, with the exception of the MSL parameters and Transmatrix, when on-dryer measurements are used as inputs:

- [[

]]

- The potential SRV acoustic resonance load signals identified in Sections 3 and 5 of this appendix are included in the time segment data.
- [[

  ]] the PBLE MATLAB® scripts are run and dryer loads are obtained.

The resulting load definition is applied to the structural finite element model as described in the following section.

7.0 FATIGUE STRESS EVALUATION

The dryer structural analysis must demonstrate that the dryer will maintain its structural integrity without failing due to fatigue during normal plant operation. Appendix E describes the methodology for constructing the finite element structural models and performing the fatigue stress evaluation using the fluctuating pressure load definition described in Section 6 of this appendix.

8.0 STRESS ADJUSTMENT FOR END TO END BIAS AND UNCERTAINTY

8.1 METHOD

This section identifies the biases and uncertainties in the overall evaluation of the steam dryer, explains how the biases and uncertainties are combined, and how these bias and uncertainties are applied to the stress results to determine the adjusted peak stress [[
]]. This adjustment includes projection to EPU.

The GEH acoustic model uses frequency dependent medium properties in which the harmonic frequency domain solution is linear. Therefore uniform frequency dependent changes in the input will have a proportional affect on the output at the same frequency. The GEH finite element dryer structural model employs the time domain direct integration solution method. This is performed assuming all linear model properties. [[

]] During the power ascension at Vermont Yankee, Entergy first used the [[ ]] method (Reference 7). Later GEH used the [[ ]] method and added the [[ ]] method to support the Susquehanna power ascension testing (Reference 8). Because these techniques are linear, and because the acoustic load and stress models are linear, the bias, uncertainty, and EPU adjustment that affect the loads can be combined with the structural model bias and uncertainty and applied directly to the peak stress results.

The process for determining the peak stress for the steam dryer is based on the following steps:

1. Obtain plant MSL data and generate PBLE loads at CLTP and lower power test points for trending.
2. Generate simulated dryer loads of nominal amplitude (referred to as “SRV resonance load adders”) for potential SRV resonant frequencies that may appear between CLTP and EPU.
3. Select time segments of the PBLE loads at CLTP that contain excitation over all frequencies and strong loads at frequency bands that contribute significantly to the dryer stress in the most limiting locations. This last selection is based on a preliminary stress analysis.
4. Combine the simulated SRV resonance loads with CLTP loads at selected time segments.
5. Run the FE time history stress analysis for the nine load time step variation cases. The load time step is varied from the nominal case by ±10%, ±7.5%, ±5% and ±2.5%. This is done for both a low frequency analysis to cover the structural response from 2-135Hz, and a high frequency analysis to cover the structural response from 135Hz to 250Hz.
6. Elements with high peak stress from all areas of the dryer for all nine LF and nine HF time step conditions are then selected for stress adjustment.

The following parameters are used in the peak stress adjustment:

1. Strain to Pressure Uncertainty (Bias addressed in Strain to Pressure conversion)
2. EPU Bias (for stress adjustment to EPU conditions)
3. CLTP Bias and Uncertainty (for adjustment of "SRV resonance load adders to observed CLTP amplitude.)
4. PBLE Load Projection, [[ ]], Bias and Uncertainty
5. PBLE Load Projection, [[ ]], Bias and Uncertainty
6. [[ ]] Acoustic Mesh and Model Bias and Uncertainty
7. FE Element Model Bias and Uncertainty
8. CLTP Time Interval Selection Bias

To determine the adjusted peak stresses for an evaluation, the following input is required

- [[

]]

- Biases and uncertainties described in the previous sections

The adjusted stresses are calculated for each of the nine load cases. There are [[ ]] methods for calculating the final peak stresses and all [[ ]] methods are used and for each dryer component, the maximum peak stress is selected as the limiting stress value from the [[ ]] methods. Table 8-1 summarizes the [[ ]] methods and applicable bias and uncertainty terms that are included along with the stress adjustment methodology.

Table 8-1 Peak Stress Calculation Methods

[[				

[[				
				]]

The biases and uncertainties are applied [[
]] in accordance with the methodology identified in this Appendix. The maximum of the calculated stress from the [[ ]] methods and nine load cases for each dryer component is then summarized in a final stress table.

8.2 BIASES AND UNCERTAINTIES

8.2.1 Strain to Pressure Calibration Uncertainty

The uncertainty in the measurement system can be directly quantified by comparing the variation in the gauge measurements between the converted pressures when compared to the plant instrumented pressure reading per sensing location. As discussed in Section 4.3.1.1 of this appendix, the average error or bias from this comparison is used to adjust the strain to pressure conversion factor for each strain gauge sensing location. [[

]] This uncertainty is independent [[ ]]. It represents the uncertainty in the plant specific strain gauge calibration factor (SGCF) bias values.

The larger bias and uncertainty from strain gauge measurements is introduced in dynamic measurements where mechanical vibration can be interpreted as acoustic pressure. This has been addressed in the bias and uncertainty in the PBLE benchmark comparisons between predicted pressure and on-dryer pressure gauges as discussed in Appendix C.

8.2.2 EPU Scaling Factor (Bias)

From the trending relations developed in Section 5 of this Appendix, the EPU Scaling Factor is determined [[ ]] as:

[[ ]] (8-1)

[[ ]] (8-2)

[[

]]

When expressed as a bias, for consistency with definitions of model biases, the bias associated with the EPU Scaling Factor is defined as:

$$B_{EPU} = 1 - SF_{EPU} \quad (8\text{-}3)$$

The EPU Scaling Factor is determined [[

]].

To address the potential for SRV resonances as steam flow is increased up to EPU power levels, SRV Scaling Factors are developed (Section 5 of this Appendix). These scaling factors represent the potential increase in magnitude of the pressure loading [[

]]. These scaling factors are based on a review of the plant MSL data that was obtained during power ascension and is also supplemented with available plant data from similar BWRs. The objective of the SRV scaling factor is to provide a design basis pressure loading for the evaluation of the steam dryer [[

]]. The SRV scaling factors also are part of the development of the limit curves that are used during plant startup to demonstrate compliance with the design basis stress analysis.

Similar to the treatment of the EPU Scaling Factor, the SRV Scaling Factor can then be represented as [[ ]]:

[[ ]] (8-4)

[[

]] When expressed as a bias, for consistency with definitions of model biases, the bias associated with the SRV Scaling Factor is defined as:

$$B_{SRV} = 1 - SF_{SRV} \quad (8\text{-}5)$$

The SRV Scaling Factor is initially determined based on [[

]].

By treating the EPU factors and potential SRV resonances as bias terms, there is appropriate treatment of combined bias and uncertainty; this is especially important for uncertainty terms that scale with pressure loads.

8.2.3 PBLE Loads Bias and Uncertainty

The PBLE plant benchmark evaluations (as reported in Appendix B and Appendix C) form the basis for the generic PBLE application bias and uncertainty values. The biases and uncertainties have been developed based on comparisons to plant measured data with instrumented steam dryers. The results are provided [[
]].

The bias is expressed in the following manner:

(8-6)

[[ ]]

Where,

(8-7)

[[ ]]

(8-8)

[[ ]]

[[

]]

8.2.4 PBLE Model – [[ ]] Bias and Uncertainty

The [[ ]] PBLE model bias and uncertainties are documented in Table 10 of Appendix C, which represents the biases and uncertainties for loads generated based on MSL data input. Table 8-2 summarizes the bias and uncertainty values that are applicable for loads generated based on MSL data input.

Table 8-2 PBLE Model [[ ]] Bias and Uncertainty

[[					
					]]

8.2.5 PBLE Model – [[ ]] Bias and Uncertainty

[[

]] As discussed in Appendix C, [[

]].

The PBLE [[ ]] bias and uncertainties are documented in Appendix K of Appendix C of this report. Table 8-3 provides the cross reference to the correct tables in Appendix K of Appendix C of this report.

Table 8-3 PBLE Model [[ ]] Bias and Uncertainty

[[			
			]]

8.2.6 GGNS Acoustic Mesh - Model Bias and Uncertainty

An acoustic model geometric sensitivity study is presented in Section 2.2.2 of Appendix B. [[

]]

[[

]]

Figure 8-1 [[ ]]

[[

]]

Figure 8-2 [[ ]]

[[

]]

Figure 8-3 [[ ]]

[[

]]

Figure 8-4 [[ ]]

[[

]]

Figure 8-5 [[ ]]

8.2.7 Finite Element Model Peak Stress Bias and Uncertainty

In 2009, uncertainties and bias errors associated with the finite element structural models of the steam dryer were provided to the NRC based on benchmarking against an instrumented dryer that included strain gauges and accelerometers. This information has been included in the Reference 9 GGNS submittal. The prototype steam dryer was instrumented with [[

]].

The FIV PBLE load data for this benchmark evaluation was developed using [[

]]. The FE model was run with [[

]] Nine frequency sensitivity cases were performed with time step size increments of ±2.5% up to a shift of ±10%. [[

]]

To calculate the FE model contribution to the overall bias and uncertainty, [[

]]

Table 8-4 FE Model [[ ]] Bias

[[		
		]]

8.2.8 Time Segment Selection Bias

For direct integration structural assessments, a conservative time segment that maximizes both the frequency content and amplitude [[

]]. The time interval bias factor is based on an assessment of [[

]]. Therefore, the time interval of test data in the load definition will include a conservative time segment based [[ ]] and a time interval bias factor based [[ ]].

8.3 STRESS ADJUSTMENT [[ ]] WITH BIAS AND UNCERTAINTY

[[

]]

[[(8-9)

]]

[[

]]

Table 8-5 [[ ]]

[[

]]

8.3.1 Combining Biases and Uncertainties [[ ]]

[[

]]

[[ ]] (8-10)

[[ ]] (8-11)

[[

]]

[[ ]] (8-12)

[[

]]

[[ ]] (8-13)

[[

]]

[[ ]] (8-14)

[[

]]

[[ ]] (8-15)

[[ ]] (8-16)

[[ ]]

[[ ]] (8-17)

[[ ]]

[[ ]] (8-18)

[[

]]

[[ ]] (8-19)

[[ ]] (8-20)

[[ ]] (8-21)

[[

]]

8.3.2 Calculating Bias and Uncertainty [[ ]]

The [[ ]] Biases are combined in accordance with the flow chart shown in Figure 8-6.

The [[ ]] Uncertainties are combined in accordance with the flow chart shown in Figure 8-7.

[[

]]

Figure 8-6 [[ ]] **Bias Calculation** [[ ]]

[[

]]

Figure 8-7 [[ ]] **Uncertainty Calculation** [[ ]]

8.3.3. Calculating Adjusted Stress [[ ]]

[[ ]]

[[ ]] (8-22)

[[ ]] (8-23)

[[

]]

[[ ]] (8-24)

[[

]]

[[ ]] (8-25)

8.3.4 Calculating Bias and Uncertainty [[ ]]

The [[ ]] Biases are combined in accordance with the flow chart shown in Figure 8-8.

The [[ ]] Uncertainties are combined in accordance with the flow chart shown in Figure 8-9.

[[

]]

Figure 8-8 [[ ]] Bias Calculation [[ ]]

[[

]]

Figure 8-9 [[ ]] **Uncertainty Calculation** [[ ]]

8.3.5 Calculating Adjusted Stress [[ ]]

[[

]]

8.4 STRESS ADJUSTMENT [[ ]] WITH BIAS AND UNCERTAINTY

[[

]]

8.4.1 Combining Biases and Uncertainties [[ ]]

[[ ]]

[[ ]] (8-26)

[[

]]

[[ ]] (8-27)

[[ ]] (8-28)

[[

]]

[[ ]] (8-29)

[[

]]

8.4.2 Calculating Bias and Uncertainty [[ ]]

The [[ ]] Biases are combined in accordance with the flow chart shown in Figure 8-10.

The [[ ]] Uncertainties are combined in accordance with the flow chart shown in Figure 8-11.

[[

]]

Figure 8-10 [[ ]] Bias Calculation [[ ]]

[[

]]

Figure 8-11 [[ ]] **Uncertainty Calculation** [[ ]]

8.4.3 Calculating Adjusted Stress [[ ]]

[[ ]]

[[ ]] (8-30)

[[ ]] (8-31)

[[

]]

[[ ]] (8-32)

[[

]]

[[ ]] (8-33)

8.4.4 Calculating Bias and Uncertainty [[ ]]

The [[ ]] Biases are combined in accordance with the flow chart shown in Figure 8-12.

The [[ ]] Uncertainties are combined in accordance with the flow chart shown in Figure 8-13.

[[

]]

Figure 8-12 [[ ]] Bias Calculation [[ ]]

[[

]]

Figure 8-13 [[ ]] Uncertainty Calculation [[ ]]

8.4.5 Calculating Adjusted Stress [[ ]]

[[

]]

8.5 ADJUSTED STRESS RESULTS

Table 8-6 below summarizes stress results [[ ]] used in the stress assessment, [[ ]]. This summary was done for the limiting EPU Condition, [[

]].

The table demonstrates that the [[

]]. With the conservative treatment of the uncertainty, the dryer still maintained a MASR of greater than 2.0.

[[

]]

Table 8-6 [[ ]]

	[[					

-----	-----	-----	-----	-----]]		

9.0 PRIMARY STRESS EVALUATION

The steam dryer is a non-safety component and performs no active safety function; however, the dryer must maintain structural integrity during normal, transient and accident conditions and not generate loose parts that may interfere with the operation of safety systems. Sections 7 and 8 of this appendix describe the fatigue evaluation process used to demonstrate that the dryer alternating stresses are sufficiently low to preclude the initiation of high cycle fatigue cracking during normal plant operation. This section describes the input loads and load combinations used to evaluate the primary stresses during normal, transient and accident conditions and demonstrate that the dryer will maintain structural integrity during all modes of operation. Appendix E describes the methodology for constructing the finite element structural models and performing the primary stress evaluation using the loads and load combinations described in this section.

9.1 DESCRIPTION OF DESIGN CONDITIONS

Plant operating conditions are defined in Chapter 15 of a plant's Updated Final Safety Analysis Report (UFSAR). These operating conditions are categorized and reflect varying probabilities of conditions, which are then compared against appropriate acceptance criteria. The main design conditions are defined as:

Normal	Normal steady-state operation
Upset	Anticipated operational transients (e.g., turbine trip, stuck open relief valve)
Emergency	Infrequent operational transients (e.g., inadvertent opening of ADS valves)
Faulted	Accident and rare transients (e.g., LOCA, SSE)

The limiting design basis condition for the steam dryer is the double-ended guillotine break of the MSL outside containment. For this event, the steam dryer must maintain its structural integrity and not generate loose parts that may interfere with the closure of the main steam isolation valves.

9.2 LOAD COMBINATIONS

The load combinations are plant-specific and are defined in the plant's design basis. Typically the load combinations used for the steam dryer analysis are specific to the candidate plant in question. These combinations are specified in a plant's Steam Dryer Design Specification and the analyses are performed over a range of conditions that support the licensed operating domain. The ASME load combinations for a typical plant are shown in Table 9-1. Definitions of the individual loads and calculation methodology are specified in the following section. Loads from independent dynamic events are combined by the square root sum of squares method (SRSS). The dryer is at uniform temperature at normal and transient conditions, and therefore the thermal

expansion stress is assumed zero. There is no radial constraint of the dryer, and differential expansion is accommodated by slippage.

Table 9-1 Typical Steam Dryer Load Combinations

Comb. No	Level	Combination
A-1	Normal	[[
B-1	Upset	
B-2	Upset	
B-3	Upset	
B-4	Upset	
B-5	Upset	
C-1	Emergency	
D-1	Faulted	
D-2	Faulted	
D-3	Faulted	
D-4	Faulted	
D-5	Faulted	]]

Definition of Load Acronyms:

[[

]]

9.3 INDIVIDUAL LOAD TERM DEFINITION AND SOURCE

9.3.1 Static Loads

The following loads are considered to be static loads that are applied during steady-state operating conditions.

9.3.1.1 Dead Weight (DW)

The stresses caused by metal and water weight are obtained by applying gravity (G) loading to steam dryer FE model.

9.3.1.2 Thermal Expansion

The steam and water temperatures at each dryer component are the same at saturated pressure/temperature conditions. The RPV transient temperature changes for all operating events are mild in the steam space where the dryer is located. The materials for the steam dryer components are of the same type of stainless steel and, therefore, have the same thermal expansion coefficient. Although the RPV is carbon steel and has a lower thermal expansion coefficient, the dryer support ring is not radially constrained by the RPV and therefore the loads due to thermal expansion effects on the dryer are negligible and do not need to be analyzed.

9.3.1.3 Differential Pressure Loads ($\Delta P_N, \Delta P_U$)

The operating pressure differentials across each dryer component are based on reactor internal pressure differences (RIPD) calculated for the applicable plant operating conditions. The ΔP loads assumed in the analysis depend on the service condition and event being analyzed. At normal conditions, the calculation of steady state pressure drops through the core is performed using the ISCOR computer program (Reference 10). This method has been applied to BWR/2

through BWR/6 designs as well as the ABWR to calculate the Normal condition reactor internal pressure differentials (RIPD). [[

]]

The static pressure drop across the steam dryer hoods is determined by the pressure drop through the vane banks plus the static pressure drop along the steam dryer hoods at the steam line nozzle locations (see Figures 9-1 and 9-2). The pressure drop across the dryer outer hoods has generally been determined for BWRs at OLTP conditions. For operation at higher steam flows experienced during EPU, the increased steam flow will increase the pressure drop along the steam dryer hoods. [[

]]

[[ ]] (9-1)

Where,

[[

]]

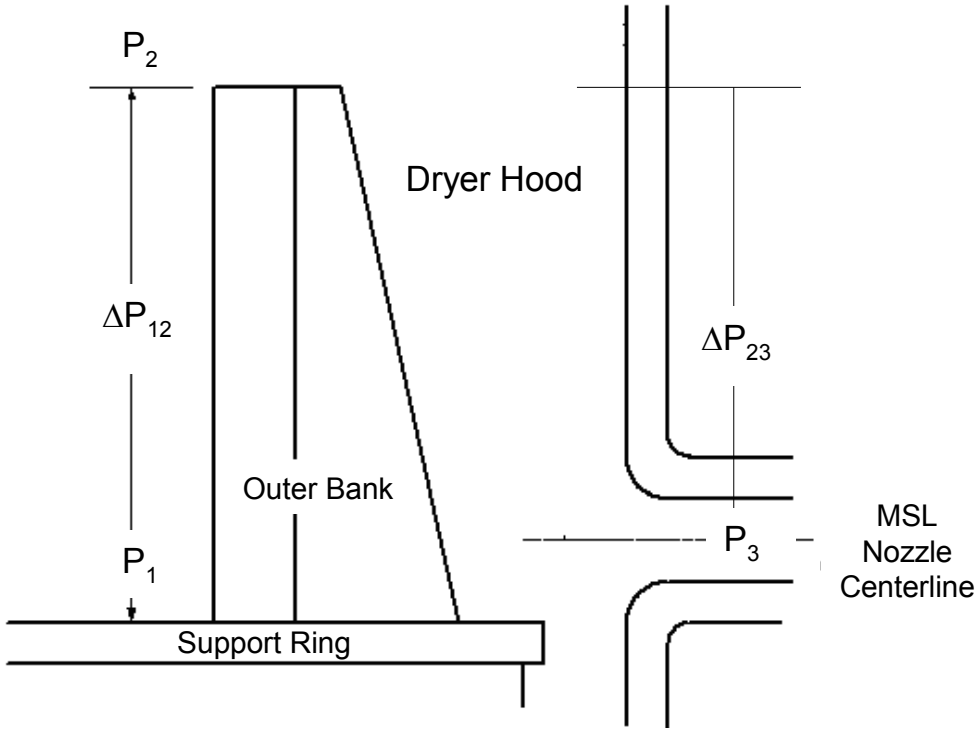

Figure 9-1 Steam Dryer Vane Bank and Outer Hood Pressure Drops

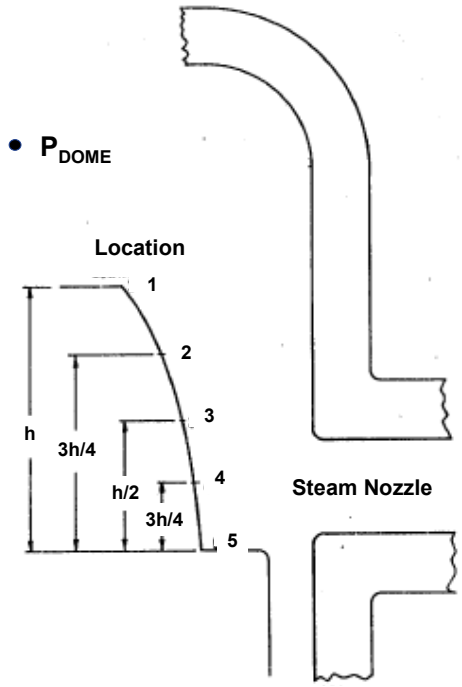

Figure 9-2 Steam Dryer Outer Hood Pressure Drops vs Elevation

The pressure drop resulting from Anticipated Operational Occurrences, or Upset Conditions, is calculated [[

]]

The opening of a safety relief valve can also result in loads on the dryer directly through the resulting pressure effects in the steamline and indirectly by transmission of the discharge loads through the containment structure and RPV. The flow transient produced by rapid opening of a single SRV generates a decompression wave in the MSL that affects the RPV dryer. The development of [[ ]] did not consider the case of one stuck open relief valve and this must be evaluated separately to confirm or replace the generic increment factor.

The one stuck open SRV event methodology develops [[
]] during the SRV event. [[

]]

[[ ]] (9-2)

[[ ]]

[[ ]] (9-3)

Where,

[[

]]

[[

]]

For accidents, or Faulted conditions, the pressure differentials across the steam dryer components [[

]]. These dynamic loads are discussed in more detail in the following section.

9.3.2 Dynamic Loads

Dynamic loads result from various off-normal operating conditions for the plant. The most basic dynamic load is the result of flow-induced vibration (FIV) where small variations in the pressure field of the steam flow are caused by turbulence, acoustic resonances and other sources. Other dynamic loads are the result of plant operational transient and accident conditions. The

following sections provide a discussion of the various dynamic loads and the methodology for calculation of the steam dryer loading.

9.3.2.1 Flow-induced Vibration (FIV_N, FIV_U)

The primary concern for the steam dryer structure is fatigue failure of the components from the FIV loading during normal operation. There are two primary sources of flow-induced vibration loads on the dryer. The first load is an acoustic pressure loading caused by the steam flow through the steam piping system. Based on in-plant measurements, the acoustic pressure loading is the dominant FIV load on the steam dryer. The second load is turbulent buffeting caused by the steam flow through and across the steam dryer structure. The velocities through the dryer are low; therefore, the contribution of the buffeting load to the total FIV load is negligible.

The detailed methodologies for determining the FIV loads for the steam dryer are outlined in Section 7 of this Appendix and in Appendix E. The FIV primary bending stresses and maximum primary membrane stresses for different components of the steam dryer are calculated with consideration for biases and uncertainties as discussed in Section 8 of this Appendix. Because the ASME Code load combination stress analysis is the primary structural stress assessment, the weld factor effect is not included in the final FIV loading (FIV_N).

The FIV load for the Upset Condition (FIV_U), is calculated [[

]]

9.3.2.2 Turbine Stop Valve Loads [[ ]]

A turbine stop valve closure produces [[ ]] loads on the steam dryer. [[

]]

The [[ ]] TSV loads are separated in time and are therefore applied separately.

The key assumptions of the methodology are summarized as follows;

- [[

]]

The TSV and turbine control valves (TCV) are basically in series, with connecting headers to equalize the pressure both in front and behind the TSVs. The turbine bypass valves (TBV) are on a header that connects to the MSLs in a manner similar to that shown in Figure 9-4.

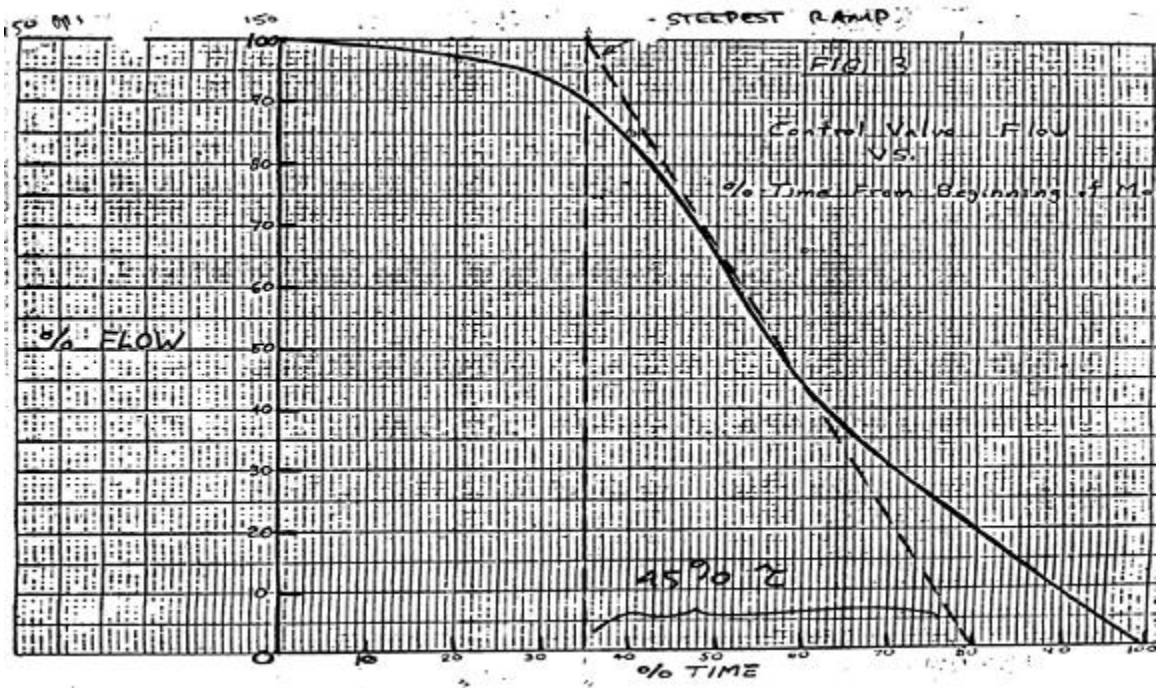

Figure 9-3 TSV Closure Characteristics

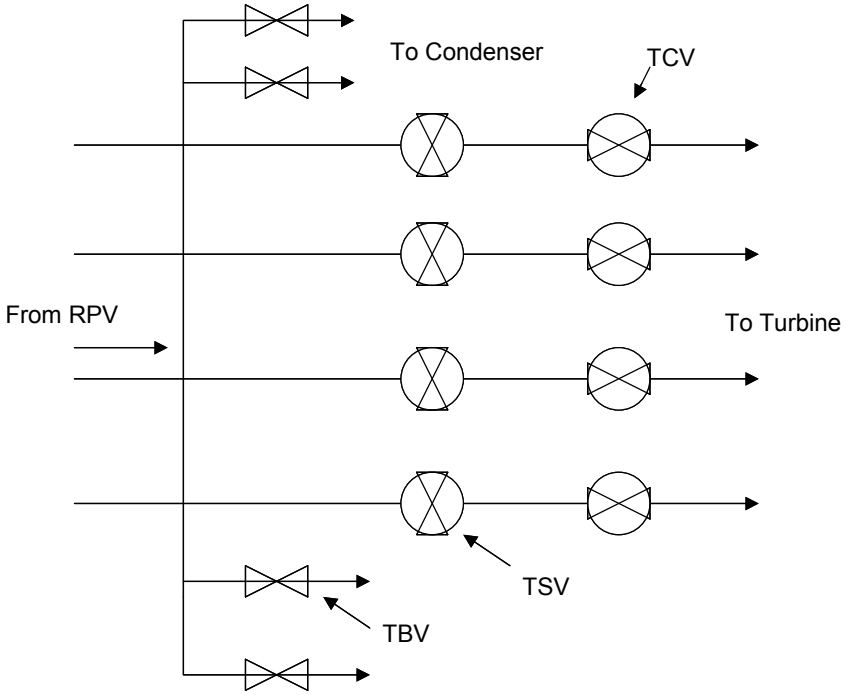

Figure 9-4 Turbine Valve Schematic

The rate of steam flow decrease during a valve closure event depends on the relative closing speeds and delay (if any) of the valves. If one valve closes faster than the other, the faster valve will control the flow. TBVs open after a delay time, and usually do not become effective until the flow to the turbine is almost shut off by TSVs or TCVs. [[

]]

9.3.2.2.1 [[ ]]

[[

]]

[[ ]] (9-4)

Where,

[[

]]

[[

]]

[[

]]

Figure 9-5 [[ ]]

[[ ]]

[[ ]] (9-5)

[[ ]]

[[ ]] (9-6)

Where:

[[

]]

[[

]]

Figure 9-6 Peak Normalized Load Distribution [[ ]]

[[						
						]]

[[ ]]

[[

]]

Figure 9-7 Finite Element Model Component for [[ ]] **Pressure Load**

9.3.2.2.2 [[ ]]

[[

]]

[[ ]] (9-7)

Where,

[[ ]] (9-8)

[[ ]]

[[ ]] (9-9)

Where,

[[ ]] (9-10)

and,

[[

]]

[[

]]

[[

]]

Figure 9-8 Projected [[ ]] **Load** [[ ]]

9.3.2.3 SRV Related Loads (SRV, SRV_{ADS})

The opening of the safety relief valves during a transient can result in loads on the dryer directly through the resulting pressure effects in the steamline and indirectly by transmission of the discharge loads through the containment structure and RPV. [[

]] The differential pressure and FIV loads related to the increase in steamline flow when the relief valves are opened are addressed in the upset condition load terms in Sections 9.3.1.3 and 9.3.2.1 of this appendix.

The SRV discharge flow to the suppression pool causes containment vibrations that may be transmitted through the containment structure and reactor vessel to the RPV internals, thus creating a load on the dryer components. The SRV containment discharge loads are transmitted to the dryer through the vessel support brackets. The horizontal SRV loads at the dryer elevation are selected per the horizontal seismic model. The vertical SRV loads at the closest node to the dryer are selected per the vertical seismic mode. SRV loads for spectral analysis are selected to

envelope spectra for all the SRV cases. Applicable structural damping (typically 2%) is applied to the response spectra. Figure 9-9 shows an example of a typical set of SRV discharge loads along with the selected bounding spectra.

9.3.2.4 Seismic Loads (OBE, SSE)

Seismic events transmit loads to the dryer through the vessel support brackets. Seismic loads for the operating basis earthquake (OBE) and safe shutdown earthquake (SSE) in the form of amplified response spectra (ARS) at the reactor dryer support elevation are used in accordance with the data documented in plant design basis seismic loads evaluations. The horizontal seismic loads are selected from the horizontal seismic model at the appropriate node representing the dryer elevation. Vertical loads are selected per the vertical seismic model at the closest node to the steam dryer. Appropriate structural damping is applied to the response spectra. Spectral analyses are performed for the seismic loads. Seismic anchor motion effects do not need to be considered because they are negligible inside the RPV.

[[

]]

Figure 9-9 Typical SRV Response Spectra

9.3.2.5 Emergency and Faulted Conditions

A general class of postulated reactor events is those where depressurization of the RPV is the limiting phenomenon. The rapid depressurization causes water in the RPV to flash into steam. The resulting two-phase level swell affects the underside of the dryer, producing a transient differential pressure loading across the dryer panels. [[

]] The Reactor Internals Pressure Differential (RIPD) calculations determine analytically the differential pressures during these conditions.

For Emergency and Faulted conditions, the pressure differentials across the steam dryer components [[

]]. This blowdown can be the result of a postulated recirculation line, steam line, or feedwater line break or depressurization through the primary system relief valves. [[

]]

Differential Pressure Load during Emergency Operation [[ ]]

The limiting event for the Emergency condition [[

]]. The additional 2% power is assumed per Regulatory Guide (RG) 1.49. The NRC withdrew this RG in April 2008. [[

]] The blow-down model (Reference 11) is used to calculate the RIPDs for the steam dryer hood and vane banks during the postulated event.

Differential Pressure Load during Faulted Condition [[ ]]

The Faulted category addresses accidents or limiting faults, which are postulated as part of the plant's design basis. For the steam dryer, the design basis Faulted event is the [[

]]. The dryer must be shown to maintain structural integrity and not generate loose parts that may interfere with the closure of the main steam isolation valves. Two reactor operating conditions are analyzed for this event:

- [[

]]

At each condition, [[ ]] is evaluated. [[

]] The blow-down model 2 is used to calculate the RIPDs for the steam dryer hood and vane banks during the postulated event.

9.3.2.6 Acoustic Loads due to MSLB Outside Containment [[ ]]

The flow transient produced by rapid opening of the break generates a decompression wave in the MSL that affects the dryer. The methodology for calculating the acoustic loads on the steam dryer vertical cover plate (hood) [[ ]] was modified to determine the steam dryer vertical cover plate acoustic loads due to the faulted MSLB event because the acoustic wave imposing the load on the outer hood is similar for both events.

[[

]]

[[ ]] (9-11)

[[ ]]

[[ ]] (9-12)

[[ ]]

[[ ]] (9-13)

Where,

[[

]]

[[

]]

Figure 9-10 Peak Normalized Acoustic Loads for MSLB

[[										
										]]

[[ ]]

10.0 REFERENCES

1. U.S. Nuclear Regulatory Commission, NUREG-0800, Revision 3, March 2007, Section 3.9.5, "*Reactor Pressure Vessel Internals*."
2. U.S. Nuclear Regulatory Commission, NUREG-0800, Revision 3, March 2007, Section 3.9.2, "*Dynamic Testing and Analysis of Systems, Structures, and Components*."
3. U.S. Nuclear Regulatory Commission, Regulatory Guide 1.20 Revision 3, March 2007, "*Comprehensive Vibration Assessment Program for Reactor Internals During Preoperational and Initial Startup Testing*."
4. SIL No. 644 Rev. 2, BWR Steam Dryer Integrity, August 30, 2006.
5. BWRVIP-139-A: BWR Vessel and Internals Project, Steam Dryer Inspection and Flaw Evaluation Guidelines, EPRI Technical Report 1018794, July 2009. Errata issued September 2005, BWRVIP letter 2005-422, report corrected.
6. S. Ziada, S. Shine, Strouhal Numbers of Flow-Excited Acoustic Resonance of Closed Side Branches, Journal of Fluids and Structures Volume 13, Issue 1, January 1999, Pages 127-142.
7. Letter, Entergy to USNRC, "Vermont Yankee Nuclear Power Station Report on the Results of Steam Dryer Monitoring," BVY 06-056 (Docket No. 50-271, TAC No. MC0761), dated June 30, 2006.
8. 0000-0101-0766-P-R0, DRF 0000-0080-2990 R0, Engineering Report, "Main Steam Line Limit Curve Adjustment During Power Ascension," Susquehanna Replacement Dryer, April 2009
9. GNRO-2012-00011, Entergy letter to the NRC, Request for Additional Information Regarding Extended Power Uprate, dated February 20, 2012.
10. NEDE-24011-P-A, "GESTAR II: General Electric Standard Application for Reactor Fuel," Licensing Topical Report, latest approved version.
11. NEDE-20566-P-A, "Analytical Model for Loss-of-Coolant Analysis in Accordance with 10 CFR 50 Appendix K," Volumes I, II and III, September 1986.
12. "Revised Susquehanna Replacement Steam Dryer Limit Curves -- Main Steam Line Mounted Instrumentation," 0000-0096-5766-P-R1, February 2009.

Appendix B

GGNS Plant Based Load Evaluation Methodology

Table of Contents

List of Tables

List of Figures

Acronyms and Abbreviations

BWR	Boiling Water Reactor
CAD	Computer-Aided Design
CLTP	Current Licensed Thermal Power
CFD	Computational Fluid Dynamics
CFR	Code of Federal Regulations
DOE	Design Of Experiments
EPU	Extended Power Uprate
FE / FEM	Finite Elements / Finite Element Method / Finite Element Model
FRF	Frequency Response Function
GDC	General Design Criteria
GEH	GE Hitachi Nuclear Energy
GGNS	Grand Gulf Nuclear Station
Hz	Hertz
LTR	Licensing Topical Report
MSL	Main Steam Line
OLTP	Original Licensed Thermal Power
NRC	Nuclear Regulatory Commission
PBLE	Plant Based Load Evaluation
PSD	Power Spectral Density
PT	Pressure Transducer
PWR	Pressurized Water Reactor
QC2	Quad Cities 2
RG	Regulatory Guide
RPV	Reactor Pressure Vessel
SF	Singularity Factor
SRSS	Square Root of the Sum of the Squares

SRV	Safety / Relief Valve
3D	Three Dimensional

Abstract

A methodology, termed Plant Based Load Evaluation (PBLE), is presented for defining the fluctuating loads that are imposed upon the Grand Gulf Nuclear Station (GGNS) reactor steam dryer. The PBLE load definition can be applied to a structural finite element model of the steam dryer in order to determine the steam dryer alternating stresses.

1.0 INTRODUCTION

As a result of steam dryer issues at operating Boiling Water Reactors (BWRs), the US Nuclear Regulatory Commission (NRC) has issued revised guidance concerning the evaluation of steam dryers [1]. Analysis must show that the dryer will maintain its structural integrity during plant operation due to acoustic and hydrodynamic fluctuating pressure loads. This demonstration of steam dryer structural integrity comes in three steps:

(1) Predict the fluctuating pressure loads on the dryer,

(2) Use these fluctuating pressure load in a structural analysis to qualify the steam dryer design

(3) Implement a startup test program for confirming the steam dryer design analysis results as the plant performs power ascension.

The PBLE (Plant Based Load Evaluation) is an analytical tool developed by GEH to perform the prediction of fluctuating pressure loads on the steam dryer. This report provides the theoretical basis of the PBLE method that will be applied for determining the fluctuating loads on the GGNS steam dryer, describes the PBLE analytical model, determines the biases and uncertainties of the PBLE formulation and describes the application of the PBLE method to the evaluation of the GGNS steam dryer.

2.0 MODEL DESCRIPTION

2.1 Overview

[[ ]]

Figure 1. PBLE Process Flow

The PBLE can be [[

]] This is the methodology to be used in the GGNS evaluation and is described in this report. [[

]]

The PBLE is built on the commercial software packages Matlab [2] and Sysnoise[3]. Matlab is a software package designed for engineering computations. The general architecture of the PBLE scripts makes use of the Matlab programming language and graphical interface.

The vessel acoustic response is calculated with Sysnoise. Sysnoise is a program for modeling acoustic wave behavior in fluids, using implementations of the finite element and boundary

element methods. In the PBLE context, Sysnoise calculates how sound waves propagate through a FEM model of the RPV dome steam volumes. This 3D acoustic model is described in detail in Section 2.2 below.

2.2 Dome Acoustic Model

2.2.1 Sysnoise Modeling Principles

Sysnoise [3] models acoustics as a wave-phenomenon. The modeling is carried out in the frequency domain, thus using the so-called Helmholtz form of the wave equation (see e.g. [5] and [10]). [[

]] The following system of equations is solved:

$$\left[K + i\omega C - \omega^2 M\right]\{p\} = \{F_A\} \quad (1)$$

Where F_A is the vector of nodal acoustic forces, proportional to the normal velocity boundary conditions imposed on the faces of the mesh. The stiffness *[K]*, damping *[C]* and mass *[M]* matrices are computed at each frequency. The system of equations is thus set up and solved to obtain the pressure distribution *{p}*. The velocity field is obtained by differentiation of the pressure field at the Gauss points of the elements and then extrapolation and averaging at the nodes.

2.2.2 Geometry Modeling

The dome FE mesh (Figure 2) comprises all RPV steam volumes [[
]]

In all GEH BWRs, there are two steam zones with different steam qualities, upstream and downstream of the dryer. [[

]]

[[ ]]

**Figure 2. Modeled steam region (left)
and details of typical vessel meshes (right)**

[[ ]]

Figure 3. Vessel response (left) [[
]]

[[

]]

[[ ]]

Figure 4. First typical [[

]]

Table 1 First Ten RPV modes

Mode No.	Modal Frequency (Hz)
1	[[
2	
3	
4	
5	
6	
7	
8	
9	
10	]]

2.2.3 Finite Element Model

[[

]]

[[ ]]

Figure 5. [[ ]]

[[

]]

[[ ]]

Figure 6. [[ ]]

[[

]]

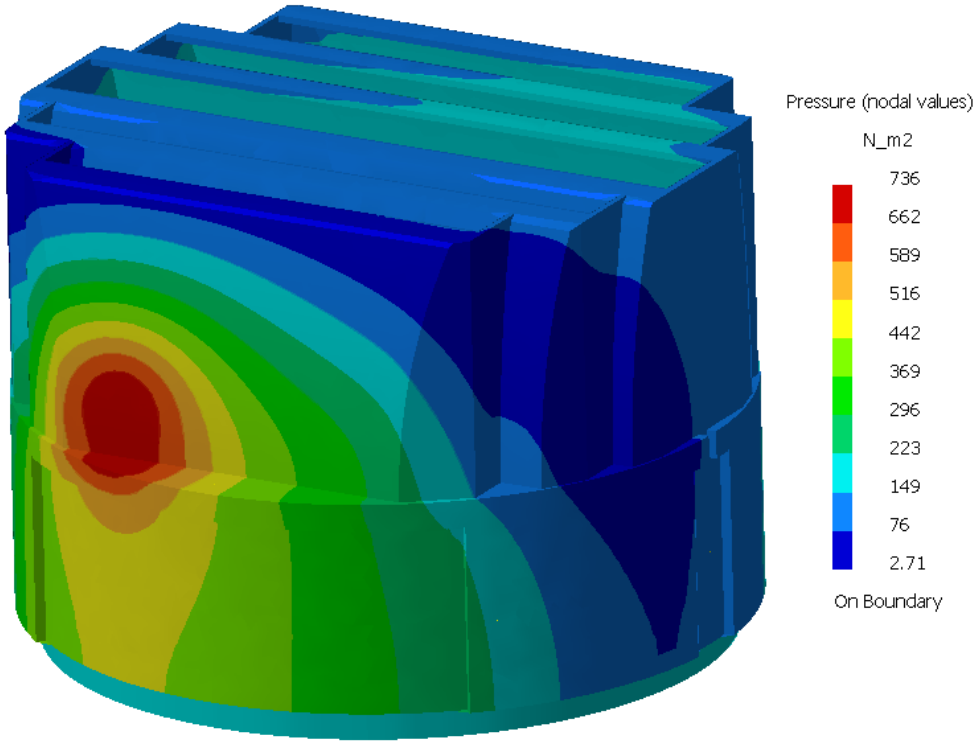

**Figure 7. Pressure amplitudes on dryer at 15 Hz (Forced Response)
View of CD side**

2.2.4 Fluid Properties and Boundary Conditions

[[

]]

Steam and water properties including impedance boundary conditions are described in detail in Section 2.4.

[[ ]]

Figure 8. Vessel passive boundary conditions

2.3 PBLE from [[ ]]

2.3.1 Solution Formulation

The pressure at any dryer point P [[

]] as shown in the benchmark assessments in Sections 3.2 and 3.3 of this report.

[[

]]

These considerations make the PBLE from in-vessel pressures a quite powerful tool.

2.3.2 Singularity Factor

The Singularity Factor (SF) is a tool to understand the mathematical limitations in PBLE. It is calculated as: [[

]]

[[ ]]

Figure 9. [[

]]

2.4 Steam and Water Acoustic Properties

This section describes all steam and water characteristic properties used in PBLE models: [[

]]

Dry steam properties, including speed of sound and density, are readily known from standard steam tables published by the International Association for the Properties of Water and Steam [6]. Petr [7] developed the [[

]] by Karplus [8].

2.4.1 [[ ]]

The following summary follows the description given in [7], Section 2. The variable nomenclature for this section is in Table 2.

[[

]]

Table 2 [[ ]]

[[	
	]]

[[

]]

[[ ]]

Figure 10. [[ ]]

2.4.2 Steam-water interface

[[

]]

[[ ]]

Figure 11. Steam-Water Interfaces

Table 3 Impedances in a Typical BWR RPV Environment

[[				
				]]

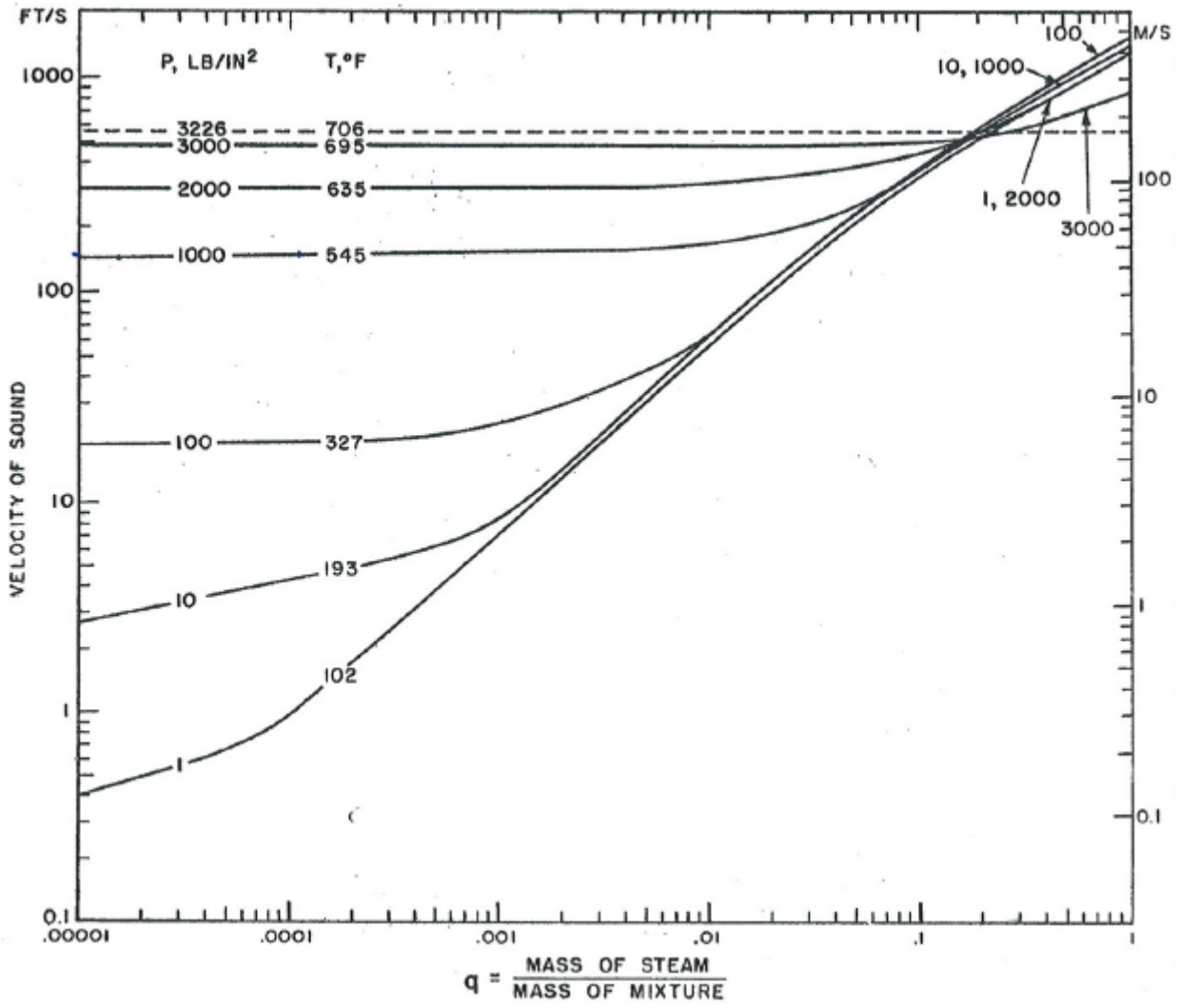

Figure 12. Speed of sound in [[ ]] (Fig. 5 in Karplus [8])

The solution that was adopted for the PBLE is to model [[

]]

3.0 MODEL QUALIFICATION: BWR PLANT VALIDATION

The Quad Cities Unit 2 (QC2) replacement steam dryer, installed in 2005, was the first GEH BWR unit instrumented with a significant number of on-dryer pressure sensors. This section presents the steam dryer fluctuating load definitions obtained with the PBLE at QC2 for two power levels, one at the QC2 Original Licensed Thermal Power (OLTP) level and at Extended Power Uprate (EPU) conditions.

3.1.1 Procedure for QC2 benchmarks

The QC2 dryer instrumentation comprised 27 PT sensors, labeled P:1 through P:27 [9]. Pressure sensor P:26, which was installed on the stream dryer temporary instrumentation mast, is not considered in this benchmark since the main interest is in pressure on the dryer surface. [[

]]

[[ ]]

Figure 13. Sensor Positions for Dryer Data Benchmark

[[

]]

Table 4 QC2 Frequency Bands for Main Acoustic Peaks

OLTP		EPU	
Begin Frequency (Hz)	End Frequency (Hz)	Begin Frequency (Hz)	End Frequency (Hz)
8	10	8	10
13	16	13	16
22	26	22	26
29	31	28	34
32	35	38	46
44	48	48	58
61	69	132	145
130	136	146	153
137	142	154	158
147	149	159	168
150	153	146	158
154	158		
150	158		

[[

]] The last segment PSDs at all sensors locations are plotted in Appendix A and Appendix B.

3.2 QC2 Benchmark at OLTP

3.2.1 From [[ ]]

[[ ]]

Figure 14. [[ ]]
(Numbers in parenthesis refer to the equation numbers)

3.2.2 From [[**]]**

[[ ]]

Figure 15. [[**]]**

3.3 QC2 Benchmark at EPU

3.3.1 From [[ ]]

[[ ]]

Figure 16. QC2 EPU Benchmark from [[ ]]

3.3.2 From [[ ]]

[[ ]]

Figure 17. QC2 EPU Benchmark from [[ ]]

3.4 QC2 Benchmark Conclusions

The PBLE predictions using [[ ]] are highly accurate: the low frequency content below [[

]] These good results validate the main assumption that [[ ]] to reproduce measured dryer pressures, including at low frequencies.

Using [[ ]] is on the conservative side. [[

]] This demonstrates the [[
]].

The main limitations in these dryer data benchmark lie within the FE model. [[

]] at both power levels.

The modeling of the region inside the dryer is also challenged; [[
]] are generally less accurate.

Overall the PBLE from [[ ]] emerges as a viable tool for developing dryer load definitions. The frequency content and the spatial distribution are well matched, the amplitude predictions are generally conservative and pressures away from the MSL nozzles are consistent with plant test data from other dryers.

4.0 APPLICATION METHODOLOGY

4.1 Scope of Application and Licensing Requirements

4.1.1 Scope of Application

The scope of the application for the Plant Based Load Evaluation Licensing Topical Report is to provide a methodology for determining the fluctuating pressure loads that the GGNS steam dryer will experience during normal operation. This fluctuating load definition can then be applied to a finite element model of the GGNS steam dryer in order to determine the structural qualification of the dryer.

4.1.2 Specific Licensing Requirements

Plant components, such as the steam dryer in a BWR nuclear power plant, perform no safety function but must retain their structural integrity to avoid the generation of loose parts that might adversely impact the capability of other plant equipment to perform their safety function. Potential adverse flow effects must be evaluated for the steam dryer to meet the requirements of GDC 1 and 4 in Appendix A of 10 CFR Part 50.

Standard Review Plan [12], Section 3 requires that the dynamic responses of structural components with the reactor vessel caused by steady-state and operational flow transient conditions should be analyzed for prototype (first of a design) reactors. The analytical assessment of the vibration behavior of the steam dryer includes the definition of the input-forcing function including bias errors and uncertainty. References [12] and [13] contain specific acceptance criteria related to formulating forcing functions for vibration prediction. Reference 1 provides guidance on acceptable methods for formulating the forcing functions for vibration prediction.

4.2 Proposed Application Methodology

The PBLE method for formulating the forcing function for vibration prediction for the GGNS steam dryer is in conformance with the guidance contained in Regulatory Guide 1.20 Revision 3.

4.2.1 Conformance with Regulatory Guide 1.20 Rev 3

The following table provides the conformance of the PBLE to the requirements contained in Section 2.1 of Regulatory Guide 1.20 Revision 3 [1].

RG 1.20 Section	Criteria	PBLE Conformance
2.1.(1)(a)	Determine the pressure fluctuations and vibration in the applicable plant systems under flow conditions up to and including the full operating power level. Such pressure fluctuations and vibration can result from hydrodynamic effects and acoustic resonances under the plant system fluid flow conditions.	Acceptable -The PBLE method is applicable up to the full power level of the plant. Since the PBLE approach in this LTR uses [[ ]], all pressure fluctuation, either hydrodynamic or acoustic are captured.
2.1.(1)(b)	Justify the method for determining pressure fluctuations, vibration, and resultant cyclic stress in plant systems. Based on past experience, computational fluid dynamics (CFD) analyses might not provide sufficient quantitative information regarding high-frequency pressure loading without supplemental analyses. Scale testing can be applied for the high-frequency acoustic pressure loading and for verifying the pressure loading results from CFD analyses and the supplemental analyses, where the bias error and random uncertainties are properly addressed.	The justification of the PBLE method is acceptable based on the benchmarking shown in Section 4.5 of this report. Stress analysis is not applicable to the scope of this LTR. CFD modeling is not applicable to the PBLE
2.1.(1)(c)	Address significant acoustic resonances that have the potential to damage plant piping and components including steam dryers, and perform modifications to reduce those acoustic resonances, as necessary, based on the analysis.	Acceptable – the PBLE is capable of determining acoustic resonances that may be detrimental to the steam dryer. Modifications for reducing acoustic resonances is beyond the scope of this LTR
2.1.(1)	Scale Model Testing	Not applicable - Scale model Testing is not used in the PBLE for determination of the steam dryer loads
2.1.(1)	Computational Fluid Dynamic (CFD) modeling	Not applicable - CFD modeling is not used in the PBLE for determination of the steam dryer loads

RG 1.20 Section	Criteria	PBLE Conformance
2.1.(2)	Describe the structural and hydraulic system natural frequencies and associated mode shapes that may be excited during steady-state and anticipated transient operation, for reactor internals that, based on past experience, are not adversely affected by the flow-excited acoustic resonances and flow-induced vibrations. Additional analyses should be performed on those systems and components, such as steam dryers and main steam system components in BWRs and steam generator internals in PWRs, that may potentially be adversely affected by the flow-excited acoustic resonances and flow-induced vibrations. These additional analyses are summarized below.	Acceptable - The PBLE is capable of determining the acoustic mode shapes within the reactor steam dome. It will simulate the acoustic response of the steam dome from the significant excitation sources.
2.1.(2)	Determine the damping of the excited mode shapes, and the frequency response functions (FRFs, i.e., vibration induced by unit loads or pressures, and stresses induced by unit loads or pressures), including all bias errors and uncertainties.	Acceptable – FRF are determined by the PBLE. Bias errors and uncertainties have been addressed.
2.1.(3)	Describe the estimated random and deterministic forcing functions, including any very-low-frequency components, for steady-state and anticipated transient operation for reactor internals that, based on past experience, are not adversely affected by the flow-excited acoustic resonances and flow-induced vibrations. Additional analyses should be performed on those systems and components, such as steam dryers and main steam system components in BWRs and steam generator internals in PWRs, that may potentially be adversely affected by the flow-excited acoustic resonances and flow-induced vibrations. These additional analyses are summarized below.	Acceptable – the PBLE is capable of determining the forcing functions in the frequency range important to BWR dryers.
2.1.(3)	Evaluate any forcing functions that may be amplified by lock-in with an acoustic and/or structural resonance (sometimes called self-excitation mechanisms). A lock-in of a forcing function with a resonance strengthens the resonance amplitude. The resulting amplitudes of the forcing function and resonance response can therefore be significantly higher than the amplitudes associated with non-lock-in conditions.	Lock in assessment is not required for PBLE loads [[ ]]

RG 1.20 Section	Criteria	PBLE Conformance
2.1.(3)	The applicant/licensee should determine the design load definition for all reactor internals, including the steam dryer in BWRs up to the full licensed power level, and should validate the method used to determine the load definitions based on scale model or plant data. BWR applicants should include instrumentation on the steam dryer to measure pressure loading, strain, and acceleration to confirm the scale model testing and analysis results. BWR licensees should obtain plant data at current licensed power conditions for use in confirming the results of the scale model testing and analysis for the steam dryer load definition prior to submitting a power uprate request.	Acceptable – The PBLE uses in plant data for the determination of the steam dryer load definition.
2.1.(3)	In recent BWR EPU requests, some licensees have employed a model to compute fluctuating pressures within the RPV and on BWR steam dryers that are inferred from measurements of fluctuating pressures within the MSLs connected to the RPV. Applicants should clearly define all uncertainties and bias errors associated with the MSL pressure measurements and modeling parameters. The bases for the uncertainties and bias errors, such as any experimental evaluation of modeling software, should be clearly presented. There are many approaches for measuring MSL pressures and computing fluctuating pressures within the RPV and the MSLs. Although some approaches reduce bias and uncertainty, they still have a finite bias and uncertainty, which should be reported. Based on historical experience, the following guidance is offered regarding approaches that minimize uncertainty and bias error:	Acceptable – the PBLE methodology in this report uses [[ ]] for determination of the load definition. The PBLE methodology in this report demonstrates the methodology to determine bias errors and uncertainties associated with the PBLE methodology [[ ]].
2.1.(3)(a)	At least two measurement locations should be employed on each MSL in a BWR. However, using three measurement locations on each MSL improves input data to the model, particularly if the locations are spaced logarithmically. This will reduce the uncertainty in describing the waves coming out of and going into the RPV. Regardless of whether two or three measurement locations are used, no acoustic sources should exist between any of the measurement locations, unless justified.	Not applicable – the PBLE methodology in this report [[ ]].

RG 1.20 Section	Criteria	PBLE Conformance
2.1.(3)(b)	Strain gages (at least four gages, circumferentially spaced and oriented) may be used to relate the hoop strain in the MSL to the internal pressure. Strain gages should be calibrated according to the MSL dimensions (diameter, thickness, and static pressure). Alternatively, pressure measurements made with transducers flush-mounted against the MSL internal surface may be used. The effects of flow turbulence on any direct pressure measurements should be accounted for in a bias error and uncertainty estimate.	Not applicable – the PBLE uses [[ ]] The effects of flow turbulence on the pressure measurement is included in the PBLE uncertainty assessment.
2.1.(3)(c)	The speed of sound used in any acoustic models should not be changed from plant to plant, but rather should be a function of temperature and steam quality.	Acceptable – the speed of sound in the PBLE is a function of the steam fluid conditions within the RPV.
2.1.(3)(d)	Reflection coefficients at any boundary between steam and water should be based on rigorous modeling or direct measurement. The uncertainty of the reflection coefficients should be clearly defined. Note that simply assuming 100-percent reflection coefficient is not necessarily conservative.	Acceptable – the conditions of the steam water interface and the associated uncertainty is developed for the PBLE method.
2.1.(3)(e)	Any sound attenuation coefficients should be a function of steam quality (variable between the steam dryer and reactor dome), rather than constant throughout a steam volume (such as the volume within the RPV).	Acceptable – the PBLE formulation uses the steam quality in the reactor steam dome and dryer for the sound attenuation coefficients.
2.1.(3)(f)	Once validated, the same speed of sound, attenuation coefficient, and reflection coefficient should be used in other plants. However, different flow conditions (temperature, pressure, quality factor) may dictate adjustments of these parameters.	Acceptable – the speed of sound is based on the thermodynamic properties of steam in the RPV
Other	Model Benchmarking	PBLE is benchmarked against previously instrumented dryer data
Other	Determination of Biases and Uncertainty	Biases and Uncertainty have been calculated

Note that other sections of Reference 1 refer to structural analysis of the steam dryer or preoperational/startup testing that is outside of the scope of this Licensing Topical Report.

4.3 Range of Application

The PBLE method described in this report is capable of determining the vibratory forcing function for the entire operating range of the GGNS steam dryer.

4.4 Plant-Specific Application Methodology

4.4.1 [[ ]] Model Inputs

The vessel [[

]]

Acoustic Finite Element Model Mesh

A FE model of the [[

]]

[[ ]]

Figure 18. [[ ]]

[[

]]

4.4.2 Plant Input Measurements

Sensor Type and Location

For the PBLE [[

]]

Error in Measured Dryer Pressures

This error, [[

]]

4.4.3 Plant-Specific Load Definition

The following steps are involved in the calculation of dryer loads with the PBLE: [[

]]

4.4.4 Application Uncertainties and Biases

This section describes the processes for how to calculate the PBLE uncertainties for a plant-specific application.

The methodology presented here provides an uncertainty due to errors in the PBLE inputs: [[

]]

4.4.4.1 Method Presentation

This section describes constituting elements of the uncertainty analysis: the varying input parameters, the statistical methods in use, the nominal case and how deviations from the nominal case are calculated.

Parameters in the Uncertainty Analysis

The code parameters and variables that have an influence in the load definition are listed in Table 5. All influence [[ ]]

Table 5 Parameters in the [[ ]]

Phenomena	**Parameter**
[[	
	]]

Analysis Techniques

The techniques used in the evaluation of the uncertainty are briefly introduced in the following paragraphs.

Design of Experiments

A Design of Experiment (DOE) is a structured, organized method for determining the relationship between parameters affecting a process and the output of that process. Forced changes are made methodically to the input parameters as directed by mathematically systematic tables and the impact on the results is assessed. It is suitable for the present study since it allows maximizing information with a limited number of well-chosen parameter variations. The effect of input variables can be judged when acting alone, or in combination with others.

For each input parameter, a number of possible values are defined, representing the known variation range for each variable. [[

]]

Monte Carlo Analysis

The Monte Carlo method is a way to statistically evaluate a system using random samples. The larger the number of random samples is, the more accurate the results. From the mathematical point of view it consists of choosing a large number of parameter values at random from within a variation interval. It is useful to assess uncertainty when the ranges of the input parameters can not be given in a deterministic way (upper and lower bounds), but their probability density functions are known.

Deviations from Nominal Case

The nominal case corresponds to the PBLE results with all parameters at their best known values. These results are obtained by following the guidelines outlined in Section 4.4. [[

]]

4.4.4.2 Step 1 – Sensitivity of [[ ]]

Aside from parameters related to numerical accuracy, a range of values is known for each parameter in Table 5. [[

]]

Based on the results of these DOEs, [[

]]

[[ ]]

Figure 19. [[ ]]

Numerical Accuracy

The uncertainty due to [[

]]

4.4.4.3 Step 2 - Uncertainty in [[ ]]

Once [[ ]] that take into account the influence of the sensitive parameters in Table 5 have been pre-computed, the overall uncertainty in the PBLE loads can be evaluated.

[[

]]

4.4.4.4 Combination of Uncertainties and Biases

Individual uncertainties (due to different parameters or groups of parameters) are combined into a single one by taking the square root of the sum of the squares (SRSS):

$$U = \sqrt{\sum u_i^2} \quad \text{(22)}$$ where:

U = Total uncertainty

u_i = Individual uncertainties

If the parameters or groups of parameters are not independent from each other, the combined uncertainty is conservative.

A benchmark against measured dryer pressures would produce a bias and an uncertainty in each frequency band. Then the total bias of the PBLE loads is the benchmark bias and the total uncertainty is a SRSS in which the benchmark uncertainty is a term of the sum.

4.5 Demonstration Analysis

This section details how uncertainties are combined in the example of Section 3.3.2: QC2 at EPU condition, [[ ]] The QC2 at OLTP had a different set of acoustic frequencies and benchmark results, but the bias and uncertainties would be calculated and assessed in the same manner.

The deviation from measured data (bias and uncertainty) is covered in the benchmark section (Section 3.3.2). The bias [Equation (17)] indicates any [[

]]

For QC2 at EPU, the biases and uncertainties from the comparison between nominal projections and measured pressures are in Figure 17. The uncertainties due to the model parameters is calculated in detail in Appendix C.

For the PBLE from in-vessel pressures, the contributors are: [[

]]

The consolidated results are shown in Table 6 and Figure 20. In Figure 20 the predicted summed PSDs are also corrected with the biases from the benchmark against test data.

[[ ]]

Figure 20. PBLE [[ ]] - Range of Predictions Versus Measurements

Table 6 Total Bias and Uncertainty for PBLE from [[ ]] for QC2 at EPU

Frequency Band (Hz)	8 -10	13 - 16	22 - 28	28 - 34	38 - 46	48 - 58	132 - 145	146 - 153	154 - 158	159 - 168	146 - 158
BIAS (%)											
[[ ]]	**-8.36**	**-6.43**	**8.49**	**6.28**	**5.47**	**-12.04**	**-14.20**	**20.99**	**-4.70**	**-4.70**	**9.60**
UNCERTAINTY (%)											
[[	8.74	4.79	2.98	2.06	1.44	2.67	2.89	0.76	0.97	3.00	1.08
	0.86	0.82	0.95	0.66	0.76	6.07	3.85	10.64	2.18	4.62	6.30
	2.89	3.57	3.99	3.83	3.11	2.96	3.07	4.03	3.69	2.69	3.87
	0.38	0.49	0.36	0.24	0.62	0.66	2.69	2.46	1.31	1.88	1.99
]]	0.91	1.12	1.24	0.95	0.64	0.76	3.08	4.63	1.56	3.41	3.40
Total uncertainty (SRSS)	**9.30**	**6.15**	**5.23**	**4.51**	**3.62**	**7.33**	**7.02**	**12.55**	**4.84**	**7.26**	**8.45**

5.0 CONCLUSIONS

The Plant Based Load Evaluation methodology [[ ]] is available to predict dryer pressure loads and their associated uncertainty.

A built-in [[

]]

The PBLE technique is validated by the Quad Cities 2 application case. From comparison between measurements and projections, the PBLE predicts good frequency content and spatial distribution. The SRV valve resonances are well captured. The PBLE predictions are highly accurate: the low frequency content below [[

]] These good results validate the main assumption that [[ ]] to reproduce measured dryer pressures, including low frequencies.

The PBLE addresses a wide range of load cases:

- MSL valve resonance (SRV/branch line) or broadband excitations (venturi)
- Sources in the vicinity of nozzles
- Hydrodynamic loading (pseudo-pressures)

The effects from the last two types of sources can be advantageously modeled by [[ ]]; for this reason the PBLE from [[ ]] is adequate to predict fluctuating dryer loads at any BWR plant.

6.0 REFERENCES

[1] U.S. Nuclear Regulatory Commission, Regulator Guide 1.20 Revision 3, March 2007, "Comprehensive Vibration Assessment Program for Reactor Internals During Preoperational and Initial Startup Testing."

[2] MATLAB ®, Copyright 1984-2008, The MathWorks, Inc.

[3] Sysnoise® Revision 5.6, LMS International, Users Manual Revision 1.0, March 2003.

[4] S.H. Jang and J.G. Ih, On the multiple microphone method for measuring in-duct acoustic properties in the presence of mean flow, J. Acous. Soc. Am., Vol. 103, No. 3, March 1998.

[5] P.M. Morse and K.U. Ingard, *Theoretical Acoustics*, McGraw-Hill, New York, 1968, p.519.

[6] W. Wagner et al., The IAPWS Industrial Formulation 1997 for the Thermodynamic Properties of Water and Steam, ASME J. Eng. Gas Turbines and Power, 122, 150-182 (2000)

[7] V. Petr, *Wave propagation in wet steam*, Proc. Instn. Mech. Engrs Vol 218 Part C 2004, p 871-882.

[8] H. B. Karplus, *Propagation of pressure waves in a mixture of water and steam*, Armour Research Foundation of Illinois Institute of Technology, United States Atomic Energy Commission contract No. AT (11-1) 528, ARF No. D132A13, 1961

[9] GE-NE-0000-0044-2240-01, "Quad Cities Unit 2 Replacement Steam Dryer, Vibration Instrumentation Program, Plant Startup Test Report"

[10] L.E. Kinsler, A.R. Frey, A.B. Coppens, J.V. Sanders, *Fundamentals of Acoustics*, Fourth Edition, John Wiley and Sons, 2000.

[11] GE report number GE-NE-0000-0037-1951-01, Y. Dayal, Quad Cities Unit 2 Nuclear Power Plant, Dryer Vibration Instrumentation Uncertainty, Revision 0, April 2005

[12] U.S. Nuclear Regulatory Commission, NUREG-0800, Revision 3, March 2007, Section 3.9.2, "Dynamic Testing and Analysis of Systems, Structures and Components."

[13] U.S. Nuclear Regulatory Commission, NUREG-0800, Revision 3, March 2007, Section 3.9.5, "Reactor Pressure Vessel Internals."

APPENDIX A QC2 OLTP BENCHMARKS PSDS

[[ ]]

Measured –Red
[[ ]] - Green
[[ ]] - Blue

[[ ]]

Measured - Red
[[ ]] - Green
[[ ]] - Blue

[[ ]]

Measured - Red
[[ ]] - Green
[[ ]] - Blue

[[ ]]

Measured - Red
[[ ]] - Green
[[ ]] - Blue

[[ ]]

Measured - Red
[[ ]] - Green
[[ ]] - Blue

[[ ]]

Measured - Red
[[ ]] - Green
[[ ]] - Blue

[[ ]]

Measured - Red
[[ ]] - Green
[[ ]] - Blue

[[ ]]

Measured - Red
[[ ]] - Green
[[ ]] - Blue

[[ ]]

Measured - Red
[[ ]] - Green
[[ ]] - Blue

APPENDIX B QC2 EPU BENCHMARK PSDS

[[ ]]

Measured - Red
[[ ]] - Green
[[ ]] - Blue

[[ ]]

Measured - Red
[[ ]] - Green
[[ ]] - Blue

[[ ]]

Measured - Red
[[ ]] - Green
[[ ]] - Blue

[[ ]]

Measured - Red
[[ ]] - Green
[[ ]] - Blue

[[ ]]

Measured - Red
[[ ]] - Green
[[ ]] - Blue

[[ ]]

Measured - Red
[[ ]] - Green
[[ ]] - Blue

[[ ]]

Measured - Red
[[ ]] - Green
[[ ]] - Blue

[[ ]]

Measured - Red
[[ ]] - Green
[[ ]] - Blue

[[ ]]

Measured - Red
[[ ]] - Green
[[ ]] - Blue

APPENDIX C QC2 EPU UNCERTAINTY ASSESSMENT

C.1. VARIATIONS IN PBLE INPUT PARAMETERS

Table 7 Nominal, Upper and Lower Bound Parameter Values for QC2

	Units	Nominal	Lower	Upper
[[				
				]]

Table 7 gives the nominal values and the upper and lower limits for all the input parameters. The [[ ]] is described in Section 2.2.2. In addition to the content of Table 7, [[

]]

C.2. STEP 1 – SENSITIVITY OF FRFS

The goal of this step is to determine which variables in the vessel have an influence in [[

]]

Mesh Independent Parameters

Figure 21 shows results, for high and low frequency respectively, for the DOE [[
]]

The curves for all experiments lay on top of each other. No variability is observed due to these parameters in their variation range.

Figure 22 shows results [[ ]] For this group of variables some differences are observed. By observing the [[

]]

[[ ]]

Figure 21. DOE on [[ ]]

[[ ]]

Figure 22. DOE on [[ ]]
Black Thick Line is the Nominal Experiment

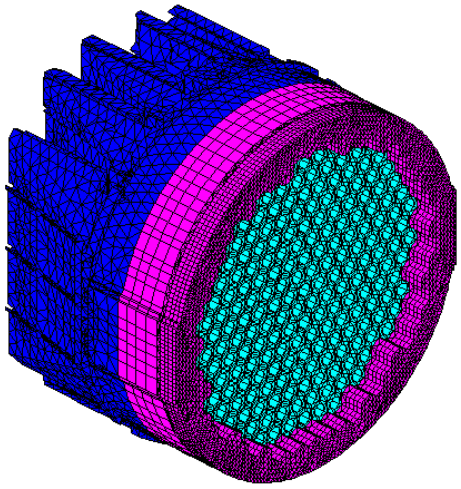

Figure 23. FEM Mesh Upstream the Dryer Showing the Regions With [[
]]

[[

]]

Table 8 Changes in [[ ]]

	[[	
Mesh 1		
Mesh 2		
Mesh 3		]]

Table 9 Acoustic Modes (Hz) of the Nominal and Modified Meshes

Modes	Nominal	Mesh 1	Mesh 2	Mesh 3
1	[[			
2				
3				
4				
5				
6				
7				
8				
9				
10				]]

[[ ]]

Figure 24. FRFs for Different FE Meshes With [[ ]]

[[ ]]

In view of [[

]]

Table 10 [[ ]]

	[[	
		]]

[[

]] In any case, the curves reproduce each other reasonably well.

[[ ]]

Figure 25. FRFs With Finer FE Mesh

Figure 26 [[

]]

[[ ]]

Figure 26. [[ ]]

C.3. STEP 2 – UNCERTAINTY IN DRYER LOADS

From the previous section, it is clear that [[

]]

[[ ]]

Figure 27. [[ ]]

Table 11 [[

]]

[[						
						]]

Table 12 [[

]]

[[					
					]]

Uncertainty due to Errors in the Measurement Loop

It has been shown in a previous report [11] that this measurement loop, [[

]] The results are shown in Figure 28 and quantified in Table 13 and Table 14.

Table 13 PBLE predictions – Measurement Loop Deviations from Nominal at Low Frequencies

Frequency band (Hz)	8 – 10	13 – 16	22 – 28	28 – 34	38 – 46	48 – 58
Upper deviation (%)	[[					
Lower deviation (%)						]]

Table 14 PBLE predictions – Measurement Loop Deviations from Nominal at High Frequencies

Frequency band (Hz)	132 – 145	146 – 153	154 – 158	159 – 168	146 – 158
Upper deviation (%)	[[				
Lower deviation (%)					]]

[[ ]]

Figure 28. PBLE Predictions – Uncertainty Due to the Measurement Loop

Uncertainty due to [[ ]]

The uncertainty [[

]]

Table 15 [[

]]

[[						
Deviation (%)						
Deviation (%)						]]

Table 16 [[

]]

[[					
Deviation (%)					
Deviation (%)					]]

C.4. CONSOLIDATED UNCERTAINTY

The results are shown in Figure 29, Table 17 and Table 18. The largest contribution to uncertainty [[

]]

The overall uncertainty remains below 10%, except for the 146 – 153 Hz bands, where it peaks at a value of 12.55%.

Table 17 Consolidated Uncertainty – [[ ]]

Frequency Bands (Hz)	8 -10	13 - 16	22 - 28	28 - 34	38 - 46	48 - 58
[[						
						]]

Table 18 Consolidated Uncertainty – [[ ]]

Frequency Bands (Hz)	132 - 145	146 - 153	154 - 158	159 - 168	146 - 158
[[					
					]]

In Figure 29, the PBLE uncertainties are quite small but some bias compared to the measured PSDs remains; this is reconciled by the benchmark against measured pressures in Section 3.3.2.

[[ ]]

Figure 29. PBLE from [[ ]]

Appendix C

GGNS Steam Dryer - Plant Based Load Evaluation Methodology, Supplement 1

A nonproprietary version of this Appendix is not being submitted in accordance with NRC Information Notice 2009-07, Requirements for Submittals, (2): "In instances in which a nonproprietary version would be of no value to the public because of the extent of the proprietary information, the agency does not expect a nonproprietary version to be submitted."

Appendix D

Not Used

Appendix E

Steam Dryer Structural Analysis Methodology

TABLE OF CONTENTS

Page

LIST OF TABLES

LIST OF FIGURES

Acronyms and Abbreviations

Acronym	Definition
ABWR	Advanced Boiling Water Reactor
ASME	American Society of Mechanical Engineers
B&PV	Boiler and Pressure Vessel
BWR	Boiling Water Reactor
DLF	Dynamic Load Factor
DOF	Degrees of Freedom
FE	Finite Element
FEM/FEA	Finite Element Model/Finite Element Analysis
FIV	Flow Induced Vibration
GEH	GE Hitachi Nuclear Energy
GGNS	Grand Gulf Nuclear Station
HCF	High Cycle Fatigue
HF	High Frequency
LF	Low Frequency
MASR	Minimum Alternating Stress Ratio
MPa	Mega Pascals
MSL	Main Steam Line
MSLB	Main Steam Line Break
PBLE	Plant Based Load Evaluation
PB	Bending Stress
PL	Local Primary Membrane Stress
PM	General Primary Membrane Stress
PT	Penetrant Testing
Q	Secondary Stress Range
RMS	Root-Mean-Square
RPV	Reactor Pressure Vessel
SI	Stress Intensity
SCF	Stress Concentration Factor
SRSS	Square Root of the Summed Squares

1.0 OVERVIEW

The purpose of this licensing topical report is to define the methodology used by GE Hitachi Nuclear Energy (GEH) for performing the structural analysis of steam dryers. This includes the analysis methodology for predicting the structural response of steam dryers to the flow induced vibration (FIV), the procedure for fatigue evaluation and the procedure for performing the primary structural analyses for load combinations at different service level conditions. The described fatigue evaluation and load combinations are consistent with the American Society of Mechanical Engineers Boiler and Pressure Vessel Code (ASME B&PV Code).

This Appendix is part of the overall methodology used by GEH to evaluate the steam dryer structural response under all service conditions. It belongs to a group of licensing topical reports that together define the methodology for evaluation of steam dryers. Each report covers certain aspects of the methodology. Appendix A, Steam Dryer Integrity Analysis Methodology, defines the overall steam dryer evaluation methodology, which covers plant and dryer instrumentation, load definition, structural analysis, limit curve development and power ascension monitoring. Appendices B, GGNS Steam Dryer-Plant Based Load Evaluation Methodology, and C, GGNS Steam Dryer-Plant Based Load Evaluation Methodology Supplement 1, define the acoustic-based Plant Based Load Evaluation (PBLE) - the GEH proprietary load definition methodology. This Appendix defines the subsequent structural analysis methodology applicable to the GGNS replacement steam dryer.

2.0 STEAM DRYER DESCRIPTION

This section describes the design features of the typical BWR parallel bank steam dryer that are relevant to the dryer structural evaluation. Examples of finite element models are also provided.

The steam dryer is designed to remove the remaining liquid from the mixture of steam and water (wet steam) that exits upward from the steam separators. Wet steam enters the bottom of the dryer through inlet enclosures, flows horizontally through dryer vanes that remove the water droplets, and finally exits the dryer vertically through outlet areas into the dome of the reactor pressure vessel (RPV). The water removed from the steam is collected in troughs below the vanes and returned through the drain channels to the RPV water. Figure 2.0-1 shows the steam path and a schematic of the dryer bank. Figure 2.0-2 and Figure 2.0-3 provide an overall illustration of the main components of a steam dryer. The dryer skirt and hood panels direct the steam flow from the separators through the drying vanes. The support ring and troughs form the main support structure for the dryer. The support ring rests on four to six steam dryer support brackets that are welded attachments to the RPV wall. The dryer skirt is suspended from the support ring and extends below the water surface in the RPV in order to form a water seal around the steam separators.

The dryer vanes are vertically oriented chevron plates. Typically, 70 to 80 of these chevron-shaped vane plates are tied together by horizontal tie rods into a vane module or dryer unit. End plates provide support for the tie rods. Figure 2.0-4 shows top views of the vane module for both early and later model dryers. While the vane modules are not structural components, they represent a significant portion of the total mass of the dryer (on the order of 30-40%) and, therefore, the inertia effect is significant under most dynamic loading conditions.

The significant steam dryer structural components are shown in Figure 2.0-2 and Figure 2.0-3. Multiple vane modules are aligned longitudinally to form a dryer bank. The dryer bank assembly consists of the vane modules, the drain trough, and the hood panels that form the inlet plenum to the dryer vane bundles. Four to six parallel dryer banks are used, depending on the size of the dryer. BWR/4 and later dryer designs incorporate interior vertical hood support plates to provide structural support and break up lower vibration modes of the large hood span. These interior support plates abut the end plates of the vane modules. On the hood side of the support plate, some designs incorporate a backing strip between the support plate and hood plates. This backing strip provides additional support at this critical junction. Additional horizontal plates attached to the support ring are used to close off steam flow paths between the banks. Vertical plates are attached at the ends of the banks to form an outlet plenum between banks. These plates direct the steam flow exiting the banks upward into the steam dome region.

The support ring, along with the drain troughs, forms the foundation of the dryer. The dryer bank assemblies are welded to the top of the support ring. On some dryer designs, cross beams attached to the support ring provide additional support to the troughs. Bank-to-bank tie bars on the top of the dryer provide structural support across the top of the dryer.

The support ring rests on four to six steam dryer support brackets that are welded attachments to the RPV wall. Seismic blocks are attached to the support ring at each of the bracket locations. The motion of the steam dryer in the circumferential direction is constrained by the seismic blocks, while leaving the support free in the radial direction to accommodate differential thermal expansion between the dryer and the RPV.

The dryer skirt is suspended from the support ring. A number of panels are welded to the inside of the skirt (BWR/2-3 designs) or the outside of the skirt (BWR/4 and later designs) to form the drain channels. Pipes connect the troughs to the drain channels to provide a flow path for the water removed from the steam by the vanes. Welded to the bottom of the skirt is the lower skirt ring. During refueling, the dryer rests on the lower skirt ring in the equipment pool.

GEH BWR steam dryer technology has evolved over many years and several product lines. In earlier BWR/2 and BWR/3 dryers, the typical active height of the dryer vanes is 48 inches. Vane material typically extends about 1.5 inches above and 3 inches below the active vane height. This inactive height of vane material is physically captured and supported by the bank assembly. Some BWR/2 GEH steam dryers inclined the dryer units 20° from vertical; however, later GEH BWR steam dryers install the units vertically. In BWR 4/5 steam dryers the active vane height was increased to 72 inches. The higher vanes have been carried into later product lines. Figure 2.0-5 illustrates the evolution of steam dryer banks and terminology used for the hood types. BWR/2 and BWR/3 plants used square hood dryers. It should be noted that the square hood dryers from only one fabricator incorporated internal diagonal braces. The slanted hood design was introduced with the BWR/4 product line. The curved hood design was introduced with the BWR/5 product line and has been used in subsequent plant designs. The curved hood dryer was also used in several later BWR/4 plants. These differences in hood designs affect the dryer modal response. Perforated plates are included on the inlet and outlet sides of the vanes of 72-inch height units in order to more effectively utilize the increased vane height. The addition of perforated plates results in a more uniform velocity over the height of the vanes. While not intended to be a structural component, the perforated plates do add stiffness to the dryer bank assembly.

The same basic GEH BWR steam dryer design has been used in BWR/2 through BWR/6, ABWR, and ESBWR product lines. This basic design consists of four to six parallel banks supported by a circumferential ring at about mid height of the dryer. The banks consist of hood

panels that direct the steam flow through the dryer vane assemblies. The skirt is suspended from the support ring and extends down below the reactor water level and outside the steam separator assembly. The skirt forms a water seal and directs the steam leaving the separators up through the vanes. Water removed from the steam is collected in troughs below the vane assemblies and returned to the RPV water through the drain channels.

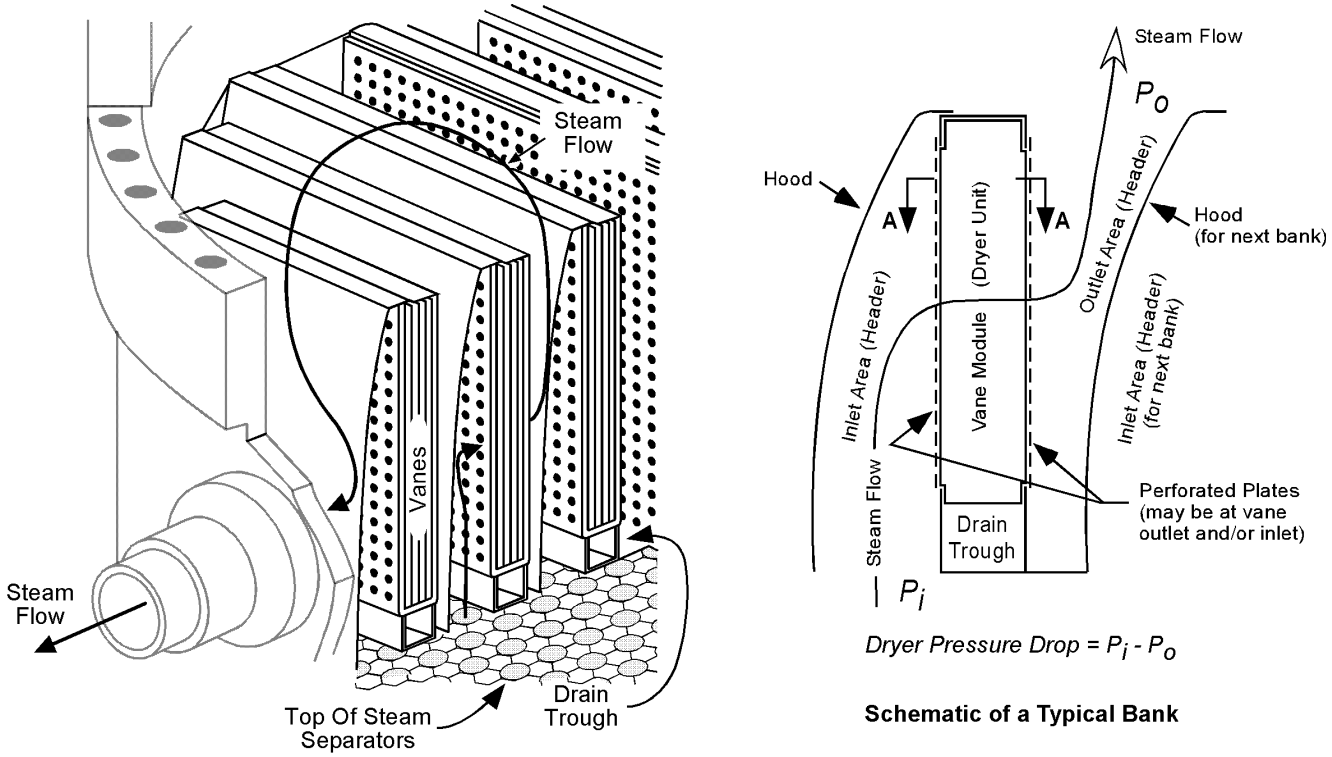

Figure 2.0-1 Steam Flow Path and Partial Dryer Profile

[[

]]

Figure 2.0-2 Structurally Significant Dryer Components

[[

]]

Figure 2.0-3 Structurally Significant Dryer Components

BWR/2/3 and 48” High BWR/4

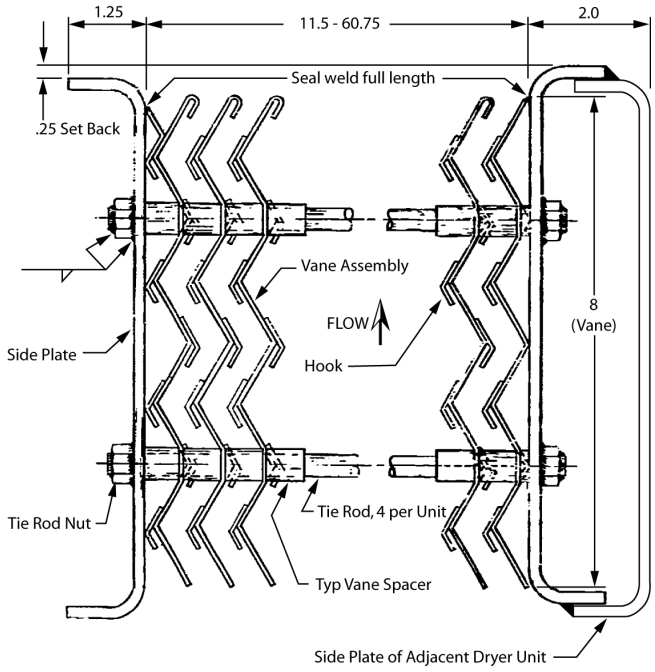

72” High BWR/4 and Later

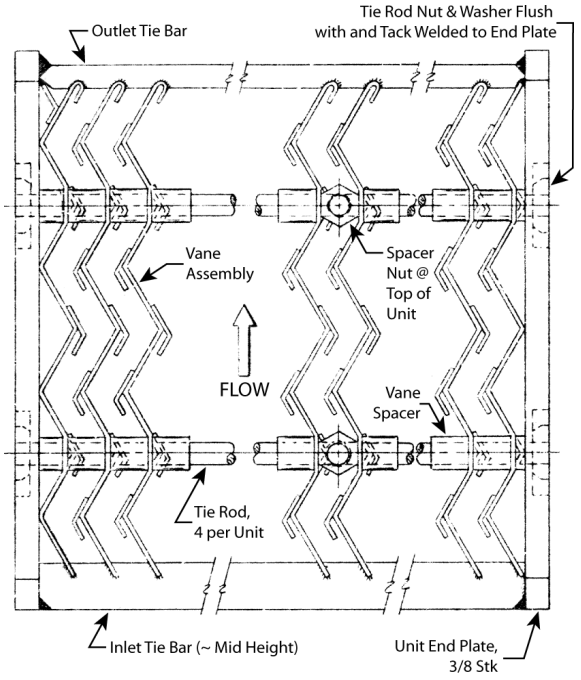

Figure 2.0-4 Schematics of Vane Modules

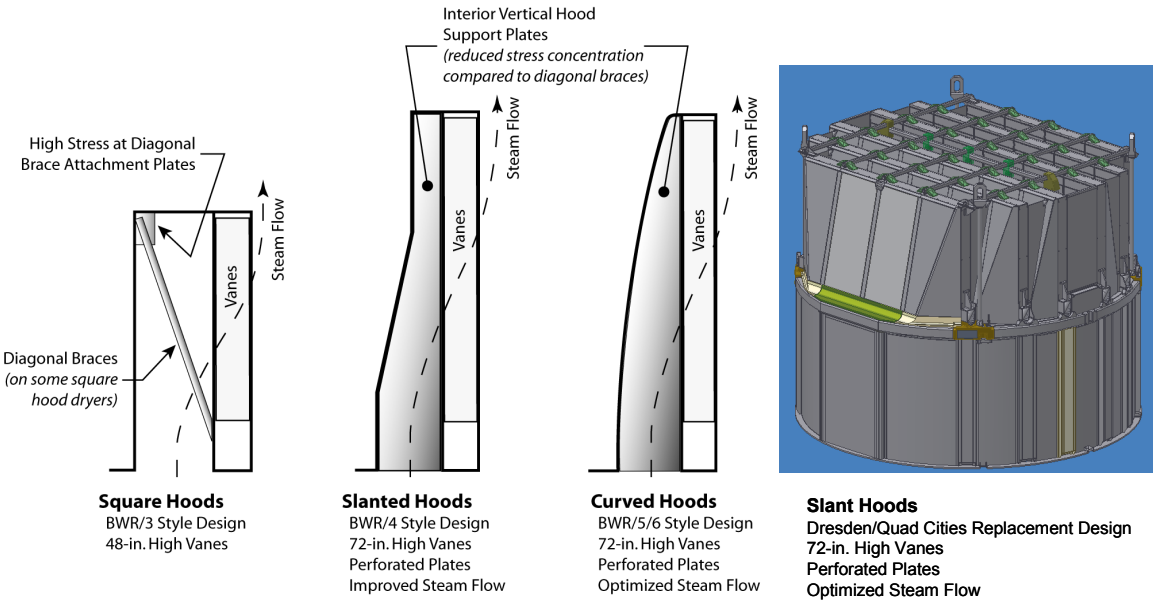

Figure 2.0-5 BWR Dryer Hood Designs

3.0 MATERIAL PROPERTIES

This section provides the guideline for the material properties used in the steam dryer structural analysis.

BWR steam dryers are manufactured from Austenitic 300 series stainless steel conforming to the GEH material and fabrication specifications. The grade most commonly used is Type 304. Recent replacement stream dryers use low carbon grade 304L to provide resistance to stress corrosion cracking. Material properties are obtained from the ASME B&PV Code (Reference 1). Steam dryers are operated at the steam saturation temperature corresponding to the RPV dome pressure. The elastic modulus of the steam dryer material will be reduced at elevated temperatures compared to that at room temperature. Specific material properties at the normal operating temperature should be used in analysis (e.g., 550°F for a dome pressure of 1045 psia). The applicable material properties from Reference 1 are shown in Table 3.0-1 below:

Table 3.0-1 Properties of SS304/SS304L at 550°F

Material/Property	Value at Operating Temperature
SS304/SS304L	
S_y, Yield Strength, psi	15,950
S_u, Ultimate Strength, psi	57,200
E, Elastic Modulus, psi	25.6×10^6

In addition, materials with properties different than the original dryer specification may have been used in modifications and repairs made to the dryer. The original material selection and repair/modification history of the individual dryer will be reviewed and the appropriate material properties for the affected components will be used in analysis.

4.0 DESIGN CRITERIA

The steam dryer, including the dryer units, is a non-safety related item and is classified as an Internal Structure as defined in Reference 1, Subsection NG, Paragraph NG-1122. The steam dryer is not an ASME Code component, but the structural evaluation methodology uses the Code as a design guide with the exception of the weld quality and fatigue factors as discussed in Subsections 4.2.1 and 7.

4.1 FATIGUE CRITERION

The steam dryer structural analyses are performed assuming that the dryer will be operated for 40 to 60 years. The stresses are expected to be well within the elastic range when the dryer is subjected to FIV loading during normal operation. Therefore, the high cycle fatigue (HCF) life is the major design consideration. The fatigue stress limit is lower than the material yield stress. Steam dryer components are subjected to cyclic acoustic pressure in normal operation where high cycle fatigue constitutes the controlling structural acceptance criterion for steam dryers. Determination of the fatigue stress limit used in the FIV structural analysis is consistent with ASME B&PV Code Section III.

The design fatigue curves and curve selection criteria for Austenitic Ni-Cr stainless steel, the group of materials used for steam dryer, are given in the ASME code (Section III, Division 1, Appendix I, Figure I-9.2.2 and Figure I-9.2.3). The ASME stress-cycle, or S-N curves plot the alternating stress intensity versus number of cycles. Alternating stress limit is dependent on mean stress. [[

]] Curve C is the most conservative of the three curves in Figure I-9.2.2 and may be used at or near the weld locations where high residual stresses may be present. Curve C also includes margin to address the residual stress from fabrication. [[

]]

4.2 WELD FACTOR

A key component of the fatigue alternating stress calculation at a specific location is the appropriate value of the stress concentration factor (SCF). The weld types of relevance for the steam dryer stress analysis are the full penetration welds, fillet welds and partial penetration groove welds. [[

]]

For the case of NG-3352 Type I and III full penetration welded joints, [[

]]

For the case of a fillet or partial penetration groove weld, there are two distinct analysis paths depending on whether the stress was obtained from a shell element or a solid element model. [[

]]

The following describes the process of determining nominal stress near the weld for the shell model. [[

]]

The stress may also be obtained from the shell finite element model peak stress intensities obtained from time history analysis. Because the shell finite element model of the full steam dryer is not capable of predicting the full stress concentrations in fillet or partial penetration welds, weld fatigue factors, and if necessary weld size reduction factors, for fillet or partial penetration welds are applied to the calculated peak stress intensities to determine the fatigue stress.

The weld size reduction factor may be needed as stated above. When using the traditional Strength of Materials formulas, the effective weld size is taken into account in the weld section properties. [[

]]

If the shell model is not capable of determining the peak stress for the fillet or partial penetration weld then a solid submodel of the weld region is created. In other words, this approach is used when the global shell model is inadequate to resolve the load path in small local regions of the steam dryer. These regions are typically places with small discontinuities in the structure where the coarser shell model or even a more refined shell model cannot adequately provide the proper local load path. [[

]]

The guidance above is based on Section III, Subsections NG and NB, of the ASME BP&V Code (Reference 1). The approaches of applying SCFs to shell and solid models described above are applicable to both bending and membrane stresses. The recommended SCF of 4 for the fillet or partial penetration welds is what has been recommended as the fatigue factor 'f' in Table NG-3352-1 of ASME Section III, Sub-section NG, for fillet or partial penetration welds. In recommending the use of this fatigue factor, Paragraph NG-3352 does not make a distinction in terms of the applicable stress types that is whether it is membrane, bending or combination of both.

The similar weld factor value for fillet welds can be derived using two sub factors: the first sub-factor (equivalent to C index in the piping fatigue stress analyses) accounts for the increase in the through-section stress over and above the nominal stress away from the weld discontinuity, and the second sub-factor (equivalent to K index in the piping fatigue stress analyses) accounts for the root discontinuities at the weld itself. A partial penetration groove weld is expected to have root discontinuities similar to those in fillet welds. [[

]] 1.8 is the maximum specified value of K index in Table NB-3681(a)-1 (i.e. for as-welded girth butt welds). Table NB-3681(a)-1 provides K index 1.2 for stress due to internal pressure, 1.8 for stress due to moment loading and 1.7 for stress due to thermal loading. [[

]]

4.2.1 Weld Quality Factor

For the case of the steam dryer, which is not a core support structure, it was judged that the use of ASME Boiler and Pressure Vessel Code Subsection NG weld quality factors needed to be further evaluated. Weld quality factors are used in the Code to assure adequate margin for static loading. For design against fatigue, margin is maintained by ensuring that the assumed loading is conservative and in the selection of the most conservative fatigue design criterion. The weld quality factor is used in the Code to reduce the allowable stress limit based on the weld inspection method. Paragraph NG-3352 of the Code states that "the use of weld quality factor *n* is for static, not fatigue applications." The same Paragraph also states that "in performing a fatigue analysis, use the fatigue factor *f*, designated in Table NG-3352-1, and the applicable fatigue curve in Table I-9.0." The referenced fatigue factor *f* is equivalent to the weld factor or SCF in Section 4.2. [[

]]

To assure high quality welds, new or replacement steam dryer fabrication employs weld processes that have been fully qualified. Additionally, root and final penetrant testing (PT) inspections are required. When both sides of the weld are accessible, penetrant test nondestructive evaluations are effective at assuring surface imperfections or discontinuities do not exceed required limitations on the root and face of the weld. Limiting surface discontinuities is of particular importance to structures subject to fatigue. Where the root side of the weld is not easily inspected, such as fillet welds, partial penetration welds and some full penetration welds, robust weld process qualifications are conducted to prevent weld defects from occurring during fabrication. Representative weld samples using the same joint design and material types as specified for the new or replacement steam dryer are destructively tested. Metallurgical evaluations demonstrating an acceptable weld root are required prior to weld procedure approval. These tests demonstrate that no defects are present at the root of production welds.

[[

]]

[[

]]

Figure 4.2-1 Weld (Fatigue) Factor Flow Diagram

4.3 ASME CODE STRESS LIMITS FOR LOAD COMBINATIONS

The ASME Code stress limits from Subsection NG of Reference 1 are listed in Table 4.3-1.

Table 4.3-1 ASME Code Stress Limits

Service level	Stress category	Core Support Structures Stress limits (NG)
Service Levels A&B	P_m	S_m
	$P_m + P_b$	$1.5S_m$
Service Level C	P_m	$1.5S_m$
	$P_m + P_b$	$2.25S_m$
Service Level D	P_m	$\text{Min}(0.7S_u \text{ or } 2.4\ S_m)$
	$P_m + P_b$	$1.5(P_m \text{ Allowable})$

Legend:

P_m:General primary membrane stress intensity
P_b:Primary bending stress intensity
S_m:ASME Code Design Stress Intensity
S_U:Ultimate strength

Note: Service Level Limits for Service Levels A, B and C are according to NG-3221 and for Service level D guidance is obtained from Appendix F Paragraph F-1331. Upset condition stress limits are increased by 10% above the limits shown in these table per NG-3223(a).

5.0 STEAM DRYER FEA MODEL AND APPLIED LOADS

A typical steam dryer and its structurally significant components have been described in Section 2.1. These components are included in the full steam dryer finite element model. The commercial finite element software ANSYS is used for the analyses. Section 5.1 provides the detailed descriptions of the finite element model. Section 5.2 describes the dynamic loading used for the fatigue evaluation. Section 5.3 describes the loads applied for the ASME Code evaluations.

5.1 FULL STEAM DRYER FINITE ELEMENT MODEL

A three-dimensional finite element model (FEM) of the steam dryer based on nominal dimensions is created using the ANSYS finite element code (Reference 2). The global FEM models all the structurally significant components of the dryer. The model consists predominantly of shell elements, [[

]] where appropriate. The model also includes the water to structure interactions for the submerged portion of the skirt. [[

]]

5.1.1 Elements and Model Simplifications

The commercial finite element software ANSYS is used in the steam dryer analysis. The finite element model of the steam dryer contains predominantly shell elements. Each node on the shell element has six degrees of freedom – three translational and three rotational. This type of shell element is of elastic formulation and allows both bending and membrane stresses. Three in-plane stress components as well as an out-of-plane normal stress are permitted. ANSYS defines three layers through the shell element thickness (i.e. top, middle and bottom layer). Locations of these layers are determined by the normal orientation of the shell element and stresses can be calculated on these layers. For the FIV analysis, stresses are evaluated and scoped for both top and bottom layers.

Besides the shell element, other types of elements are also used in dryer models. [[

]] Section 5.1.2 discusses the confirmation of the mesh convergence for the model.

Certain simplifications are made when creating a dryer model. These simplifications are made in part to maintain a reasonable model size and analysis run time. These simplifications do not sacrifice the accuracy of the overall structural response of a modeled dryer. The simplifications are explained below.

[[

]] Treatment of welds in analysis has been discussed in the light of weld factor in Section 4.2. Submodeling is discussed in Section 6.2.2.

[[

]] This modeling is further discussed in Section 5.1.5.

[[

]]

Figure 5.1-1 An Example of Steam Dryer Finite Element Model

5.1.2 Mesh Size and Mesh Sensitivity

If the finite element model mesh is not refined enough, the analysis results may be nonconservative. To determine the adequacy of the mesh, a mesh convergence study is performed. [[

]]

Table 5.1-1 Typical Mesh Size: Global FE Dryer Model

[[

]]

5.1.3 Dryer Vane Bundle Model

An overall description of the dryer vane bank has been provided in Section 2.0. A vane bank consists of multiple vane modules. Vane bundles are vane modules without end plates. Each vane bundle contains numerous chevron-shaped vanes as well as tie rods and support pads. The construction of a GEH vane bundle is shown in Figure 5.1-2 and Figure 2.0-4.

The vane modules make up a large part of the total mass of a dryer (Section 2.0). [[

]]

A global dryer FEM contains the degrees of freedom (DOF) used directly in the FIV analysis for a full dryer. [[

]]

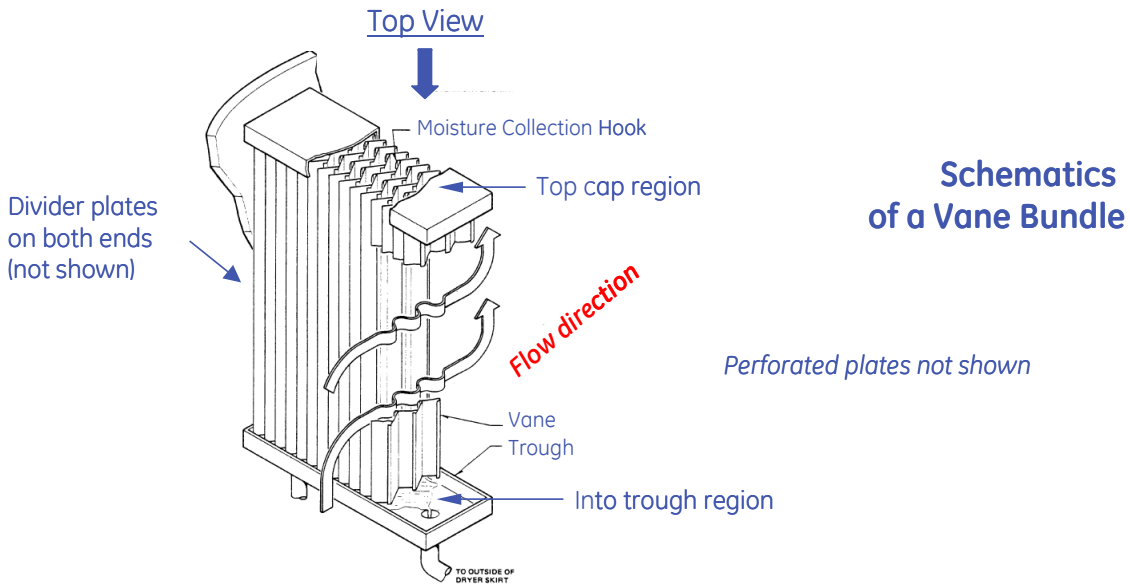

Figure 5.1-2 Vane Bundle Construction

[[

]]

Figure 5.1-3 Vane Bundle FEM and Master DOFs

5.1.4 Water Modeling

The water to structure interaction is included for the submerged portions of the steam dryer. The bottom half of the dryer skirt is submerged in the water. The water provides a resisting pressure on the skirt/drain channel panels as they vibrate through water, having being excited by the oscillating acoustic pressure. These fluid-structure interactions are manifested in the fluid resistance to the structural vibration and may significantly alter the dynamic response of the entire steam dryer.

Water inside and outside skirt is simulated in the structural finite element model. The water levels on the top of the modeled regions are different between inside and outside the skirt. The top surface of water level outside skirt is set at the RPV water level during normal operation. The top water level inside skirt is lower by the equivalent static head of the pressure drop of the steam flow through the vane banks. The bottom water level is determined from the bottom level of steam separator. The bottom of water typically extends below the lower skirt ring.

The outer diameter of the water model is equal to the reactor vessel inner diameter. The inner diameter of the water model is equal to the minimum diameter of an inner circle containing all the steam separator tubes. Water movement is unobstructed within the annular belts between skirt and the separators, and between skirt and the vessel wall. Thus, the modeled water is annular in shape with two stepped levels as shown in Figure 5.1-4. The outer level (higher step) represents the water outside skirt and the inner level (lower step) represents the water inside skirt.

[[

]]

The displacement boundary conditions are applied to the water model in the following manner. All nodes from the water model that are located on the surface of water outer or inner diameter are fixed only in the radial direction, representing the solid boundary of either the reactor vessel

wall or steam separator. Most nodes on the bottom of the modeled water are fixed in the reactor axial direction.

The water surrounding the skirt and drain channels contains a large number of steam bubbles from the steam entrained in the separator spillover flow. This bubbly water is modeled in the fluid elements. The bubbly water properties are significantly different than those of solid water because of the presence of steam bubbles. The carry-under fraction (the mass fraction of the *wet* steam in the mixture of water and bubbles) is used to determine the characteristics of the bubbly water mixture. [[

]] Figure 5.1-5 shows a schematic of *carry-under* as well as the steam-bubbly water interfaces. Further discussions of the effects of the bubbly water on the dryer analyses can be found in Appendices B and C.

Density and bulk modulus are the two major properties required for the ANSYS fluid elements in the model. The bulk modulus measures the resistance to uniform compression, namely, the volumetric deformation under pressure. It also defines the compressive sound wave in fluids and is a significant parameter in determining the sound speed in a fluid medium.

The following is the general equation used to calculate the density of the mixture of fluids. It applies to the density of bubbly water as well as the density of wet steam. If the mixture is bubbly water, the density of the entrapped wet steam is used for ρ_{steam} in the equation. If the mixture is wet steam, the density of dry steam should be used instead. Such dry steam is the compressed steam in the BWR environment of elevated temperature and pressure.

$$\rho_{mixture} = \frac{1}{\frac{q}{\rho_{steam}} + \frac{1-q}{\rho_{water}}} \qquad (5.1\text{-}1)$$

where

$\rho_{mixture}$ = Density of mixture, e.g., the bubbly water or wet steam.

ρ_{steam} = Density of wet or dry steam.

ρ_{water} = Density of the saturated water in a typical BWR RPV environment.

q = Steam quality. If the mixture is bubbly water, q will be carry-under fraction.

For downstream wet steam, the steam quality q is over 99.9% and 1-q is almost zero. Substituting them into Equation (5.1-1), the density of wet steam ($\rho_{mixture}$ in the equation) is found nearly identical with the density of compressed dry steam (ρ_{steam}). Appendix B provides the density of the saturated water in a typical BWR RPV environment (approximately 550°F), which is about 0.026~0.027 lbs/in^3. This value is significantly lower than that of water at ambient temperature. Appendix B also provides the density of the typical wet steam found in a BWR RPV environment. Its value is approximately 0.0013 lbs/in^3. Equation (5.1-1) is then applied once again to obtain the density of bubbly water using those of the saturated water and wet steam.

Derived from the wave equation, the speed of sound in the bubbly water is related to the density and bulk modulus of the bubbly water. The relation may be expressed in the following equation,

[[ ]] (5.1-2)

Where:

[[

]]

The speed of sound within the bubbly water in the typical BWR RPV of elevated temperature and pressure (approximately 550°F and 1050 psi) is obtained from the curves in Figure 12 of Appendix B. [[

]] For dryers with significantly different carry-under fraction and operation conditions, those parameters should be re-calculated using the above equations and relevant data. The bulk modulus of the bubbly water in a typical BWR RPV environment is less than one thousandth of the bulk modulus of pure water at ambient temperature. Bubbly water provides less resistance than solid water to the vibration of the submerged skirt and drain channels.

[[

]]

Figure 5.1-4 Modeling Water

[[

]]

Figure 5.1-5 Schematics of Bubbly Water and Steam

5.1.5 Perforated Plate

In BWR/4 and later dryers, vane bundles are enclosed by perforated plates on each side. The small holes in the perforated plates distribute the steam uniformly over the height of the vane bank. These openings will reduce the mass and stiffness of the plate compared to a plain plate without openings.

A large perforated plate attached to one side of a dryer bank is made of multiple rectangular smaller plates. The perforated plates are welded around their periphery to the top caps, vane module end plates, and trough to provide a steam seal. As a result, the perforated plates provide a direct load path from top caps to the troughs. They also interact with the hoods through hood supports and vane module end plates. In addition, these perforated plates carry significant amount of weight due to their large area despite the fact that they are typically only 1/8" thick. Perforated plates have both inertia and stiffness effects on the FIV response.

[[

]]

[[

]]

Figure 5.1-6 Modeling Perforated Plates

5.1.6 Submodel

Submodeling of high stress regions becomes necessary if the relatively coarse global model is not considered adequate enough to resolve the stress, or if the stress is significantly affected by the local features not modeled in the global model. Section 6.2.2 provides the details on the steam dryer-related submodeling including modeling requirement, analysis procedure and post processing of stresses.

5.2 DYNAMIC LOADS

5.2.1 FIV Pressure Loads

The driving force in the FIV structural analysis is the oscillating acoustic pressure generated by the steam flow inside the reactor dome and four main steam lines (MSL). The FIV load definition is generated based on measurements from on-dryer pressure transducers or pressure measurements taken on the MSLs (typically using strain gages to measure the pipe hoop stress). The PBLE methodology (Appendices B and C) is used to determine the acoustic pressures acting on the dryer from the plant measurements. [[

]] so that the FIV loads determined by the stress analysis will have considered the peak stress intensities that occur at frequencies as low as 1 cycle per 100 seconds. Events that occur less frequently are expected to have a diminished contribution to the FIV fatigue life. The process for selecting the analysis time interval and determining the time interval bias is described in Section 5.2.4. The solved acoustic pressures are then mapped and applied to the structural model to determine the forced response of the steam dryer. Figure 5.2-1 shows the flow chart of the acoustic pressure load definition process leading to the FIV structural analysis. The process for acquiring the plant measurements and developing the plant-specific FIV load definition is provided in Appendix A.

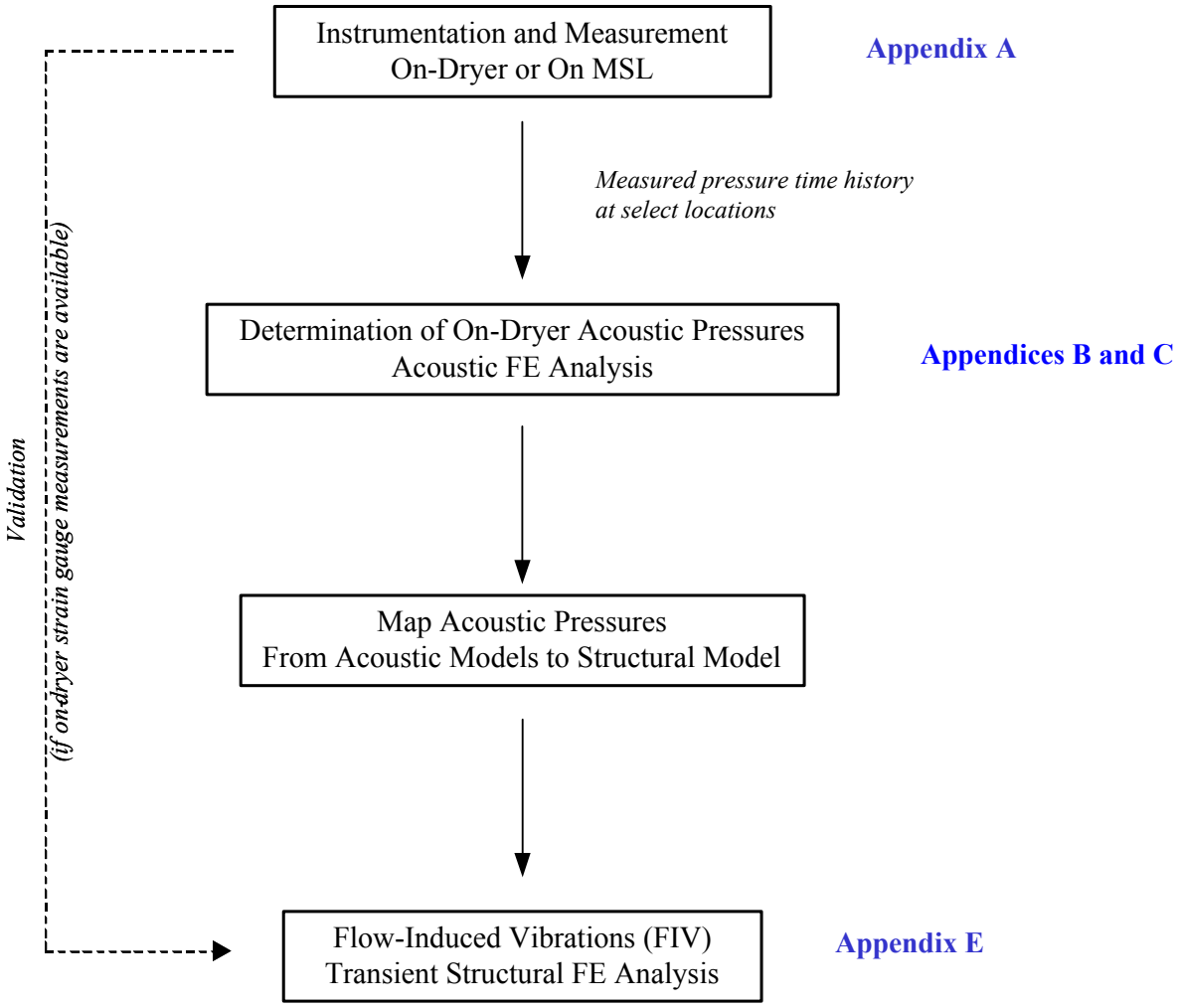

Figure 5.2-1 Process of the FIV Analysis

The acoustic finite element analysis is conducted in the frequency domain. The structural finite element analysis is performed in the time domain (Section 6.1). To apply the acoustic loads to the structural analysis, the acoustic pressure spectra of a steam dryer obtained from an acoustic analysis in the frequency domain have to be transformed first into the time history representations of acoustic pressures in the time domain at the respective locations. There are acoustic pressures on both sides of the dryer panels. The pressures on each side of the panel are resolved into a differential pressure, which is then applied as a pressure force to the structural model.

Typically, the mesh (in the form of nodes and elements) of the acoustic FEM does not match the mesh of the corresponding structural FEM. From an acoustic analysis in the frequency domain, acoustic pressures are evaluated at the acoustic nodes associated with the steam dryer pressure surfaces and then transformed to the form of nodal pressure force time histories. In order to map the acoustic pressures onto a structural model, the mesh from the structural model is first overlaid with the nodes from the corresponding part of the acoustic model (i.e. the acoustic nodes on the steam dryer surfaces). The pressure value of a structural node at each time step is then extracted from that of the acoustic node closest to it at the same time step. Pressures at all structural nodes are mapped in the same manner. This process is repeated for all time steps.
[[

]]

[[

]]

Figure 5.2-2 Contours of Evaluated and Mapped Acoustic Pressures

5.2.2 Bias and Uncertainty of the Steam Dryer FIV Stress

The bias and uncertainty error in the FIV structural analysis comes from various sources. There are uncertainties in the predicted dynamic response and structural modes of the steam dryer, owing to the approximations in the structural model and the uncertainties in the as-fabricated structure. [[

]] Section 8 of Appendix A provides a detailed description of the bias and uncertainty terms for the analysis process.

5.2.3 Dynamic Testing for Prototype Dryers

On a new plant or a prototype replacement dryer where there is more time and space to accommodate frequency response testing, shaker testing may be used in lieu of hammer testing. Either a hammer or a shaker with a force transducer will provide the excitation. Hammer or shaker testing is not practical on an irradiated dryer; however, the bias and uncertainty estimates based on the comparison of simulations and measurements taken on new dryers are applicable to operating dryers because the dryer construction is similar.

The excitation is applied at different accessible regions of the dryer: banks, skirt, end plates, and top caps. [[

(5.2-1)

]] The bias error is represented by frequency band and component. The bias and uncertainty is represented by the average and standard deviation of the error based on multiple tests for a dryer region.

5.2.4 Period of Peak Response for FIV Assessment

The FIV loading used in the finite element stress analysis considers peak stress intensities that occur at frequencies as low as ~1 cycle per 100 seconds. [[

]]

For direct integration structural finite element analysis, to achieve better low and high frequency response resolution while maintaining storage within supercomputer capacity, separate low and high frequency analyses are typically performed. [[

]]

In the F-Factor method, [[

(5.2-2)

(5.2-3)

]] (5.2-4)

This process is repeated over each of the frequency bands to generate the peak stress contribution from each band, Sn.

[[

]]

Table 5.2-1 Time Domain Strain Gage Data Statistics

[[

]]

Assume that [[

. (5.2-5)

. (5.2-6)

. (5.2-7)

(5.2-8)

(5.2-9)

(5.2-10)

(5.2-11)

(5.2-12)

(5.2-13)

]]

5.2.5 Bias and Uncertainty and Benchmarking Using Harmonic FE FIV Solution

The FE benchmark performed in Reference 3 was performed using an ANSYS solution with the direct integration method. If the ANSYS harmonic method is used for the dryer analysis, the

harmonic analysis and associated post processing is also benchmarked against test data and with the direct integration method results. The benchmarking will compare the predicted dryer response against test data and the harmonic stress predictions are compared against direct integration methods to demonstrate that the harmonic post processing methodology successfully identifies maximum stress regions of steam dryer subcomponents. The FE harmonic model bias and uncertainty is determined based on these benchmark comparisons.

5.3 ASME LOADS

Section 8 provides the detailed information on the load combinations assumed for the ASME B&PV Code analyses. The process for defining the various ASME load terms is provided in Appendix A.

6.0 VIBRATION ANALYSIS AND PREDICTED COMPONENT STRESSES

This section describes the process used to perform the FIV structural analysis. The commercial finite element software ANSYS is used in the solution. For the flow-induced vibration of steam dryers, GEH applies the ANSYS transient dynamic analysis (i.e. direct integration method) in the time domain with [[

]].

6.1 DYNAMIC ANALYSIS APPROACH

6.1.1 Structural Damping

Structural damping exists in steam dryers, which dissipates part of the vibration energy. [[

]] consistent with the recommendation in the USNRC Regulatory Guide 1.20 Revision 3.

Rayleigh damping is assumed and applied to all structural finite element models of steam dryers. Rayleigh damping assumes that damping matrix (**C**) is a *linear combination* of mass matrix (**M**) and stiffness matrix (**K**) in the equation of motion; namely,

$$\mathbf{C} = \alpha\,\mathbf{M} + \beta\,\mathbf{K} \qquad (6.1\text{-}1)$$

Where α and β are the alpha and beta Rayleigh damping constants.

[[

]]

[[ ]] (6.1-2)

Therefore, the damping ratio, i.e. the ratio of the damping constant over critical damping constant, varies [[ ]]. On a curve of damping ratio *versus* frequency, no more than two frequencies can have the same damping ratio. [[

]]

[[ ]] (6.1-3)

The Rayleigh damping ratio as described is frequency dependent if the alpha and beta damping constants are invariant. A constant damping ratio is prescribed at the anchoring frequencies ω_1 and ω_2. [[

]] damping ratio (ζ) for the structural analysis is assumed in the dryer analyses. In the time domain transient dynamic analysis with ANSYS, frequency-dependent and material-dependent alpha and beta damping constants cannot be defined and therefore, it is not possible to enforce the same damping ratio at all frequencies. As a result, two anchoring frequencies have to be selected [[ ]]. The anchoring frequencies are defined by the frequency range where significant pressure loads are present. This is to ensure that within the analyzed frequency range, the damping ratio is [[ ]] for the frequencies at which the structure is being driven.

In the typical dryer structural analysis, a wide range of frequency is covered. As shown by Curve 2 of Figure 6.1-1, a single damping curve covering the entire frequency range results in an effective damping ratio of much less than [[ ]] over a large portion of the frequency range. Thus, depending on the measured frequency content in the acoustic loads, [[

]] structural analyses may be performed, each with its own governing damping curve. Curve 1 of Figure 6.1-1 shows [[

]]

The damping used for harmonic analyses in the frequency domain does not have the limitations imposed by Rayleigh damping in the time domain. A harmonic analysis in the frequency domain permits frequency-dependent damping ratios to be used. Harmonic analyses in the frequency domain will use a [[ ]] applied for all frequencies.

[[

]]

Figure 6.1-1 [[ ]]

6.1.2 Dynamic FIV Analysis

The commercial finite element software ANSYS is used in the FIV analysis for the steam dryer. The time domain full transient dynamic analysis method (transient analysis type and full solution method) in ANSYS is used for the structural analysis. This analysis employs direct integration over the time domain and therefore, it is also referred to as the direct integration method. Alternately, the harmonic analysis method in ANSYS may be used. Linear elastic analysis is performed for the FIV analyses because all the dryer materials are expected to remain within the linear elastic range during normal operation and there is no large nonlinear deformation involved.

The acoustic pressure load definition process is described in Section 5.2.1. The process for selecting the analysis time segment and determining the residual time segment bias is described in Section 5.2.4. The acoustic loads are periodic and contain a full spectrum of frequencies. In the time domain analysis, multiple time steps are needed in order to preserve the fidelity of the load definition at the highest frequency considered. For a cyclic acoustic load, at least eight (8) time steps per cycle are used to define the peak and valley of the load definition at its highest frequency. For example, for an analysis with input frequencies up to 125 Hz, at least 1000 time steps per second are required. An acoustic time step is defined for each time step in the ANSYS solution in order to preserve the fidelity of the frequency content throughout the evaluation.

In order to address the limitations of the applied structural damping in the time domain analysis, the acoustic load definition is divided into [[ ]] portions and analyzed as separate cases. [[

]]

The available test data from instrumented steam dryers show that there is no significant pressure loading or structural response for [[

]]

When the analytical acoustic loads are first applied to the dryer at the beginning of the analysis, the structural response goes through a startup transient due to the inertia effect of the dryer (i.e. the dryer is initially assumed to be at rest). The structural response during this initial startup transient stage is not representative of steady-state operation because it is still strongly

influenced by the initial condition of the dryer. The structural response in the analysis will become independent of the initial condition of the dryer only after a large number of time steps. To minimize the initial condition effect and capture the low frequency response, the beginning of acoustic load is gradually ramped up from zero to full amplitude during the initial series of time steps. Therefore, the initial portion of the applied load time history is spent to achieve a stabilized response. A window function is applied to smooth the time history data of acoustic pressure and reduce the time needed to phase out significant initial condition effect. In the dryer analyses, direct integration solutions after half a second are generally considered sufficiently removed from the initial condition effect. [[

]] The analysis time intervals are long enough to ensure that the startup transient effects have passed.

There is an uncertainty in the predicted structural mode frequencies and dynamic response of steam dryers because of the approximations in the structural model and variations in the as-built dryer as compared to the nominal design dimensions (e.g. tolerances on plate thickness). The uncertainties in the pressure load frequency content and damping also contribute to the uncertainty in the structural analysis. Coupling of structural and acoustic modes is often a major contributor to severe stress response. Structural model uncertainty, if not addressed properly, may result in underestimating peak stress response by overlooking the actual structural modes that may be significantly excited by acoustic loads, owing to a difference between the predicted mode and the real mode.

[[

]]

Displacement boundary conditions are applied to the lug support locations in the dryer model as shown in Figure 6.1-2. The support ring rests on four to six steam dryer support brackets that are welded attachments to the RPV wall. Seismic blocks are attached to the support ring at each of the bracket locations. The motion of the steam dryer in the circumferential direction is constrained by the seismic blocks, while leaving the support free in the radial direction to

accommodate differential thermal expansion between the dryer and the RPV. Under FIV loading during normal operation, constraints in the radial direction have only a minor effect on the dryer response. Motion in the vertical direction is constrained by the dryer dead weight. For simplicity, the nodes at the locations of the support brackets are fixed in the translational degrees of freedom.

The direct integration method in the time domain was used in the FEA benchmark against the on-dryer strain measurements in Reference 3. [[

]]

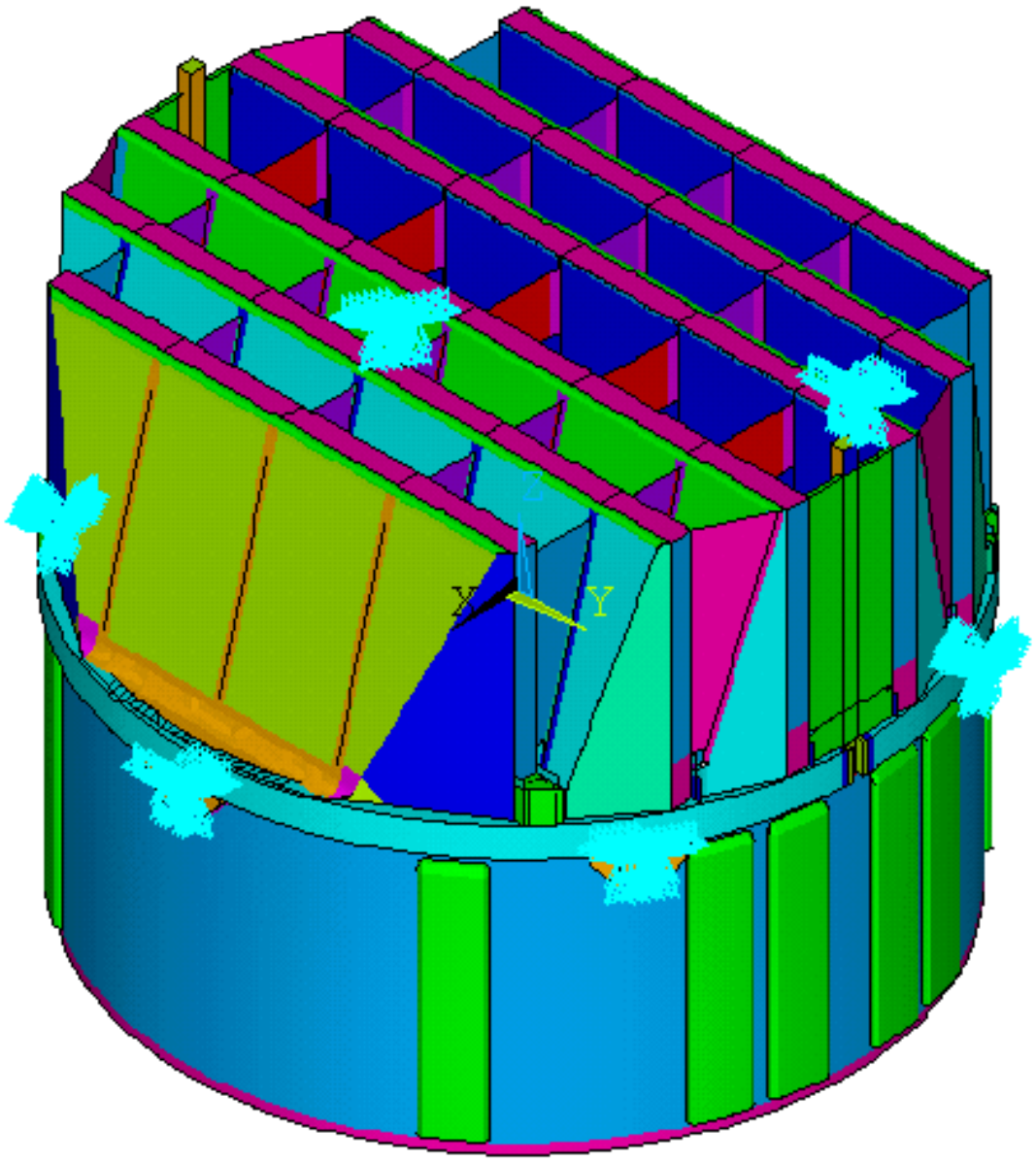

Figure 6.1-2 Steam Dryer Boundary Conditions – Dryer with Six Brackets

6.2 STRESS RECOVERY

6.2.1 Post Processing of Global FEM Analysis

The results of the dynamic stress analysis consist of time histories of the structural response of all the elements in the FEM. In the post-processing of the analysis results, the stresses of all time steps are searched in order to determine the maximum stress intensities for the dryer components. This process is called stress scoping. These maximum stress intensities are then used in the fatigue evaluation. The results for each component are scoped to obtain the maximum stress intensity directly from the analysis. In addition, the weld lines are scoped and the results adjusted by the appropriate weld factor to determine the maximum stress intensities in the weld regions. The scoping results are tabulated individually for each of the modeled steam dryer components.

Element stress intensities from ANSYS are used to represent the steam dryer stress results. Stress intensity is defined as the difference between maximum and minimum principal stresses, equivalent to twice the maximum shear stress. Element stress intensities at an element's nodal locations are extracted during the post-processing of the ANSYS results. For each shell element at a given time step, four stress intensity values are extracted from the upper layer at the four nodes associated with the element, and four more values from its bottom layer (refer to Section 5.1.1 for the definition of shell layers). The maximum of these eight values is used to represent the maximum stress intensity of this shell element at this time step. The maximum of all time steps is therefore the maximum stress intensity for this element.

In the global dryer FEM, the components of the dryer model are defined and grouped based on their common design features and relative loading. The scoping described previously for a single element is extended to all elements in a pre-defined dryer component. The maximum stress intensity is then determined for that dryer component, which is used in the fatigue evaluation. The resulting FIV stress table contains the maximum stress intensities directly from the analysis for each dryer component. An example of stress table is provided in Section 9.0. The maximum stress intensity is used in the high cycle fatigue evaluation. As described in Section 7.1, this approach is in general more conservative than using the alternating stress intensity. During the scoping process, the membrane stresses are saved for use in the ASME code-based load combination evaluations described in Section 8.0.

Stress contour plots can be generated from ANSYS based on the scoping results. They are useful in visualizing high stress regions. Figure 6.2-1 shows an example of stress contour for the inner hood panels at the time of the peak stress intensity for the panels. The plot shows that the

location of the maximum stress intensity is on the border to a hood tee. The global distribution of the relatively high stresses at this time step is also evident from the color contours.

For the high stress intensity elements located on a weld, the stress intensity value has to be modified by the appropriate weld SCF described in Section 4.2. All elements from the FEM that are either lying astride or bordering on the weld lines are identified. In addition, all nodes that are located on the weld lines are also identified. Each weld location may join together two or more different dryer components. The results are scoped for the element stress intensities for the components on both sides of the weld lines. To obtain the weld stress intensities, these stress intensities are multiplied by the appropriate weld SCF for the type of weld. The maximum weld stress intensity is then determined for each component that is associated with welds.

Each dryer component is thus identified with two values after scoping, the maximum stress intensity from the component scoping and the maximum weld stress intensity after application of the appropriate weld stress concentration factor. The larger of these two values is then used to represent the maximum stress intensity for this dryer component.

[[

]]

Figure 6.2-1 Stress Intensity Contour at Max Stress Intensity (SI) Time Step – Inner Hoods

6.2.2 Submodel Analysis and Local Stress

Submodeling is a finite element technique to obtain more accurate results in a particular region of a model. For the global dryer model, mesh convergence has been established for the general membrane and bending stresses (nominal stress). Therefore, for the high stress seen in the middle of a plate (e.g., hood panel) with no discontinuities or other stress concentration factors in its vicinity, these stresses are veritable and there is no further need for submodeling the stressed area. However, submodeling may be necessary for the high stress seen in a region of the model where stress concentration factors exist but not captured by the model. Examples include the welded connections, fillets and other geometric discontinuities. A global dryer model typically does not include these details. In summary, submodeling of steam dryers may be justified if the weld stress is significantly high in the global model, or if the high stress area is influenced by geometric discontinuities not adequately captured in the global model. Typical applications of submodeling include high-stressed welds identified by the global model results.

A submodel with much finer mesh and employing solid elements is built that includes the necessary geometric details not included in the global model. A dynamic analysis of the submodel is performed using the same time step definition from the global model. The cut boundary conditions at each time step from the global model are extracted and mapped onto the submodel. For the submodel of a weld, the analysis stress results are linearized along the weld throat to be used in the weld stress fatigue evaluation. If there is a theoretical solution applicable to the particular stress condition in a dryer region and the global model in that region is not adequate to determine the local stress, a closed form solution may be employed instead of submodeling to re-evaluate the predicted stresses from the global model in that region. To perform the closed form solution, structural forces and moments across relevant cross-sections are extracted from the global finite element model and used in the closed-form formulae from the Strength of Materials or other theoretical solutions to estimate more accurate stresses at the interested locations. An example of a closed form calculation is the stress calculation for the bank-to-bank tie bars.

For submodeling, a small area encompassing the high stress region is cut out from the global model. The size of a submodel is determined by the locations of its cut boundaries. The cut boundaries must be located sufficiently away from the high stress region so that the high gradient localized stresses will have no effect on the cut boundaries. In addition, there must be sufficient space between the cut boundaries and the high stress regions to allow adequate mesh transition. The displacement along the cut boundaries is extracted from the global model and mapped onto the same boundaries in the submodel. In order to determine whether the cut boundary conditions are applied correctly, the submodel using the original global shell mesh is first analyzed. This submodel is a portion of the global model without any modification. The same dynamic analysis

for the global model is applied to the submodel and the maximum stress results are compared to those from the global model analysis. Allowing for minimal numerical errors, the results from both models should be nearly identical.

Once the correctness of the cut boundary application is ascertained, the part of the submodel away from the cut boundaries will be refined and replaced with solid elements. Except for the area adjacent to the cut boundaries, the original mesh (typically, of shell model) is replaced with the refined solid element mesh that captures the discontinuities and other geometric details lacking in the global model. In the area adjacent to the cut boundaries, the original shell mesh is retained. In this area, the mesh is gradually transitioned to the more refined solid element mesh. Solid elements do not have the rotational DOFs that shell elements have. [[

]]

A stress convergence study is performed as described in Section 5.1.2. [[

]]

Pressure forces applied in the global model are also mapped to the submodel. After completing the submodel analysis, the submodel reaction forces at the boundaries are compared to the internal forces at the cut boundaries in the global model. This step confirms that the structural stiffness is comparable between the global model and the submodel. The force difference is found to be the smallest when the original shell mesh is retained in the vicinity of the cut boundaries in the submodel, which is the approach undertaken in meshing submodels. Figure 6.2-2 shows an example of a submodel around outlet end plates. Figure 6.2-3 shows the boundary conditions and other details of the submodel.

A full transient dynamic analysis is performed on the submodel using the same time step definition as that in the global model. This approach allows the inertia effect to be reproduced in the submodel through the time history. This is accomplished by extracting the cut boundary conditions from the global model and mapping them onto the submodel for every time step. Similar to the global model, an ANSYS load step file is generated at each time step and the transient dynamic analysis type is prescribed for the submodel.

Submodels are generally used to address the observed high stresses in the global model that are related to welds or other stress concentrations from geometry not adequately captured in the global model. [[

]]

[[

]]

Figure 6.2-2 Illustration of a Submodel Around Outlet End Plates

[[

]]

Figure 6.2-3 Boundary Conditions of a Submodel Around Outlet End Plate

[[

]]

Figure 6.2-4 Calculation of Fillet Weld Nominal Stress by Linearization

7.0 FATIGUE PREDICTION

Steam dryers are subjected to cyclic acoustic pressures that cause flow-induced vibration during normal operation. They may experience on the [[ ]] during a steam dryer's typical 40-60 year life. Therefore, HCF constitutes a major structural acceptance criterion for the steam dryer. The steam dryer fatigue evaluation described in this section is consistent with the ASME B&PV Code Section III requirements.

7.1 FATIGUE CALCULATION

In performing the fatigue evaluation for steam dryers under FIV loading, the maximum stress intensity in each dryer component is found from the FIV stress analyses described in Section 6. The maximum stress intensities are then adjusted as necessary by the appropriate weld stress concentration factors defined in Section 4.2. If the analysis is being performed in support of a plant power uprate, the adjusted stress intensities are then scaled up to the predicted EPU conditions using the EPU scaling factor described in Section 5 of Appendix A. Finally, the analysis biases and uncertainties described in Section 5.2.2 are incorporated into the results. The resulting maximum stress intensities are compared against the fatigue acceptance criterion described in Section 4.1.

The ASME Code (Section III, Div 1, NG-3222.4) prescribes the alternating stress intensity for fatigue evaluation of cyclic operations. Instead of assessing true alternating stress intensity in the dynamic cycles, the maximum stress intensity is used in the FIV fatigue evaluation of the steam dryer. The stress intensity is twice the maximum shear stress; in other words, it represents the stress range if the maximum shear stress completely reverses itself during a dynamic cycle (in this case, mean stress will be equal to zero). The alternating shear stress in the above situation is half of the stress range (or half the value of the maximum stress intensity). For the assessment of fatigue acceptance, the full value of maximum stress intensity is compared against the fatigue limit. The maximum stress intensity is in general a more conservative approach than alternating stress intensity in such fatigue evaluation.

The requirement for acceptance of a dryer component is that its maximum stress intensity has to be smaller than the fatigue limit. [[

]]

[[

]]

Figure 7.1-1 Primary and Weld Scoping for Fatigue Evaluation

7.2 FREQUENCY CONTENT OF THE STRUCTURAL RESPONSE

The frequency content of the stresses is analyzed for the components with small safety factors as identified by the fatigue evaluation. The frequency content of strain and peak stress over multiple frequency bands is factored into the calculation of the overall stress bias in the RMS method described in Section 5.2.2.

8.0 ASME LOAD COMBINATIONS

The steam dryer is not a safety component and performs no active safety function. However, the dryer must maintain its structural integrity (i.e. generate no loose parts) so as to not interfere with the function of a safety system. The following section discusses the methodology used for the primary stress assessment of the steam dryer and the RPV support brackets. The results of this assessment demonstrate that the dryer will maintain its structural integrity during transient and accident events. Guidance is provided by Article NG-3000 of Reference 1 for the steam dryer and Article NB-3000 of Reference 1 for the attachments to the RPV shell.

8.1 ASME LOAD COMBINATIONS

Load combinations are defined for the evaluation of the primary stresses in the steam dryer for Normal (Service Level A), Upset (Service Level B), Emergency (Service Level C), and Faulted (Service Level D) conditions. The load combinations are specified in the Steam Dryer Design Specification and associated data sheet. Table 8.1-1 provides a typical set of load combinations applied to the steam dryer. Plant-specific design basis load combinations will be used.

Table 8.1-1 ASME Load Combinations and Conditions

Comb. no	Level	Combination
A-1	Normal	[[
B-1	Upset	
B-2	Upset	
B-3	Upset	
B-4	Upset	
B-5	Upset	
C-1	Emergency	
D-1	Faulted	
D-2	Faulted	
D-3	Faulted	
D-4	Faulted	
D-5	Faulted	]]

Notes:

1. Loads from independent dynamic events are combined by the square root sum of the squares method.
2. The load combination table is typical. Plant-specific design basis load combinations will be used.

Definition of Load Acronyms

[[

]]

8.2 ASME APPROACH

The global FE shell model described in Section 5.1 is used in these analyses. The structural responses of the steam dryer to the ASME load combinations will be evaluated using the ANSYS finite element code for the loads defined in Section 8.1. The results of the individual load analyses are then combined for each event as specified in Table 8.1-1. The type of finite element structural analysis for each load term in Table 8.1-1 is identified in Table 8.2-1. [[

]].

Table 8.2-1 Type of Analysis for the Load Terms in ASME Load Combinations

Load Term	Description	Type of Analysis for the Load
[[		
		]]

Note:

DLF Dynamic Load Factor: The static analysis stress results are multiplied by this factor to adjust for the effect from transient events.

8.3 ASME LOAD CASE STRESS RESULTS

The stress intensity representing the FIV membrane stress is obtained from the FIV analysis for every component and every load. The results of the individual load analyses are then combined for each event as specified in Table 8.1-1. The resulting stresses are then compared to the criteria from Section 4.1. Table 9.0-4 in Section 9 provides a template table for reporting the maximum stress intensity values of dryer components. Minimum stress margins are also calculated in the table.

8.4 ASME CODE ANALYSIS OF THE RPV DRYER BRACKETS

The following section covers the steam dryer components that support the dryer within the RPV. These components are the steam dryer support brackets and the guide rod brackets. While the steam dryer analyses take guidance from Article NG-3000 of Section III of the ASME BPV Code (Reference 1), the brackets attached to the RPV are governed by Article NB-3000 and Appendix F of the same Code. Also, note that the analyses of these brackets falls into the "Safety Related" category because these brackets are attached to the reactor vessel pressure boundary.

The guide rod bracket provides a load path to the RPV only during dryer installation; therefore, the following paragraphs will primarily focus on the support brackets (lugs) and the RPV near the lugs.

Table 9.0-5 shows a typical minimum margin stress summary table. This table will be referred to throughout the following paragraphs.

8.4.1 Load Cases

The load combinations to be considered are defined by the design basis for the plant and the RPV. The certified design specification for the steam dryer brackets provides guidance with regard to the load combinations and load types that are to be considered. The load combinations considered are similar to those in Table 8.1-1 and additional design and installation load combinations are analyzed per the steam dryer bracket design specification.

8.4.2 Primary Stress

The primary stress intensity values required by the code are general primary membrane (Pm), local primary membrane (PL) and membrane plus bending (PL + PB). Special stress categories such as the maximum shear stress and bearing stress are also calculated as part of the primary stress assessment.

The primary stress values in the RPV shell and the steam dryer brackets are determined differently. [[

]]

8.4.2.1 RPV Primary Stress Assessment

The primary membrane stress intensity due to the design pressure is determined using closed form equations. This stress intensity value is compared to Sm (see Table 9.0-5).

[[

]]

[[

]]

Figure 8.4-1 Typical Steam Dryer Bracket FEM

The forces experienced by the bracket for the load combinations for the various service levels are applied to the contact area between the bracket and the steam dryer and run using static analysis. The model is then post processed to determine the following stress intensity values for each load combination:

1. [[

2.

]]

8.4.2.2 Dryer Bracket Primary Stress Calculations

[[

]]

[[

]]

Figure 8.4-2 Bracket Stress Calculation Locations

[[ ]] The calculations include the evaluation of primary membrane stress intensity, primary membrane plus bending stress intensity, and the primary and maximum shear stress in the bracket. [[

]]

The code allowable values for the general and local primary membrane, local membrane plus bending, and the average and maximum shear stress values are provided in Table 9.0-5. Note that the upset condition (Service Level B) allowable values are increased by 10% over the normal operating condition values per Code (Reference 1). The faulted (Service Level D) condition allowable stress values are governed by Appendix F of Reference 1.

8.4.3 Secondary Stress Range

For the normal and upset plant conditions, the code requires a check of the local primary membrane (PL) plus primary bending (PB) plus the secondary stress range (Q) at this location. The PL + PB + Q stress is compared to 3.0Sm.

8.4.3.1 RPV Shell

For the RPV shell in the evaluation of the primary plus secondary stress range (PL + PB + Q) for the normal and upset conditions, the pressure stress in the RPV shell dominates. Therefore, the maximum primary local membrane plus bending (PL + PB) is increased by the secondary stress range (Q) from the thermal cycling due to the start up and shut down transients. This stress range is usually obtained from the original stress report for the RPV. This report has the thermal stress due to the startup and shutdown transients at various locations of the RPV shell. [[

]]

8.4.3.2 Steam Dryer Bracket

Because the materials used for the support bracket are usually similar with respect to thermal expansion coefficients, the only loading that produces a secondary stress in the dryer bracket at the bracket-to-RPV interface is due to internal pressure cycling. [[

]]

8.4.4 Analysis for Cyclic Operation

An assessment is performed to determine the suitability of the bracket and shell at the bracket location to the vibratory environment. This assessment is governed by paragraph NB-3222.4 (d) of the Code (Reference 1). This paragraph is entitled "Components Not Requiring Analysis for Cyclic Operation," and sets forth the criterion for fatigue analysis exemption (i.e. no cycle counting required). This is also known as a fatigue exemption assessment.

Parts NB-3222.4 (d)(1) - (5) discuss the requirements on the usage with regard to the atmospheric to service pressure cycles, normal service pressure fluctuations, and temperature differences. The Reactor Pressure Vessel Stress Report for the particular plant in operation typically provides evidence that these criteria are met for the RPV shell and its attachments.

Part NB-3222.4 (d)(6) discusses mechanical loads. The locations evaluated for the mechanical fatigue assessment are the same as those for the bracket primary stress analysis in Section 8.4.2.2. This approach is appropriate for the evaluating the bracket fatigue with regard to mechanical loading where the resulting stress range is then compared with the allowable stress amplitude. Here the code is assigning a stress concentration value of two, with the total cumulative number of significant cycles used for the fatigue exemption determination of a load condition.

In the mechanical load fatigue exemption, the specified full range of mechanical loads excluding pressure must not result in load stresses whose range exceeds the alternating stress allowable (Sa) value from the applicable fatigue curve for the total specified number of significant load fluctuations. [[

]]

[[

]] This value is compared with the Sa allowable for the total design cycles for significant loads.

[[

]]

9.0 PLANT SPECIFIC REPORT CONTENT

The plant-specific steam dryer stress report includes information on the finite element model, material properties, analysis methodology, FIV load definition, design basis load combinations, and structural acceptance criteria used in the analysis. It presents the results of the fatigue analysis and the primary stress analysis. Plant-unique special analyses and supporting justifications are also provided in the plant-specific steam dryer stress report.

This subsection provides templates for tabulated final stress processing that are common to all dryer analyses. Typical dryer components are listed. Tables 9.0-1 and 9.0-2 document the process of determining the maximum stress intensity of each dryer component for the [[ ]] analyses, respectively. The maximum stress intensities from both the primary scoping and the weld scoping are tabulated for the nominal run and all time shift runs so that both weld stress and structural uncertainty are included in the maximum component stresses. Table 9.0-3 documents the process of determining the final stress intensities. It includes combining the [[ ]] stresses, scaling to EPU and adjusting for the analysis bias and uncertainty. For the example shown in Table 9.0-3, a single bias and uncertainty factor is applied to both [[ ]] results. If the bias and uncertainty is different for the [[ ]] stress intensities will be scaled to EPU and adjusted for the bias and uncertainty separately prior to final combination. Table 9.0-3 also documents the final safety factor calculation.

The primary stress analysis results table templates are shown in Tables 9.0-4 and 9.0-5.

Table 9.0-1 Maximum Stress Intensities after Scoping – [[ ]] (Template)

COMPONENT	[[ ]] - Maximum Stress Intensity (psi)																		Applied Weld Factor for weld scoping	LF Max Stress Intensity (psi)	Load Case at Max Stress
	NOM		P10		P75		P5		P25		M25		M5		M75		M10				
	Primary scoping	Weld scoping	Primary scoping	Weld scoping	Primary scoping	Weld scoping	Primary scoping	Weld scoping	Primary scoping	Weld scoping	Primary scoping	Weld scoping	Primary scoping	Weld scoping	Primary scoping	Weld scoping	Primary scoping	Weld scoping			
Dryer Base Plate																					
Trough Thin Section																					
Trough Thick Section																					
Bank Top Cap - Inner																					
Bank Top Cap - Outer																					
Bank End Plates - Inner																					
Bank End Plates - Outer																					
Outlet End Plates - Inner																					
Outlet End Plates - Outer																					
Hoods - Inner																					
Hoods - Outer																					
Divider Plates																					
Inlet End Plates - Inner																					
Inlet End Plates - Outer																					
Skirt																					
Drain Pipes																					
Drain Channels																					
Lower Skirt Ring																					
Cover Plates																					
Hood Tees - Inner																					
Hood Tees - Outer																					
Support Ring																					
Tie Bars Bank-to-Bank																					
Hood Supports																					

Table 9.0-2 Maximum Stress Intensities after Scoping – [[ ]] (Template)

COMPONENT	[[ ]] - Maximum Stress Intensity (psi)																		Applied Weld Factor for weld scoping	HF Max Stress Intensity (psi)	Load Case at Max Stress
	NOM		P10		P75		P5		P25		M25		M5		M75		M10				
	Primary scoping	Weld scoping	Primary scoping	Weld scoping	Primary scoping	Weld scoping	Primary scoping	Weld scoping	Primary scoping	Weld scoping	Primary scoping	Weld scoping	Primary scoping	Weld scoping	Primary scoping	Weld scoping	Primary scoping	Weld scoping			
Dryer Base Plate																					
Trough Thin Section																					
Trough Thick Section																					
Bank Top Cap - Inner																					
Bank Top Cap - Outer																					
Bank End Plates - Inner																					
Bank End Plates - Outer																					
Outlet End Plates - Inner																					
Outlet End Plates - Outer																					
Hoods - Inner																					
Hoods - Outer																					
Divider Plates																					
Inlet End Plates - Inner																					
Inlet End Plates - Outer																					
Skirt																					
Drain Pipes																					
Drain Channels																					
Lower Skirt Ring																					
Cover Plates																					
Hood Tees - Inner																					
Hood Tees - Outer																					
Support Ring																					
Tie Bars Bank-to-Bank																					
Hood Supports																					

Table 9.0-3 Maximum Stress Intensity and MASR from FIV Analysis (Template)

DRYER COMPONENT	CLTP MAXIMUM STRESS INTENSITY (PSI)	EPU MAXIMUM STRESS INTENSITY (PSI)					MAX STRESS INTENSITY (PSI)	MASR
		SRV Freq #1	SRV Freq #2	SRV Freq #3	SRV Freq #4	SRV Freq #5		
Dryer Base Plate								
Trough Thin Section								
Trough Thick Section								
Bank Top Cap - Inner								
Bank Top Cap - Outer								
Bank End Plates - Inner								
Bank End Plates - Outer								
Outlet End Plates - Inner								
Outlet End Plates - Outer								
Hoods - Inner								
Hoods - Outer								
Divider Plate								
Inlet End Plates - Inner								
Inlet End Plates - Outer								
Skirt								
Drain Pipes								
Drain Channel								
Lower Skirt Ring								
Cover Plate								
Hood Tee - Inner								
Hood Tee - Outer								
Support Ring								
Tie Bars Bank-to-Bank								
Tie Bars at center								
Trans Brace under Base Plate								
Trans Brace Brackets								
Hood Support								
Holddown								

Table 9.0-4 Typical ASME Stress Table for the Steam Dryer (Template)

Component	Normal		Upset						Emergency		Faulted							
	A1		B1		B2		B3		C1		D1		D2		D3		D4	
	Pm	Pm+b	Pm	Pm+b	Pm	Pm+b	Pm	Pm+b	Pm	Pm+b	Pm	Pm+b	Pm	Pm+b	Pm	Pm+b	Pm	Pm+b
Dryer Base Plate																		
Trough Thin Section																		
Trough Thick Section																		
Bank Top Cap – Inner																		
Bank Top Cap – Outer																		
Bank End Plates – Inner																		
Bank End Plates – Outer																		
Outlet End Plates – Inner																		
Outlet End Plates – Outer																		
Hoods – Inner																		
Hoods – Outer																		
Inlet End Plates – Inner																		
Inlet End Plates																		
Skirt																		
Drain Plugs																		
Lower Skirt Ring																		
Cover Plate																		
Hood Tee – Inner																		
Hood Tee – Oouter																		
Support Ring																		
Tie Bars Bank-to-Bank																		
Tie Bars at center																		
Trans Brace under Base Plate																		
Trans Brace Brackets																		
Bank Top Cap – Inner (no TieBar)																		
Bank Top Cap – Outer (no TieBar)																		
Divider Plate – Inner Banks																		
Divider Plate – Outer Banks																		
Hood Support – Inner Banks																		
Hood Support – Outer Banks																		
Drain Channel – radial leg																		
Drain Channel – circum portion																		
Bank Top Cap – Inner																		
Bank Top Cap – Outer																		
304L SS Allowable Stress	14350	21525	15785	23678	15785	23678	15785	23678	21525	32288	34440	51660	34440	51660	34440	51660	34440	51660
Max Stress / Allowable																		

Table 9.0-5 Table of Minimum Design and Operational Stress Margins (Template)

Service Condition	Component	Stress Category	Requirement	Allowable Value [psi]	Maximum Predicted Value [psi]	Stress Margin	Remarks
DESIGN	Dryer Bracket	P_m	$1.0S_m$				
	Vessel Shell		$1.0S_m$				
	Dryer Bracket	Maximum Shear	$0.8S_m$				
	Vessel Shell		$0.8S_m$				
	Dryer Bracket	$P_L + P_B$	$1.5S_m$				
	Vessel Shell		$1.5S_m$				
	Dryer Bracket	Bearing Stress	$1.0S_y$				
	Vessel Shell		N/A	N/A	N/A	N/A	
NORMAL	Dryer Bracket	P_m	$1.0S_m$				
	Vessel Shell	P_L	$1.5S_m$				
	Dryer Bracket	$P_L + P_B$	$1.5S_m$				
	Vessel Shell		$1.5S_m$				
	Dryer Bracket	Maximum Shear	$0.8S_m$				
	Vessel Shell		$0.8S_m$				
	Dryer Bracket	$P_L + P_B + Q$	$3.0S_m$				
	Vessel Shell		$3.0S_m$				
	Dryer Bracket	Bearing Stress	$1.0S_y$				
	Vessel Shell		N/A	N/A	N/A	N/A	
	Dryer Bracket	FATIGUE	Exemption from Fatigue Analysis per NB-3222.4 see Section X.XX				
	Vessel Shell						
UPSET	Dryer Bracket	P_m	$1.1S_m$				
	Vessel Shell	P_L	$1.65S_m$				
	Dryer Bracket	$P_L + P_B$	$1.65S_m$				
	Vessel Shell		$1.65S_m$				
	Dryer Bracket	Maximum Shear	$0.88S_m$				
	Vessel Shell		$0.88S_m$				
	Dryer Bracket	$P_L + P_B + Q$	$3.3S_m$				
	Vessel Shell		$3.3S_m$				
	Dryer Bracket	Bearing Stress	$1.0S_y$				
	Vessel Shell		N/A	N/A			
	Dryer Bracket	FATIGUE	Exemption from Fatigue Analysis per NB-3222.4 see Section X.XX				
	Vessel Shell						
FAULTED	Dryer Bracket	P_m	$Min(0.7S_u$ or $2.4\ S_m)$				
	Vessel Shell		$Min(0.7S_u$ or $2.4\ S_m)$				
	Dryer Bracket	P_L	$1.5*(Min(0.7S_u$ or $2.4\ S_m))$				
	Vessel Shell		$1.5*(Min(0.7S_u$ or $2.4\ S_m))$				
	Dryer Bracket	$P_L + P_B$	$1.5*(Min(0.7S_u$ or $2.4\ S_m))$				
	Vessel Shell		$1.5*(Min(0.7S_u$ or $2.4\ S_m))$				
	Dryer Bracket	Primary Shear	$0.42S_u$				
	Vessel Shell		$0.42S_u$				
	Dryer Bracket	Maximum Shear	$0.9S_u$				
	Vessel Shell		$0.9S_u$				

Table Notes:

10.0 CONCLUSIONS

This report defines the methodology for the structural analysis of steam dryers in response to FIV loads. The report describes the detailed finite element model, analysis procedures, fatigue evaluation and ASME load combinations of steam dryers used in the BWR/2 through BWR/6 and ABWR product line. The FIV loads defined in Appendices B and C are applied in the structural analysis. The structural analysis results will be used to iterate on steam dryer designs that will meet the required fatigue and ASME load combination stress criteria.

11.0 REFERENCES

1. American Society of Mechanical Engineers Boiler and Pressure Vessel Code (ASME B&PV), Section III, 2001 Edition.

2. ANSYS® Release 11.0SP1, Ansys Incorporated, 2007.

3. GNRO-2012-00011, Entergy letter to the NRC, Request for Additional Information Regarding Extended Power Uprate, dated February 20, 2012.

4. Letter, Entergy to USNRC, "Vermont Yankee Nuclear Power Station Report on the Results of Steam Dryer Monitoring," BVY 06-056 (Docket No. 50-271, TAC No. MC0761), Dated June 30, 2006.

5. 0000-0101-0766-P-R0, "Main Steam Line Limit Curve Adjustment during Power Ascension," Class III, April 2009.

Appendix F

Power Ascension Test Plan

TABLE OF CONTENTS

LIST OF TABLES

LIST OF FIGURES

F.1 Background

The GGNS replacement dryer was analyzed for CLTP loads projected to EPU based on [[ ]]. This projected load was combined with [[ ]].

The following cases describe the [[ ]] conditions considered in the design basis stress analysis:

[[

]]

During the testing performed up to CLTP (Appendix G), acoustic signals in the MSL strain gauge data [[

]]

[[

]]

Following the methodology outlined in Appendix A, design basis stress analyses were performed using the GGNS plant specific MSL strain gauge data obtained over a range of power. The design basis stress analysis accounted for the expected increase in loads as steam velocity increases, including the effect of potential SRV resonances. The stress analysis results included the analysis and measurement biases and uncertainties. The design basis peak stress represents the maximum calculated stress in any dryer component.

The limit curve approach used for dryer power ascension monitoring was first used by Entergy at Vermont Yankee in monitoring the modified steam dryer during power ascension testing in 2006. The limit curve approach was later adopted by GEH in the development of main steam line monitoring limits for the prototype BWR/4 Units 1 and 2 replacement steam dryers (Reference 1). During the power ascension at Vermont Yankee, [[

]] (Reference 2). [[

]] development of the prototype BWR/4 Limit Curve adjustment methodology (Reference 3). This methodology was employed for MSL monitoring and the adjustment of acceptance limits during power ascension testing of the prototype BWR/4 Units 1 and 2 steam dryers. This general methodology has been incorporated into the GGNS acceptance limits presented here. For the GGNS Power Ascension Test Program (PATP), [[

]] will be based on the MSL strain gauge measurements obtained during the power ascension following the same methodology [[

]].

F.2 Methodology for Development of Acceptance Limits

During power ascension testing above CLTP, the MSL strain gauge data will be used [[

]]

[[

]]

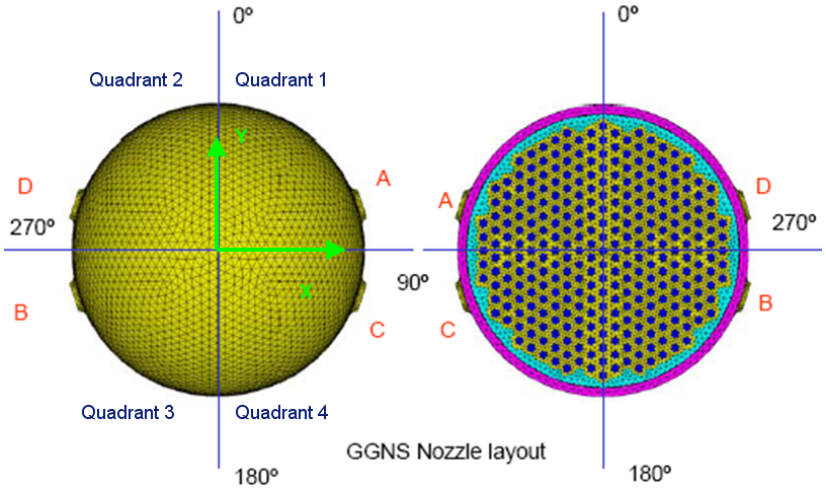

Figure F-1. GGNS MSL Layout

[[

]]

Figure F-2. [[ ]]

[[ ]]

[[

]]

Figure F-3. [[ ]]
[[ ]]

[[

]]

Figure F-4. [[ ]]
[[ ]]

[[

]] Maintaining these [[ ]] acceptance limits will assure the dryer peak stress amplitude remains below 13,600 psi, the ASME Curve C endurance limit for the dryer material. Previous steam dryer monitoring programs at the prototype BWR/4 plant (Reference 1) and Vermont Yankee (Reference 2) had developed monitoring limits based on MSL strain gauge PSD data. [[

]]

The dryer stress response was evaluated [[

]]. The structural model was evaluated for frequency variations over a ±10% range by varying the time step size for the load definition. [[

]]

[[

]]

Figure F-5. [[ ]]

[[

]]

Figure F-6. [[ ]]

The projected limiting stress at [[
]] in Table F-1. [[

]]

Table F-1. Design Basis Peak Stress Intensities

Condition	Limiting Subcomponent	Peak Stress (psi)	[[
			]]

[[ ]]

The Level 1 limit curve is established by factoring the EPU design load spectra by the Limit Curve Factor (LCF). [[

]]

The Level 1 limit is depicted as the upper red curve [[
]]. If a Level 1 limit is exceeded, power will be reduced to a level where the limit curve is satisfied. The goal during the PATP is to maintain the [[ ]] below the Level 2 limit.

During power ascension to EPU power levels, [[

]]

[[

]]

Maintaining the [[ ]] below the acceptance limits will assure that the FIV peak stress amplitude on the GGNS replacement dryer will remain below the ASME Code endurance limit.

F.3 GGNS Dryer Acceptance Limits for Operation Above CLTP

The limits provided in this section shall be evaluated at power ascension plateaus not to exceed 3.5% core thermal power intervals while the reactor steam flow and core thermal power are essentially constant. If a Level 1 limit is exceeded, power will be reduced to a level where the limit criteria are satisfied. The goal during the PAT is to maintain the [[ ]] below the Level 2 limit.

[[ ]] monitored and trended. The trends should be used to extrapolate the dryer loads to the next power ascension plateau. [[

]]

During initial power ascension above CLTP the following acceptance limits shall be maintained:

[[

]]

[[

]]

During the first complete cycle of operation with the replacement steam dryer, monitoring of plant parameters potentially indicative of steam dryer structural degradation will be conducted as recommended in Service Information Letter (SIL) 644, Revision 2 (Reference 4). During the refueling outage following the first complete cycle of operation with the replacement steam dryer, inspections of the dryer will be conducted as recommended in Reference 4.

[[

]]

Figure F-7. [[ ]]

[[

]]

Figure F-8. [[ ]]

[[

]]

Figure F-9. [[ ]]

[[

]]

Figure F-10. [[ ]]

[[

]]

Figure F-11. [[ ]]

[[

]]

Figure F-12. [[ ]]

[[

]]

Figure F-13. [[ ]]

[[

]]

Figure F-14. [[ ]]

[[

]]

Figure F-15. [[ ]]

[[

]]

Figure F-16. [[ ]]

[[

]]

Figure F-17. [[ ]]

[[

]]

Figure F-18. [[ ]]

Table F-2. [[ ]]

[[				
				]]

Table F-3. [[ ]]

[[				
				]]

Table F-4. [[

]]

[[				
				]]

Table F-5. [[

]]

[[				
				]]

Table F-6. [[

]]

[[				

]]

Table F-7. [[

]]

[[				
				]]

F.4 Requirements for Defining [[ ]]

[[

]]

[[

]]

F.5 Determine Margin for Continued Power Ascension

At each power ascension plateau, the data trending described in Section 5 of Appendix A [[

]]

F.6 Update Acceptance Limits

F.6.1 Prepare [[ ]]

Based on trending data and [[

]]

[[

]]

F.6.2 Determine Adjusted Stress with Bias and Uncertainty

With revised EPU [[

]]

F.6.3 Updated Acceptance Limits

Using revised [[

]]

F.7 References

1. GE Hitachi Nuclear Energy, "Revised Susquehanna Replacement Steam Dryer Limit Curves – Main Steam Line Mounted Instrumentation," 0000-0096-5766-P-R1, February 2009.

2. Letter, Entergy to USNRC, "Vermont Yankee Nuclear Power Station Report on the Results of Steam Dryer Monitoring," BVY 06-056 (Docket No. 50-271, TAC No. MC0761), dated June 30, 2006.

3. GE Hitachi Nuclear Energy, "Main Steam Line Limit Curve Adjustment During Power Ascension," 0000-0101-0766-P-R0, April 2009.

4. General Electric Services Information Letter SIL No. 644 Rev. 2, "BWR Steam Dryer Integrity," August 30, 2006.

Appendix G

Grand Gulf Nuclear Station Main Steam Line Test Report

TABLE OF CONTENTS

LIST OF TABLES

LIST OF FIGURES

1.0 Summary

During RFO-16 strain gauges were installed on all four main steam lines at the Grand Gulf Nuclear Station (GGNS). The data from these gauges provides input to the GEH Plant Based Load Evaluation (PBLE), which will be used to determine pressure loads on the steam dryer at Current Licensed Thermal Power (CLTP) and to predict the pressure loads at Extended Power Uprate (EPU) condition. As part of the detailed EPU analysis these loads will be utilized in conjunction with Finite Element Analysis to evaluate the dryer's structural capabilities at EPU. This report provides a preliminary evaluation of the quality of the data and the frequencies of concern.

[[ ]] strain gauges were placed in [[ ]] locations ([[ ]] locations on Main Steam Line (MSL) B and D, as well as [[ ]] locations on MSL A and C) determined by acoustic finite element modeling of the steam lines and vessel. Additional surface preparation of the MSL piping was required due to significant scale buildup. Of the [[ ]] strain gauges, [[ ]] remained functional after installation/final testing. When analyzed the signals showed very low noise and good signal quality.

Power Spectral Density (PSD) analysis of the MSL data showed notable maxima at 12 Hz, 23 Hz and 44 Hz. All of these maxima are indicative of acoustic modes in the combined steam dome and MSL system excited by flow through the upstream and downstream MSIVs and MSL venturis. SRV resonances were observed at 196 Hz, 203 Hz and possibly 208 Hz in the 100% CLTP measurements.

2.0 Purpose

The purpose of this report is to provide the results of the data acquisition and initial analysis from the MSL pressure measurements at the GGNS. Strain gauges mounted on the surface of the MSLs within the drywell were used to measure the dynamic pressure waves during power ascension and steady state operation. This data is used as input to the PBLE to define the fluctuating pressure loads for the structural analysis of the steam dryer. More detailed evaluation of this data is contained in Section 3 of the main report.

3.0 Instrumentation

3.1 Strain Gauges

The MSL sensors consisted of [[ ]] high temperature weldable strain gauges with 3-wire shielded leads (HITEC part number HBWAK-35-250-6-10FG Shield). The selection of the sensors was based on past experience of similar tests conducted on other plant MSLs. The strain gauge arrangement consisted of [[ ]] monitoring locations (upper and lower) on MSLs B and D, as well as [[ ]] monitoring locations on MSLs A and C. [[ ]] strain gauges were oriented circumferentially at each monitoring location with the strain gauge pairs on

opposite sides (i.e., 180° apart) wired in series. The strain gauges were wired in series, because there were a limited number of penetration cables available.

3.2 Sensor Installation

Strain gauge installation began on September 24, 2008 and was completed on October 11, 2008. The strain gauges were installed at the primary elevations on the MSL piping inside the primary containment. A capacitive discharge welder was used to install the strain gauges onto the MSLs. Figure 1 illustrates the primary strain gauge elevations. Field measurements of the strain gauge locations are referenced to the MSL nozzle elevation centerline (Table 1). This reference is assumed to be at [[ ]]. The installation dimensions are the vertical measurement relative to the vessel nozzle. The purpose of these as-built dimensions is to derive the adjusted distance from the inside of the vessel to gauge locations along the center of the steam line. In the acoustic model the pipe is represented as a one-dimensional component based on the pipe centerline. The linear distance dimensions used in the GEH location assessment were based on plant drawings provided by Enercon. These drawings provided as-built dimensions that permitted GEH to determine the distance from the inside wall of the vessel to riser. Linear distances from the vessel nozzle to the actual strain gauge locations were calculated from the plant drawings and the as-built dimensions, measured within 1/8”, and are shown in Table 2.

Table 1. GGNS Plant As-Built Measurements

[[

]]

Table 2. Linear Distance from Vessel Nozzle to Strain Gauge Locations

Strain Gauge Locations	Distance to Inside Nozzle, inches			
	MSL B	MSL D	MSL A	MSL C
[[				
				]]

The strain gauge installation required the removal and reinstallation of the MSL insulation at the specified strain gauge locations. The insulation was modified to accommodate space for the strain gauges on the MSL pipes and for the signal cable egress. Post installation testing identified several failed strain gauges. All were repaired and of the [[ ]] strain gauges, [[ ]] remained operational throughout the test. A sample of installed strain gauge photos can be found in Figures 2 through 8.

[[

]]

Figure 1. Primary Strain Gauge Attachment Elevations

[[

]]

Figure 2. Photo Strain Gauge MSL A 3rd

[[

]]

Figure 3. Photo Strain Gauge MSL B Upper

[[

]]

Figure 4. Photo Strain Gauge MSL B Lower

[[

]]

Figure 5. Photo Strain Gauge MSL C Upper

[[

]]

Figure 6. Photo Strain Gauge MSL C Lower

[[

]]

Figure 7. Photo Strain Gauge MSL D Upper

[[

]]

Figure 8. Photo Strain Gauge MSL D Lower

3.3 Data Acquisition System

The DAS was located on a cart inside the auxiliary building at elevation 139'. It consisted of the LMS SCADAS Mobile unit, 700-Ohm resistor bridge completion box, data acquisition laptop computer and analysis laptop computer. Signal conditioning for the strain gauges was contained in the LMS SCADAS modules. An isolation transformer was placed between the DAS and the plant AC power to eliminate electrical noise. A photo of the DAS setup inside the auxiliary building can be seen in Figure 9.

The DAS wiring diagram is shown in Figure 10 and only illustrates one shielded twisted pair of a cable. All sensor leads from the strain gauges were first wired in series. Field cabling connected the strain gauge pairs to the inboard junction box for penetration TB1CE01. These cables were connected to existing terminations. Additional field cabling connected the outside junction box at penetration TB1CE01 to the external 700-Ohm resistor bridge completion box. The bridge completion box interfaced with the DAS (LMS SCADAS Mobile Unit and interfacing laptop computer) via short cables.

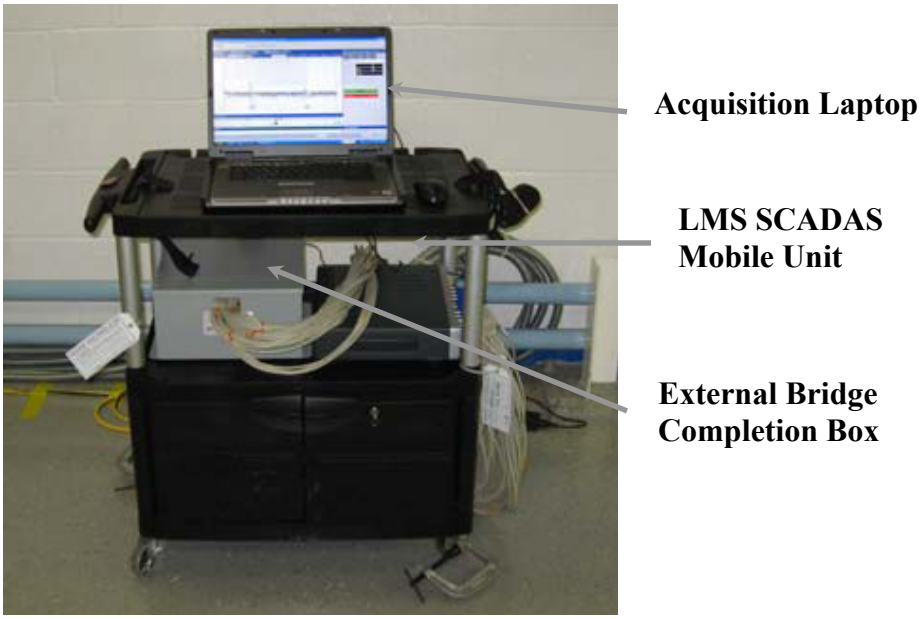

Figure 9. DAS Photo Inside Auxiliary Building

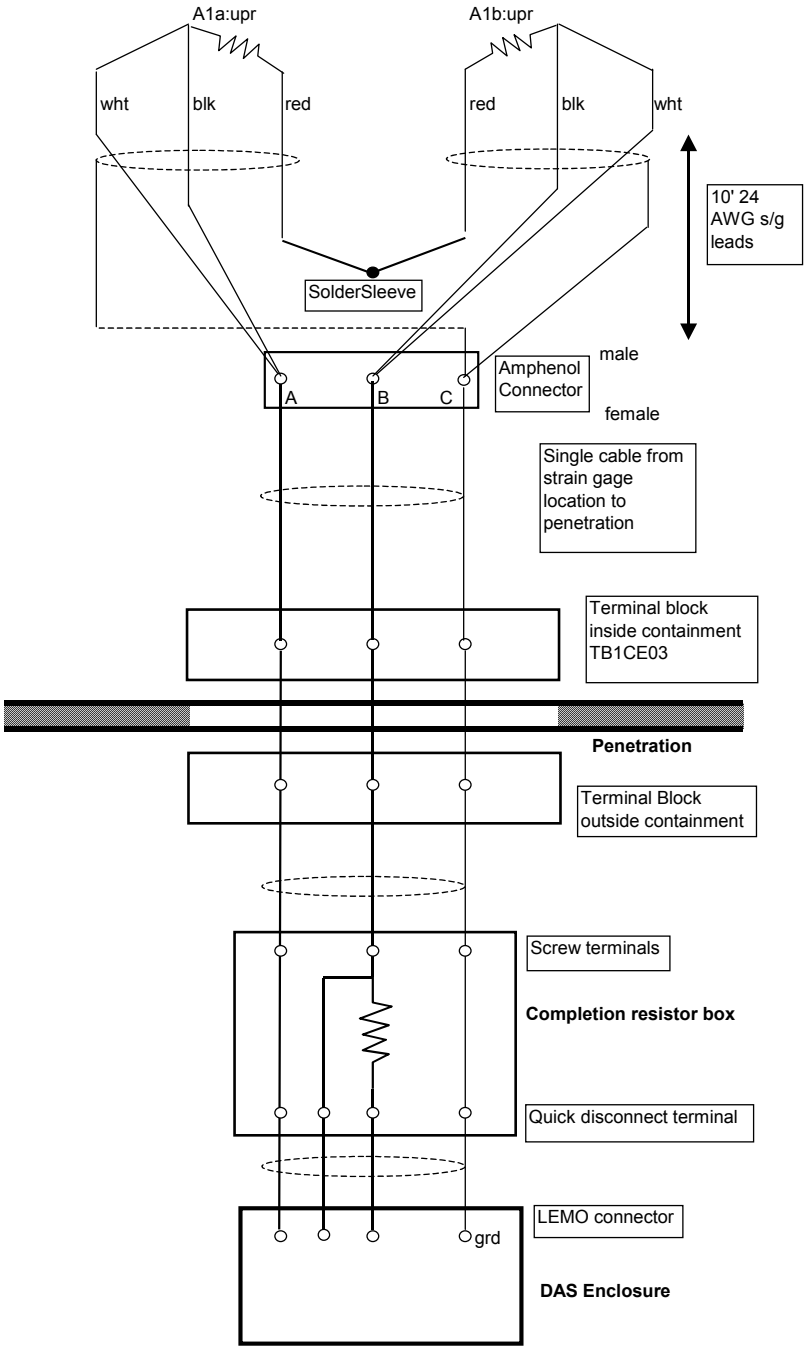

Figure 10. DAS Wiring Diagram

4.0 Tests Performed

4.1 Sensor Pre-Calibration

The sensors were pre-calibrated on October 8, 2008 at the GGNS through the LMS Data Acquisition System (DAS). No abnormalities were noted.

4.2 Primary System Pressurization Test

After the sensor pre-calibration the strain gauges were measured statically during the Primary System Pressurization Test on October 16-17, 2008. Transient records during pressurization and de-pressurization conditions were recorded. The static strain levels were then converted to equivalent pressure using the MSL dimensions and compared with plant pressure instrumentation.

4.3 Power Ascension

Steady state power conditions were used to measure the fluctuating pressure in the MSLs. Measurements were taken at approximately [[
]]. Power ascension data was taken from November 1, 2008 to November 3, 2008. After the reactor stabilized, [[ ]] additional 100% CLTP data points were collected at approximate one hour intervals on November 4, 2008.

4.4 Sensor Post-Calibration

The sensors were post-calibrated on November 5, 2008 with the LMS DAS. No abnormalities were noted.

4.5 Low Power Measurements

During RFO-17 in May 2010, these strain gauges were used to measure static and dynamic signals to evaluate the noise floor level and electrical and mechanical noise at low power levels. Steady state power conditions were used to measure the fluctuating pressure in the MSLs. Measurements were taken at [[
]]. Power ascension data was taken from May 26, 2010 to May 27, 2010. The low power measurements are summarized in Attachment D.

5.0 Data Acquisition Analysis

5.1 Data Acquisition and Analysis Process

The MSL vibration data was collected with a laptop computer and a LMS SCADAS Mobile unit using a sampling frequency of [[ ]]. The only exception was the third data set of the [[ ]] CLTP steady state point. The sampling rate was increased to [[ ]] to check

for aliasing, but no aliasing was noted. The resistance measurements at the DAS termination were entered into the LMS TestLab software package to account for lead wire resistances.

Six data logs were taken for each test condition. Three logs at 10-volt (10V) bridge excitation and three logs at 0-volt (0V) bridge excitation were taken for each power increment. The data logs alternated in the order 10V, 0V, 10V, 0V, 10V, and 0V. The data acquisition time for the 10V and 0V settings were 120 seconds and 40 seconds, respectively. The 10V and 0V log files were measured in immediate succession to identify electrical noise. Prior to each data log the strain gauges were balanced and shunt calibrated.

A data set was defined as a 10V and 0V pair. Maximum, minimum, mean and ranges were calculated for each strain gauge pair. The data was checked for saturation to make sure the data amplitude did not exceed the channel range. Saturation never occurred during testing. Averaged time history data for the strain gauge pairs at each location were calculated along with the averaged PSDs. A maximum PSD value of 250 Hz was saved and plotted. Coherence between the averaged lower and upper strain gauge pairs was also calculated.

Data set one is shown in the Attachment A plots. Data sets two and three were similar to data set one. The averaged plant processed data can be found in Attachment C.

5.2 Primary System Pressurization Test

The strain gauge installation was checked against plant processed data during the primary system pressurization check. As mentioned in Section 4.2 of this appendix, the testing consisted of continuous measurements from zero to full pressure. Then when the primary system pressurization check was complete and the plant was ready to return to ambient pressure, the DAS was nulled and calibrated and continuous measurements were made from full pressure to ambient. The reactor pressure during pressurization went from 14.4 psig to 1027.7 psig. The reactor coolant temperature went from 171°F to 182°F. The reactor pressure during depressurization went from 1032 psig to 17 psig. The reactor coolant temperature during depressurization went from 220°F to 135°F.

5.3 Strain-to-Pressure Conversion

The strain-to-pressure conversion factors were determined using the formula for a thick walled cylinder with closed ends subject to internal pressure only. The conversion factor can be calculated using the following formula:

[[

]]

MSL diameter and thickness UT measurements were taken on September 30, 2008 thru October 2, 2008.

Table 3 below summarizes the conversion factors for each of the [[ ]] strain gauge locations during the hydro test. The Modulus of Elasticity for carbon steels (A516 GR70) as a function of temperature was taken from the ASME Codes (Reference 1).

Table 3. Pipe Dimensions and Strain-to-Pressure Conversion

[[

]]

5.4 Power Ascension Measurements

Attachment A contains the PSD plots for each sensor location at each power level taken during power ascension. Following data collection at each test point, the measured signal data was processed and plotted in the frequency domain for review before ascending to the next power step. The PSD plots represent measurements averaged over 120 seconds of MSL strain data. The PSDs are averaged based on a series of two second long segments, with the adjacent segments overlapping by 50%. The individual strain gauge signals, the averaged strain gauge signals (both excited and non-excited) and coherence between averaged strain gauge signals at the upper and lower sensor locations on the same MSL are plotted on the PSDs. As can be seen in the figures in Attachment A, the individual gauge signals in many frequency bands diverge as a result of the pipe vibration. The black line shows the PSD for the time domain average of the signals for the four pairs of strain gauges. The signals are averaged to define the average hoop strain, which is proportional to the average dynamic pressure at the monitoring location.

Attachment B contains waterfall plots for each sensor location showing the frequency and amplitude content during the power ascension. Attachment C contains the plant operating data at each of the power ascension steps. Attachment D contains the report from the low power measurements taken during RFO-17 to evaluate the noise floor and electrical interference.

5.5 Coherence

Coherence is the measure of the correlation between two signals at a particular frequency. As the coherence approaches a maximum of 1.0 the correlation between the two signals is stronger. When the coherence is 1.0 the two signals are perfectly correlated. When the coherence is zero there is no relationship between the two signals.

Coherence values are included in the PSD plots in Attachment A. The coherence was calculated between the upper and lower strain gauge locations for all steam lines and between the third and lower locations for MSL A and C.

Table 4 is the tabulation of the three highest coherence levels for each power level for frequencies less than approximately 190 Hz and the frequencies at which they occur. The fourth column pair is the coherence peaks in the frequency band from approximately 190-250 Hz. High coherence between measurement locations is indicative of acoustic modes that are being excited in the vessel and MSL system.

Table 4. Coherence in MSL Measurements

[[

]]

6.0 References

1. ASME Boiler and Pressure Vessel Code, Section II, Part D, Subpart 2, Table TM-1, pg. 671.

Attachment A: PSD and Coherence Plots

[[

]]

Figure 11. A-Third PSD and Coherence, 75% CLTP

[[

]]

Figure 12. A-Upper PSD and Coherence, 75% CLTP

[[

]]

Figure 13. A-Lower PSD and Coherence, 75% CLTP

[[

]]

Figure 14. B-Upper PSD and Coherence, 75% CLTP

[[

]]

Figure 15. B-Lower PSD and Coherence, 75% CLTP

[[

]]

Figure 16. C-Upper PSD and Coherence, 75% CLTP

[[

]]

Figure 17. C-Third PSD and Coherence, 75% CLTP

[[

]]

Figure 18. C-Lower PSD and Coherence, 75% CLTP

[[

]]

Figure 19. D-Upper PSD and Coherence, 75% CLTP

[[

]]

Figure 20. D-Lower PSD and Coherence, 75% CLTP

[[

]]

Figure 21. A-Third PSD and Coherence, 80% CLTP

[[

]]

Figure 22. A-Upper PSD and Coherence, 80% CLTP

[[

]]

Figure 23. A-Lower PSD and Coherence, 80% CLTP

[[

]]

Figure 24. B-Upper PSD and Coherence, 80% CLTP

[[

]]

Figure 25. B-Lower PSD and Coherence, 80% CLTP

[[

]]

Figure 26. C-Upper PSD and Coherence, 80% CLTP

[[

]]

Figure 27. C-Third PSD and Coherence, 80% CLTP

[[

]]

Figure 28. C-Lower PSD and Coherence, 80% CLTP

[[

]]

Figure 29. D-Upper PSD and Coherence, 80% CLTP

[[

]]

Figure 30. D-Lower PSD and Coherence, 80% CLTP

[[

]]

Figure 31. A-Third PSD and Coherence, 85% CLTP

[[

]]

Figure 32. A-Upper PSD and Coherence, 85% CLTP

[[

]]

Figure 33. A-Lower PSD and Coherence, 85% CLTP

[[

]]

Figure 34. B-Upper PSD and Coherence, 85% CLTP

[[

]]

Figure 35. B-Lower PSD and Coherence, 85% CLTP

[[

]]

Figure 36. C-Upper PSD and Coherence, 85% CLTP

[[

]]

Figure 37. C-Third PSD and Coherence, 85% CLTP

[[

]]

Figure 38. C-Lower PSD and Coherence, 85% CLTP

[[

]]

Figure 39. D-Upper PSD and Coherence, 85% CLTP

[[

]]

Figure 40. D-Lower PSD and Coherence, 85% CLTP

[[

]]

Figure 41. A-Third PSD and Coherence, 90% CLTP

[[

]]

Figure 42. A-Upper PSD and Coherence, 90% CLTP

[[

]]

Figure 43. A-Lower PSD and Coherence, 90% CLTP

[[

]]

Figure 44. B-Upper PSD and Coherence, 90% CLTP

[[

]]

Figure 45. B-Lower PSD and Coherence, 90% CLTP

[[

]]

Figure 46. C-Upper PSD and Coherence, 90% CLTP

[[

]]

Figure 47. C-Third PSD and Coherence, 90% CLTP

[[

]]

Figure 48. C-Lower PSD and Coherence, 90% CLTP

[[

]]

Figure 49. D-Upper PSD and Coherence, 90% CLTP

[[

]]

Figure 50. D-Lower PSD and Coherence, 90% CLTP

[[

]]

Figure 51. A-Third PSD and Coherence, 95% CLTP

[[

]]

Figure 52. A-Upper PSD and Coherence, 95% CLTP

[[

]]

Figure 53. A-Lower PSD and Coherence, 95% CLTP

[[

]]

Figure 54. B-Upper PSD and Coherence, 95% CLTP

[[

]]

Figure 55. B-Lower PSD and Coherence, 95% CLTP

[[

]]

Figure 56. C-Upper PSD and Coherence, 95% CLTP

[[

]]

Figure 57. C-Third PSD and Coherence, 95% CLTP

[[

]]

Figure 58. C-Lower PSD and Coherence, 95% CLTP

[[

]]

Figure 59. D-Upper PSD and Coherence, 95% CLTP

[[

]]

Figure 60. D-Lower PSD and Coherence, 95% CLTP

[[

]]

Figure 61. A-Third PSD and Coherence, 100% CLTP

[[

]]

Figure 62. A-Upper PSD and Coherence, 100% CLTP

[[

]]

Figure 63. A-Lower PSD and Coherence, 100% CLTP

[[

]]

Figure 64. B-Upper PSD and Coherence, 100% CLTP

[[

]]

Figure 65. B-Lower PSD and Coherence, 100% CLTP

[[

]]

Figure 66. C-Upper PSD and Coherence, 100% CLTP

[[

]]

Figure 67. C-Third PSD and Coherence, 100% CLTP

[[

]]

Figure 68. C-Lower PSD and Coherence, 100% CLTP

[[

]]

Figure 69. D-Upper PSD and Coherence, 100% CLTP

[[

]]

Figure 70. D-Lower PSD and Coherence, 100% CLTP

Attachment B: Waterfall Plots

[[

]]

Figure 71. A-Third Average PSD vs % Power Waterfall Plot

[[

]]

Figure 72. A-Upper Average PSD vs % Power Waterfall Plot

[[

]]

Figure 73. A-Lower Average PSD vs % Power Waterfall Plot

[[

]]

Figure 74. B-Upper Average PSD vs % Power Waterfall Plot

[[

]]

Figure 75. B-Lower Average PSD vs % Power Waterfall Plot

[[

]]

Figure 76. C-Upper Average PSD vs % Power Waterfall Plot

[[

]]

Figure 77. C-Third Average PSD vs % Power Waterfall Plot

[[

]]

Figure 78. C-Lower Average PSD vs % Power Waterfall Plot

[[

]]

Figure 79. D-Upper Average PSD vs % Power Waterfall Plot

[[

]]

Figure 80. D-Lower Average PSD vs % Power Waterfall Plot

Attachment C: Plant Data

[[

]]

[[

]]

[[

]]

[[

]]

Attachment D: Grand Gulf Nuclear Station Main Steam Line Low Power Measurement Report

D1.0 Purpose

The purpose of this attachment is to provide the results of the data acquisition and initial analysis from the MSLs at the GGNS during RFO-17. Strain gauges mounted on the surface of the MSLs within the drywell were used to measure the dynamic pressure waves during power ascension at low power levels. This data will be used to evaluate the signal noise floor and interference not visible in higher power data.

D2.0 Instrumentation

D2.1 Sensor Installation

The original strain gauge installation during RFO-16 was done in Sept.-Oct. 2008. During RFO-17 in May 2010, these strain gauges were used to measure static and dynamic signals to evaluate the noise floor level and electrical and mechanical noise at low power levels. The installation locations and procedure used during RFO-16 are described in Section 3 of this attachment.

D2.2 Data Acquisition System

The DAS was located on a cart inside the auxiliary building at elevation 139'. It consisted of the LMS SCADAS Mobile unit, 700-Ohm resistor bridge completion box, data acquisition laptop computer and analysis laptop computer. Signal conditioning for the strain gauges was contained in the LMS SCADAS modules. An isolation transformer was placed between the DAS and the plant AC power to provide clean power to the acquisition system. A photo of the DAS setup inside the auxiliary building can be seen in Figure 9 of this appendix.

D3.0 Tests Performed

D3.1 System Checkout

Resistance measurements were made to establish the survival rate of the strain gauges since installation in 2008. From these measurements, it was determined that a majority of the strain gauges had survived. These measurements indicated that five channels had changed in resistance by more than 10%. Upon arrival on site, these measurements were repeated with similar results. To improve the ability of the data acquisition system to balance, resistors were added in the bridge completion box to bring the arms of the bridge closer together. Channels [[ ]] had resistors added.

D3.2 Sensor Pre-Calibration

During RFO-16 it was concluded that two channels were unusable, [[ ]]. These channels were turned off during data acquisition in 2008.

For RFO-17, the sensors were pre-calibrated on May 20, 2010 at the GGNS through the LMS DAS. During calibration, the DAS was not able to stabilize two channels. These channels, [[ ]], were turned off and not used in the data acquisition. [[ ]] original channels were used throughout the testing.

D3.3 Primary System Pressurization Test

After the sensor pre-calibration, the strain gauges were measured statically during the Primary System Pressurization Test on May 20-21, 2010. Transient records during pressurization and de-pressurization conditions were recorded. The static strain levels were then converted to equivalent pressure using the MSL dimensions and compared with plant pressure instrumentation.

D3.4 Power Ascension

Steady state power conditions were used to measure the fluctuating pressure in the MSLs. Measurements were taken at [[
]]. Power ascension data was taken from May 26, 2010 to May 27, 2010.

D3.5 Sensor Post-Calibration

The sensors were post-calibrated on May 28, 2010 with the LMS DAS. [[ ]] channels were found to be out of tolerance during the Post Cal Checkout. Data from these sensors was not used for the analysis.

D4.0 Data Acquisition Analysis

D4.1 Data Acquisition and Analysis Process

The MSL vibration data was collected with a laptop computer and a LMS SCADAS Mobile unit using a sampling frequency of [[ ]]. The resistance measurements at the DAS termination were entered into the LMS TestLab software package to account for lead wire resistances.

Six data logs were taken for each test condition. Three logs at 10V bridge excitation and three logs at 0V bridge excitation were taken for each power increment. The data logs alternated in the order 10V, 0V, 10V, 0V, 10V and 0V. The data acquisition time for the 10V and 0V settings were 120 seconds and 40 seconds, respectively. The 10V and 0V log files were measured in immediate succession to identify electrical noise. In the third set an additional 0V without nulling was performed. Prior to each data log the strain gauges were balanced and shunt calibrated.

A data set was defined as a 10V and 0V pair. The entire unfiltered data log was evaluated. Maximum, minimum, mean and ranges were calculated for each strain gauge pair. The data was checked for saturation to make sure the data amplitude did not exceed the channel range. Saturation never occurred during testing. Averaged time history data for the strain gauge pairs at each location were calculated along with the averaged PSDs. A maximum PSD value of 250 Hz was saved and plotted. Coherence between the averaged lower and upper strain gauge pairs was also calculated.

Data set one is shown in the attachment plots. Data sets two and three were similar to data set one.

D4.2 Primary System Pressurization Test

The strain gauge installation was checked against plant-processed data during the primary system pressurization check. As mentioned in Section D3.3, data was recorded during both pressurization and depressurization. The DAS was nulled and calibrated and continuous measurements were made from zero to full pressure. When the primary system pressurization check was complete and the plant was ready to return to ambient pressure, the DAS was nulled and calibrated and continuous measurements were made from full pressure to ambient. The reactor pressure during pressurization went from 6.7 psig to 1023.5 psig. The reactor pressure during depressurization went from 1027.7 psig to 20.1 psig.

D4.3 Noise Analysis

Measurements at 0V bridge excitation were taken for each test condition. The average 0V PSD data is included in the attachment plots. Comparing this measurement with the 10V average PSD data indicates the noise floor and points out potential electrical or mechanical

noise in the measurement. Table 1D below shows the noise frequencies at each power level identified by this measurement. These potential noise frequencies appear across all measurement channels at the specified power levels.

Table 1D. Measurement Noise Frequencies

Power level	Noise Frequencies (Hz)		
[[			
			]]

The 60Hz and 180Hz are typical electrical noise from the line frequency (and higher harmonics). There is other noise that only appeared on the channels for the Lower B and Lower D strain gauges. The identified frequencies are shown in Table 2D. Below 30% CLTP the recirculation pumps were operating at low speed, corresponding to a drive frequency of 15 Hz. Above 30% CLTP they are switched to high speed. At high speed the recirculation pumps were operating at a drive frequency of 60 Hz. At high speed the recirculation pumps are operating at about 1793 rpm (Pump A – 1789 rpm, Pump B – 1797 rpm). This would correspond to a rotational frequency of 29.8 Hz. The 149 Hz corresponds to a fifth harmonic of the rotational frequency. These pumps have a five-vane impeller. The vane passing frequency for a five-vane impeller at 1793 rpm is 149 Hz. Because the recirculation pump motors are induction motors, this electrical interference could be induced by the pressure resistance as the impeller blade passes the cutwater. The momentary slowing of the blade increases the rotor's field strength to handle the extra load. This would then feed back into the current on the bus, where it would show up as electrical interference that is synchronized with the vane passing frequency.

Table 2D. Local Noise Frequencies

Power Level	Noise Frequencies (Hz)
[[	
	]]

Figures 1D through 10D show waterfall plots of the 0V noise for each strain gauge location. Figures 11D through 30D show PSD plots of locations where an orthogonal set of strain gauges produced quality data. Other locations had two sets of quality strain gauges but these were not an orthogonal pair and are not shown here.

[[

]]

Figure 1D. A-Third 0V Average PSD vs % Power Waterfall Plot

[[

]]

Figure 2D. A-Upper 0V Average PSD vs % Power Waterfall Plot

[[

]]

Figure 3D. A-Lower 0V Average PSD vs % Power Waterfall Plot

[[

]]

Figure 4D. B-Upper 0V Average PSD vs % Power Waterfall Plot

[[

]]

Figure 5D. B-Lower 0V Average PSD vs % Power Waterfall Plot

[[

]]

Figure 6D. C-Upper 0V Average PSD vs % Power Waterfall Plot

[[

]]

Figure 7D. C-Third 0V Average PSD vs % Power Waterfall Plot

[[

]]

Figure 8D. C-Lower 0V Average PSD vs % Power Waterfall Plot

[[

]]

Figure 9D. D-Upper 0V Average PSD vs % Power Waterfall Plot

[[

]]

Figure 10D. D-Lower 0V Average PSD vs % Power Waterfall Plot

[[

]]

Figure 11D. B-Upper Average PSD and Coherence, 10% CLTP

[[

]]

Figure 12D. B-Lower Average PSD and Coherence, 10% CLTP

[[

]]

Figure 13D. C-Lower Average PSD and Coherence, 10% CLTP

[[

]]

Figure 14D. D-Lower Average PSD and Coherence, 10% CLTP

[[

]]

Figure 15D. B-Upper Average PSD and Coherence, 20% CLTP

[[

]]

Figure 16D. B-Lower Average PSD and Coherence, 20% CLTP

[[

]]

Figure 17D. C-Lower Average PSD and Coherence, 20% CLTP

[[

]]

Figure 18D. D-Lower Average PSD and Coherence, 20% CLTP

[[

]]

Figure 19D. B-Upper Average PSD and Coherence, 24% CLTP

[[

]]

Figure 20D. B-Lower Average PSD and Coherence, 24% CLTP

[[

]]

Figure 21D. C-Lower Average PSD and Coherence, 24% CLTP

[[

]]

Figure 22D. D-Lower Average PSD and Coherence, 24% CLTP

[[

]]

Figure 23D. B-Upper Average PSD and Coherence, 40% CLTP

[[

]]

Figure 24D. B-Lower Average PSD and Coherence, 40% CLTP

[[

]]

Figure 25D. C-Lower Average PSD and Coherence, 40% CLTP

[[

]]

Figure 26D. D-Lower Average PSD and Coherence, 40% CLTP

[[

]]

Figure 27D. B-Upper Average PSD and Coherence, 50% CLTP

[[

]]

Figure 28D. B-Lower Average PSD and Coherence, 50% CLTP

[[

]]

Figure 29D. C-Lower Average PSD and Coherence, 50% CLTP

[[

]]

Figure 30D. D-Lower Average PSD and Coherence, 50% CLTP

Attachment 3

GNRO-2012/00011

Grand Gulf Nuclear Station Extended Power Uprate

Response to Request for Additional Information

Mechanical and Civil Engineering Branch, Steam Dryer

GEH Affidavit for Withholding Information from Public Disclosure

GE-Hitachi Nuclear Energy Americas LLC

AFFIDAVIT

I, Edward D. Schrull, PE state as follows:

(1) I am the Vice President, Regulatory Affairs, Services Licensing, GE-Hitachi Nuclear Energy Americas LLC ("GEH"), and have been delegated the function of reviewing the information described in paragraph (2) which is sought to be withheld, and have been authorized to apply for its withholding.

(2) The information sought to be withheld is contained in Enclosures 1 and 3 of GEH letter, 173280-JB-060, "Grand Gulf Steam Dryer: Transmittal of Steam Dryer Responses to Requests for Additional Information 8, 10, and 12," dated February 19, 2012. The GEH proprietary information in Enclosure 1, which is entitled "GEH Responses to GGNS Steam Dryer Requests for Additional Information 8 and 12, GEH Proprietary Information – Class III (Confidential)" is identified by a dotted underline inside double square brackets. [[This sentence is an example.{3}]] Figures, equations and some tables containing GEH proprietary information are identified with double square brackets before and after the object. In each case, the superscript notation {3} refers to Paragraph (3) of this affidavit, which provides the basis for the proprietary determination. Enclosure 3, which is entitled "GEH Input to RAI 10, GEH Proprietary Information - Class III (Confidential)" is proprietary in its entirety. The header of each page in Enclosure 3 carries the notation "GEH Proprietary Information – Class III (Confidential){3}." In all cases, the superscript notation {3} refers to Paragraph (3) of this affidavit, which provides the basis for the proprietary determination.

(3) In making this application for withholding of proprietary information of which it is the owner or licensee, GEH relies upon the exemption from disclosure set forth in the Freedom of Information Act ("FOIA"), 5 USC Sec. 552(b)(4), and the Trade Secrets Act, 18 USC Sec. 1905, and NRC regulations 10 CFR 9.17(a)(4), and 2.390(a)(4) for trade secrets (Exemption 4). The material for which exemption from disclosure is here sought also qualifies under the narrower definition of trade secret, within the meanings assigned to those terms for purposes of FOIA Exemption 4 in, respectively, Critical Mass Energy Project v. Nuclear Regulatory Commission, 975 F2d 871 (DC Cir. 1992), and Public Citizen Health Research Group v. FDA, 704 F2d 1280 (DC Cir. 1983).

(4) The information sought to be withheld is considered to be proprietary for the reasons set forth in paragraphs (4)a. and (4)b. Some examples of categories of information that fit into the definition of proprietary information are:

a. Information that discloses a process, method, or apparatus, including supporting data and analyses, where prevention of its use by GEH's competitors without license from GEH constitutes a competitive economic advantage over other companies;

b. Information that, if used by a competitor, would reduce their expenditure of resources or improve their competitive position in the design, manufacture, shipment, installation, assurance of quality, or licensing of a similar product;

c. Information that reveals aspects of past, present, or future GEH customer-funded development plans and programs, resulting in potential products to GEH;

d. Information that discloses trade secret and/or potentially patentable subject matter for which it may be desirable to obtain patent protection.

(5) To address 10 CFR 2.390(b)(4), the information sought to be withheld is being submitted to NRC in confidence. The information is of a sort customarily held in confidence by GEH, and is in fact so held. The information sought to be withheld has, to the best of my knowledge and belief, consistently been held in confidence by GEH, not been disclosed publicly, and not been made available in public sources. All disclosures to third parties, including any required transmittals to the NRC, have been made, or must be made, pursuant to regulatory provisions or proprietary and/or confidentiality agreements that provide for maintaining the information in confidence. The initial designation of this information as proprietary information, and the subsequent steps taken to prevent its unauthorized disclosure, are as set forth in the following paragraphs (6) and (7).

(6) Initial approval of proprietary treatment of a document is made by the manager of the originating component, who is the person most likely to be acquainted with the value and sensitivity of the information in relation to industry knowledge, or who is the person most likely to be subject to the terms under which it was licensed to GEH. Access to such documents within GEH is limited to a "need to know" basis.

(7) The procedure for approval of external release of such a document typically requires review by the staff manager, project manager, principal scientist, or other equivalent authority for technical content, competitive effect, and determination of the accuracy of the proprietary designation. Disclosures outside GEH are limited to regulatory bodies, customers, and potential customers, and their agents, suppliers, and licensees, and others with a legitimate need for the information, and then only in accordance with appropriate regulatory provisions or proprietary and/or confidentiality agreements.

(8) The information identified in paragraph (2), above, is classified as proprietary because it contains detailed GEH design information of the methodology used in the design and analysis of the steam dryers for the GEH Boiling Water Reactor (BWR). Development of these methods, techniques, and information and their application for the design, modification, and analyses methodologies and processes was achieved at a significant cost to GEH.

The development of the evaluation processes along with the interpretation and application of the analytical results is derived from the extensive experience databases that constitute major GEH asset.

(9) Public disclosure of the information sought to be withheld is likely to cause substantial harm to GEH's competitive position and foreclose or reduce the availability of profit-making opportunities. The information is part of GEH's comprehensive BWR safety and technology base, and its commercial value extends beyond the original development cost. The value of the technology base goes beyond the extensive physical database and analytical methodology and includes development of the expertise to determine and apply the appropriate evaluation process. In addition, the technology base includes the value derived from providing analyses done with NRC-approved methods.

The research, development, engineering, analytical and NRC review costs comprise a substantial investment of time and money by GEH. The precise value of the expertise to devise an evaluation process and apply the correct analytical methodology is difficult to quantify, but it clearly is substantial. GEH's competitive advantage will be lost if its competitors are able to use the results of the GEH experience to normalize or verify their own process or if they are able to claim an equivalent understanding by demonstrating that they can arrive at the same or similar conclusions.

The value of this information to GEH would be lost if the information were disclosed to the public. Making such information available to competitors without their having been required to undertake a similar expenditure of resources would unfairly provide competitors with a windfall, and deprive GEH of the opportunity to exercise its competitive advantage to seek an adequate return on its large investment in developing and obtaining these very valuable analytical tools.

I declare under penalty of perjury that the foregoing affidavit and the matters stated therein are true and correct to the best of my knowledge, information, and belief.

Executed on this 19th day of February 2012.

Edward D. Schrull, PE
Vice President, Regulatory Affairs
Services Licensing
GE-Hitachi Nuclear Energy Americas LLC
3901 Castle Hayne Rd.
Wilmington, NC 28401
Edward.Schrull@ge.com

GE-Hitachi Nuclear Energy Americas LLC

AFFIDAVIT

I, Edward D. Schrull, PE state as follows:

(1) I am the Vice President, Regulatory Affairs, Services Licensing, GE-Hitachi Nuclear Energy Americas LLC ("GEH"), and have been delegated the function of reviewing the information described in paragraph (2) which is sought to be withheld, and have been authorized to apply for its withholding.

(2) The information sought to be withheld is contained in GEH proprietary report NEDC-33601P, "Engineering Report Grand Gulf Replacement Dryer Fatigue Stress Analysis Using PBLE Methodology," Revision 1, dated February 2012. The GEH proprietary information in NEDC-33601P is identified by a dotted underline inside double square brackets. [[This sentence is an example.{3}]] Figures, equations and some tables containing GEH proprietary information are identified with double square brackets before and after the object. Appendix C of NEDC-33601P is proprietary in total, thus, it carries the notation "GEH Proprietary Information - Class III (Confidential){3}" in the header. In all cases, the superscript notation {3} refers to Paragraph (3) of this affidavit, which provides the basis for the proprietary determination.

(3) In making this application for withholding of proprietary information of which it is the owner or licensee, GEH relies upon the exemption from disclosure set forth in the Freedom of Information Act ("FOIA"), 5 USC Sec. 552(b)(4), and the Trade Secrets Act, 18 USC Sec. 1905, and NRC regulations 10 CFR 9.17(a)(4), and 2.390(a)(4) for trade secrets (Exemption 4). The material for which exemption from disclosure is here sought also qualifies under the narrower definition of trade secret, within the meanings assigned to those terms for purposes of FOIA Exemption 4 in, respectively, Critical Mass Energy Project v. Nuclear Regulatory Commission, 975 F2d 871 (DC Cir. 1992), and Public Citizen Health Research Group v. FDA, 704 F2d 1280 (DC Cir. 1983).

(4) The information sought to be withheld is considered to be proprietary for the reasons set forth in paragraphs (4)a. and (4)b. Some examples of categories of information that fit into the definition of proprietary information are:

a. Information that discloses a process, method, or apparatus, including supporting data and analyses, where prevention of its use by GEH's competitors without license from GEH constitutes a competitive economic advantage over other companies;

b. Information that, if used by a competitor, would reduce their expenditure of resources or improve their competitive position in the design, manufacture, shipment, installation, assurance of quality, or licensing of a similar product;

c. Information that reveals aspects of past, present, or future GEH customer-funded development plans and programs, resulting in potential products to GEH;

d. Information that discloses trade secret and/or potentially patentable subject matter for which it may be desirable to obtain patent protection.

(5) To address 10 CFR 2.390(b)(4), the information sought to be withheld is being submitted to NRC in confidence. The information is of a sort customarily held in confidence by GEH, and is in fact so held. The information sought to be withheld has, to the best of my knowledge and belief, consistently been held in confidence by GEH, not been disclosed publicly, and not been made available in public sources. All disclosures to third parties, including any required transmittals to the NRC, have been made, or must be made, pursuant to regulatory provisions or proprietary and/or confidentiality agreements that provide for maintaining the information in confidence. The initial designation of this information as proprietary information, and the subsequent steps taken to prevent its unauthorized disclosure, are as set forth in the following paragraphs (6) and (7).

(6) Initial approval of proprietary treatment of a document is made by the manager of the originating component, who is the person most likely to be acquainted with the value and sensitivity of the information in relation to industry knowledge, or who is the person most likely to be subject to the terms under which it was licensed to GEH. Access to such documents within GEH is limited to a "need to know" basis.

(7) The procedure for approval of external release of such a document typically requires review by the staff manager, project manager, principal scientist, or other equivalent authority for technical content, competitive effect, and determination of the accuracy of the proprietary designation. Disclosures outside GEH are limited to regulatory bodies, customers, and potential customers, and their agents, suppliers, and licensees, and others with a legitimate need for the information, and then only in accordance with appropriate regulatory provisions or proprietary and/or confidentiality agreements.

(8) The information identified in paragraph (2), above, is classified as proprietary because it contains detailed GEH design information of the methodology used in the design and analysis of the steam dryers for the GEH Boiling Water Reactor (BWR). Development of these methods, techniques, and information and their application for the design, modification, and analyses methodologies and processes was achieved at a significant cost to GEH.

The development of the evaluation processes along with the interpretation and application of the analytical results is derived from the extensive experience databases that constitute major GEH asset.

(9) Public disclosure of the information sought to be withheld is likely to cause substantial harm to GEH's competitive position and foreclose or reduce the availability of profit-making opportunities. The information is part of GEH's comprehensive BWR safety and technology base, and its commercial value extends beyond the original development cost. The value of the technology base goes beyond the extensive physical database and analytical methodology and includes development of the expertise to determine and apply the appropriate evaluation process. In addition, the technology base includes the value derived from providing analyses done with NRC-approved methods.

The research, development, engineering, analytical and NRC review costs comprise a substantial investment of time and money by GEH. The precise value of the expertise to devise an evaluation process and apply the correct analytical methodology is difficult to quantify, but it clearly is substantial. GEH's competitive advantage will be lost if its competitors are able to use the results of the GEH experience to normalize or verify their own process or if they are able to claim an equivalent understanding by demonstrating that they can arrive at the same or similar conclusions.

The value of this information to GEH would be lost if the information were disclosed to the public. Making such information available to competitors without their having been required to undertake a similar expenditure of resources would unfairly provide competitors with a windfall, and deprive GEH of the opportunity to exercise its competitive advantage to seek an adequate return on its large investment in developing and obtaining these very valuable analytical tools.

I declare under penalty of perjury that the foregoing affidavit and the matters stated therein are true and correct to the best of my knowledge, information, and belief.

Executed on this 19th day of February 2012.

Edward D. Schrull, PE
Vice President, Regulatory Affairs
Services Licensing
GE-Hitachi Nuclear Energy Americas LLC
3901 Castle Hayne Rd.
Wilmington, NC 28401
Edward.Schrull@ge.com